E.O. Paton Electric Welding Institute of the National Academy of Sciences of Ukraine

International Scientific-Technical and Production Journal

The Paton WELDING JOURNAL

Issue 2 2021

Published Monthly Since 2000

English Translation of the Monthly «Avtomatychne Zvaryuvannya» (Avtomaticheskaya Svarka/Automatic Welding) Journal Published in Ukrainian and Russian Since 1948

Founders
E.O. Paton Electric Welding Institute
International Association «Welding»

Publisher
International Association «Welding»

Translators
A.O. Fomin, I.M. Kutianova
Editor
N.G. Khomenko
Electron galley
D.I. Sereda, T.Yu. Snegiryova

Address
E.O. Paton Electric Welding Institute,
International Association «Welding»
11 Kazymyr Malevych Str. (former Bozhenko),
03150, Kyiv, Ukraine
Tel.:/Fax: (38044) 200 82 77
E-mail: journal@paton.kiev.ua
www://patonpublishinghouse.com/eng/journals/tpwj

State Registration Certificate
KV 4790 of 09.01.2001
ISSN 0957-798X
DOI: http://dx.doi.org/10.37434/tpwj

Subscriptions
12 issues per year, back issues available.
$384, subscriptions for the printed (hard copy) version, air postage and packaging included.
$312, subscriptions for the electronic version (sending issues of Journal in pdf format or providing access to IP addresses).
Institutions with current subscriptions on printed version can purchase online access to the electronic versions of any back issues that they have not subscribed to.
Issues of the Journal (more than two years old) are available at a substantially reduced price.

CONTENTS

SCIENTIFIC AND TECHNICAL

INDUSTRIAL

https://doi.org/10.37434/tpwj2021.02.01

FEATURES OF FORMATION OF STRUCTURE OF COAXIAL JOINTS OF COPPER AND ALUMINIUM IN EXPLOSION WELDING WITH VACUUMING OF WELDING GAP

M.O. Pashchin, P.S. Shlonskyi, A.G. Bryzgalin, O.S. Kushnaryova and **N.L. Todorovych**
E.O. Paton Electric Welding Institute of the NAS of Ukraine
11 Kazymyr Malevych Str., 03150, Kyiv, Ukraine. E-mail: office@paton.kiev.ua

The results of the study of intermetallics formation in explosion welding of copper and aluminium coaxial joints depending on the length of the joint and the environment in the welding gap (air and vacuum) are presented. The metallographic analysis of the boundary of the coaxial joint in copper-aluminium rods showed that at different areas of bimetallic rods in welding under different conditions both in air as well as in the presence of vacuum in the gap, intermetallic layers of different thickness are formed. The growth, observed in the volume fraction and thickness of the intermetallic layer in the joint area, as it moves away from the initiation point, regardless of the environment in the welding gap (air or vacuum), is natural and is explained by the channel effect in explosion welding. 14 Ref., 1 Table, 9 Figures.

Keywords: explosion welding, channel effect, intermetallics, contact point speed

As is known, in aircraft industry, manufacturers seek to reduce the weight of aircrafts. Therefore, manufacture of conductive elements with a copper solid gap, which inspite of a high electrical conductivity at the same time has a high density, is irrational. In current-carrying elements (Figure 1) an alternating current of high frequency flows and, taking into account the skin effect, the current is distributed nonuniformly in the cross-section — mainly in a thin surface layer [1].

The length of the pipe cladding can be characterized by the coefficient of length in the form of the ratio of its length L_p to diameter d_p

$$K_l = L_p d_p^{-1}.$$

Among the reasons that cause the need in cladding long-length workpieces, two main reasons can be distinguished:

- producing or restoring standard products;
- increase in efficiency and economy of expensive materials.

Until now, the possibilities of technologies for explosive cladding pipes and rods were limited to short-length products (K_l < 5–10) [2] and the nomenclature of coating materials (stainless steel, titanium) [3–6]. These works show the need in further development and improvement of technologies, in particular, for the development of the range K_l > 5–10 and cladding with electrical materials.

In [7] the possibility of producing long-length coaxial joints (K_l ~ 30) is presented, but at the same time it is indicated that the continuity of the joint, on average, amounts to 50 % from the total contact area of welded surfaces, which may be quite acceptable for conductivity and unsatisfactory when a product is subjected to mechanical action (bending, flattening, etc.).

Despite numerous successes achieved in the field of studying the process of explosion welding of copper and aluminium, due to investigations by Ukrainian and foreign scientists Kudinov V.M., Dobrushin L.D., Petushkov V.G., Derybas A.A., Sedykh B.S., Lysak V.I., Trykov Yu.P., Kuzmin S.V., Pervukhin L.B., Crossland V., Bahrani, etc. most of the works are devoted to the problem of producing sheet bimetal or three-layer composite material produced according to the battery scheme (simultaneous cladding on both sides).

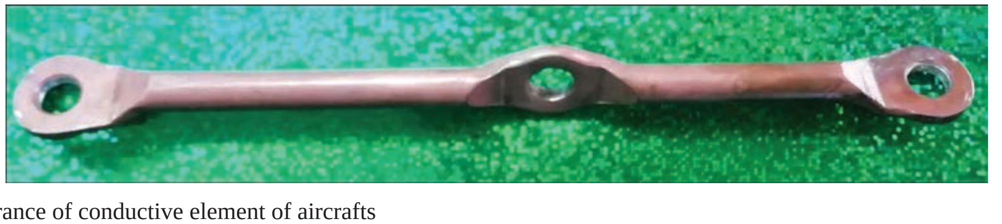

Figure 1. Appearance of conductive element of aircrafts

M.O. Pashchin — https://orcid.org/0000-0002-2201-5137, P.S. Shlonskyi — https://orcid.org/0000-0002-3566-1752,
A.G. Bryzgalin — https://orcid.ord/0000-0001-5886-3069, O.S. Kushnaryova — https://orcid.org/0000-0002-2125-1795,
N.L. Todorovych — https://orcid.org/0000-0002-3872-5790

The process of joint formation during explosion welding of coaxial joints of copper with aluminium is greatly influenced by an shock-compressed gas, which fills the gap between the welded surfaces and moves at a speed exceeding the speed of the point contact [8]. For combination (joining) of copper-aluminium, the atmosphere in the welding gap affects the formation of the joint structure because of a low melting point of aluminium and the eutectic $Al_2Cu + \kappa$, which has a melting point of 548 °C [9]. A high temperature of the gas before the contact point results in heating the welded surfaces [10–12]. An increase in the size of the eddy zones (up to the melts and destruction of the cladding layer) with moving away from the beginning of the welding process indicates an increase in the amount of energy absorbed by the metal in the zone of the welded joint formation. The abovementioned results of investigations allowed formulating the aim of this work.

The aim of this work was to study the effect of the length and vacuuming of the welding gap on the structure of the joint of copper with aluminium during explosion welding of long-length cylindrical products.

Materials and procedures of investigations. To determine the maximum length, at which it is possible to produce a high-quality welded coaxial joint of copper and aluminium, as well as the effect of vacuuming, explosion welding experiments were performed on the conditions mentioned in Table, with and without vacuuming of the welding gap.

As welded materials, M1 grade copper pipe with an outer diameter of 28 mm and a wall thickness of 1 mm and AD1 grade aluminium rod were used (Figure 2), and the welded area was ground to a diameter of 24 mm. The length of the welded workpieces was 1000 mm. Explosion welding was carried out on two conditions at collision speeds of 320 and 390 m/s, the speed of the contact point of 2000 and 2600 m/s, respectively, with and without vacuuming of the welding gap. Before welding, the copper pipes were etched in a 10 % solution of nitric acid to remove scale after annealing, and aluminium rods were cleaned by a sandpaper with a grain size of P120. During vacuuming of the welding gap, the value of vacuum was 20 kPa. For uniformity of loading, the container was used consisting of several parts (Figure 2, *b*).

Cutting out of specimens for the subsequent manufacture of sections from them was carried out mechanically by means of a corner saw, according to the scheme

Numbers of sections cut out from rods, welded on different conditions

Conditions	V_c = 2000, m/s	V_c = 2600, m/s
Air	No.1 — beginning 70–100 mm	No.7 — beginning 70–100 mm
Same	No.2 — middle 450–500 mm	No.8 — middle 450–500 mm
»	No.3 — end 870–900 mm	No.9 — end 870–900 mm
Vacuum	No.4 — beginning 70–100 mm	No.10 — beginning 70–100 mm
Same	No.5 — middle 470–500 mm	No.11 — middle 470–500 mm
»	No.6 — end 870–900 mm	No.12 — end 870–900 mm

Figure 2. Workpieces for explosion welding (*a*), loading of explosives into a folded container (*b*)

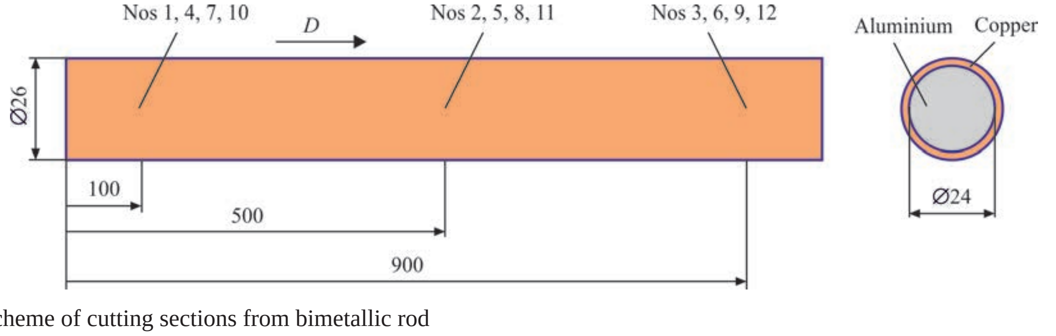

Figure 3. Scheme of cutting sections from bimetallic rod

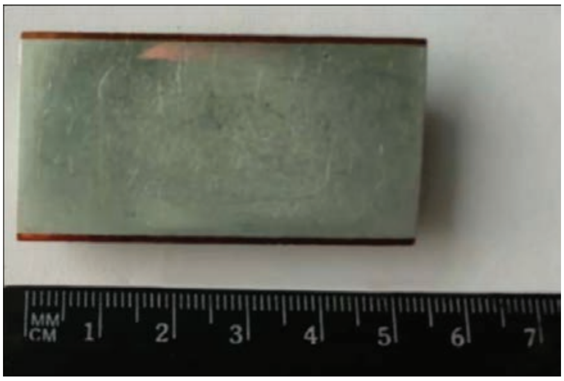

Figure 4. Specimen of microsection of bimetallic rod for metallographic examinations after explosion welding

presented in Figure 3. In all cases, the cut was made using coolant to prevent overheating of the joint area.

Table describes the place of cutting out of the specimen to study the microstructure and indicates the conditions, on which the explosion welding was carried out.

A specimen of a microsection of copper-aluminium joints after explosion welding is shown in Figure 4. To reveal the microstructure, copper etching was performed. Etching of microsections was performed in a mixture from 1 part of nitric acid (50 %) and 1 part of water (50 %).

The hardness tests were performed by the Vickers method. Into the surface of the material, a tetrahedral diamond pyramid with an angle at the apix $\alpha = 136°$ is pressed.

The measurements of microhardness were performed in a microhardness tester PMT-3. The measurements were performed by the method of reconstructed impression, which consists in applying the impression to the tested surface after application of a static load of 0.1 N for copper M1 and aluminium AD1 to the diamond tip. The measuring step was set in the range from 0.05 to 0.2 mm depending on the hardness of the material and the distance from the boundary of the joint d (with an increase in d the step increased) was investigated. Setting up of PMT-3 device on touch of the specimen was carried out at a load $P = 0.005$ N.

Results of experiments and their discussion. The produced specimens were subjected to metallographic examinations, the results of which are presented in Figure 5. The volume fraction of intermetallics and the width of intermetallic layer were studied. Based on their results the diagrams of dependence of the abovementioned parameters on the conditions of explosion welding and the presence or absence of vacuum in the welding gap were plotted (Figures 6, 7).

Figure 5, *a*, *b*, c shows the photos of the microstructure of different zones (beginning, middle, end) of the bimetallic rod produced at V_c = 2000 m/s in air, and in Figure 5, *d*, *e*, *f* in vacuum. The photos of microstructure of different zones of the bimetallic rod (beginning, middle, end), produced in air and in vacuum at V_c = 2600 m/s are presented in Figure 5 (*g*, *h*, *i*) and Figure 5 (*j*, *k*, *l*), respectively.

The carried out metallographic analysis of the boundary of the coaxial joint in copper-aluminium rods showed that at different areas of bimetallic rods in welding on different conditions and in air, and in the presence of vacuum in the gap, it is impossible to produce a joint without the formation of intermetallics.

In explosion welding of copper with aluminium at the speed of the contact point V_c = 2000 m/s, the joint line has a configuration close to a wave-like one with the presence of areas of molten metal near the base of the deformation mounds. Intensification of welding conditions (increase in the speed of the contact point to 2600 m/s) leads to the formation of a wave-like configuration of the joint with unstable parameters of waves and the formation of a continuous interlayer of intermetallics both in vacuum and without it.

In this case, an eddy is formed at the beginning of a wave formation, inside which looseness, copper particles and other inclusions are observed (see Figure 5).

The observed increase in the volume fraction (Figure 6) and thickness of the interlayer (Figure 7) of intermetallics in the joint zone as they move away from the initiation point, regardless of the environment in the welding gap (air or vacuum), has a natural character and is explained by the channel effect in explosion welding [13].

During welding in air on the conditions V_c = = 2000 m/s at the beginning of the specimen the volume fraction of intermetallics is equal to 60 %, during welding in vacuum on the same conditions it is equal to 48 % (Figure 6), which is 1.25 times lower. At the same time, the ratio of the volume fraction of intermetallics in air to the same fraction in vacuum at the beginning of the specimen in welding at V_c = 2600 m/s amounts to 1.08. This indicates the fact that with an increase in speed of the contact point, the transition of kinetic energy into heat energy occurs mainly due to plastic deformation of the metal of the near-weld zone, and to a lesser extent due to the channel effect, which is weak expressed at a short distance from the initiation of the explosion welding process.

In the middle and at the end of the specimen, the ratio of the volume fraction of intermetallics in air to the same fraction in vacuum during welding on the conditions V_c = 2000 m/s amounts to 1.05 and 1.03, respectively, i.e. they are almost equalized. This indicates the fact that at a distance of more than ten diameters of the workpiece in the welding with vacuuming gap, air «plug» of a shock-compressed air and parti-

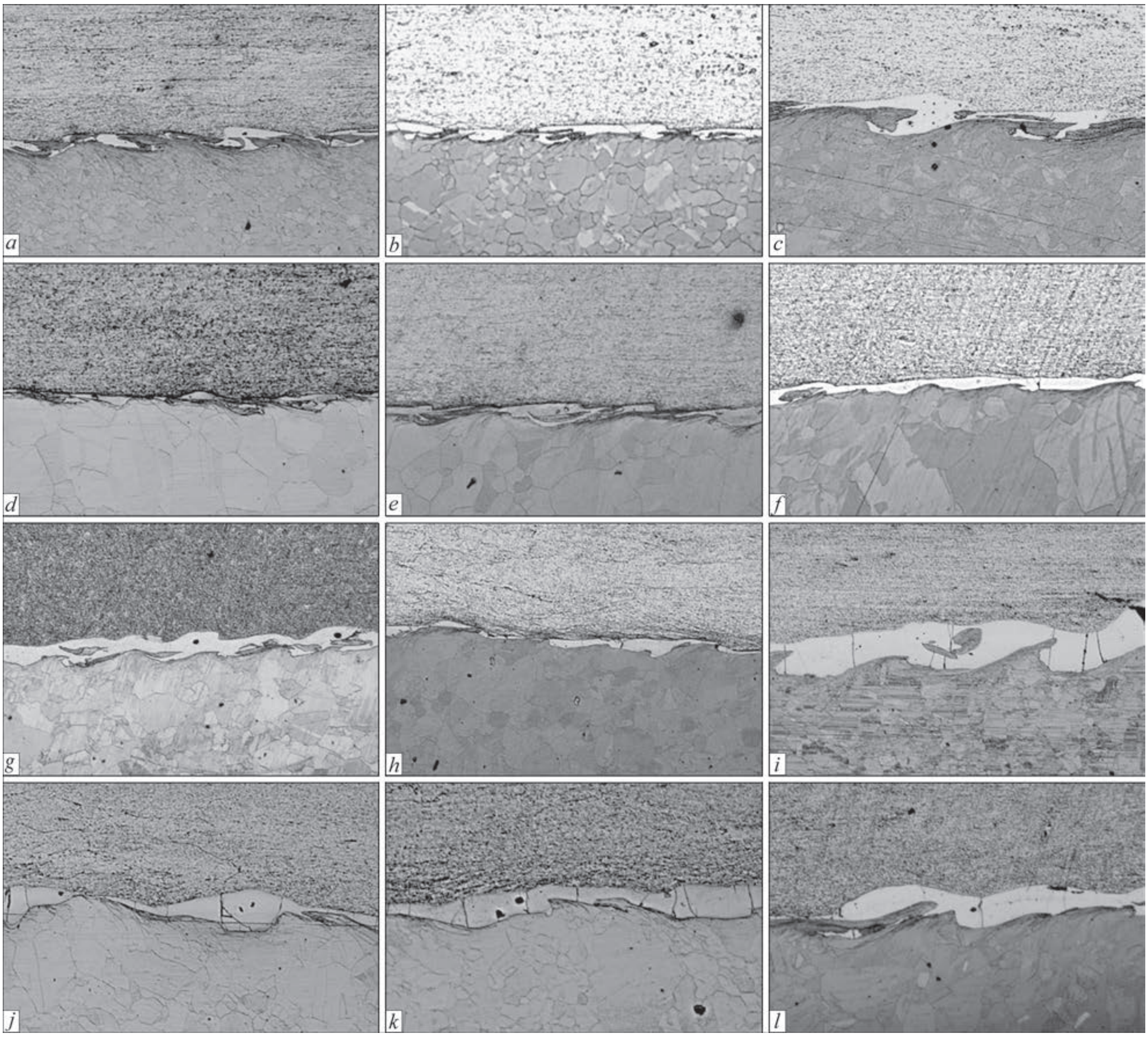

Figure 5. Change in the microstructure of the joint zone depending on the distance from the beginning of welding and environment in the welding gap at different speeds of the contact point (×150, aluminium is above): *a*, *b*, *c* — beginning, middle, end, V_c = 2000 m/s in air; *d*, *e*, *f* — beginning, middle, end, V_c = 2000 m/s in vacuum; *g*, *h*, *i* — beginning, middle, end, V_c = 2600 m/s in air; *k*, *l*, *m* — beginning, middle, end, V_c = 2600 m/s in vacuum

cles of welded materials is accumulated, which heats welded surfaces.

As is seen from Figure 6, the ratio of the volume fraction of intermetallics in air to the same fraction in vacuum in the middle of the specimen in welding on the conditions V_c = 2600 m/s, is equal to 0.61. Thus, the volume fraction of intermetallics produced by welding in vacuum is 1.5 times higher than during

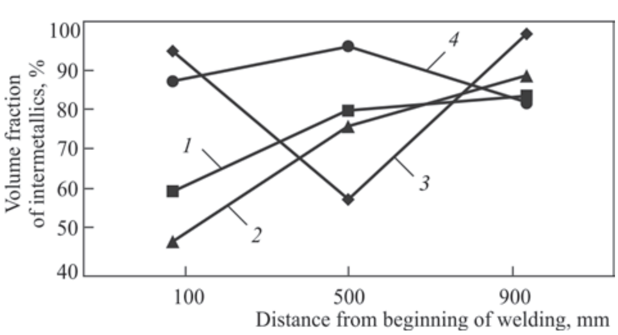

Figure 6. Dependence of the volume fraction of intermetallics on conditions and distance from the beginning of welding: *1* — V_c = = 2000 m/s — in air; *2* — V_c = 2000 m/s — in vacuum; *3* — V_c = = 2600 m/s — in air; *4* — V_c = 2600 m/s — in vacuum

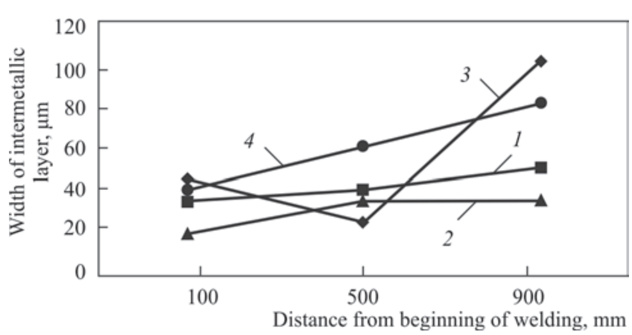

Figure 7. Dependence of width of intermetallic layer on the conditions and distance from the beginning of welding: *1* — V_c = = 2000 m/s — in air; *2* — V_c = 2000 m/s — in vacuum; *3* — V_c = = 2600 m/s — in air; *4* — V_c = 2600 m/s — in vacuum

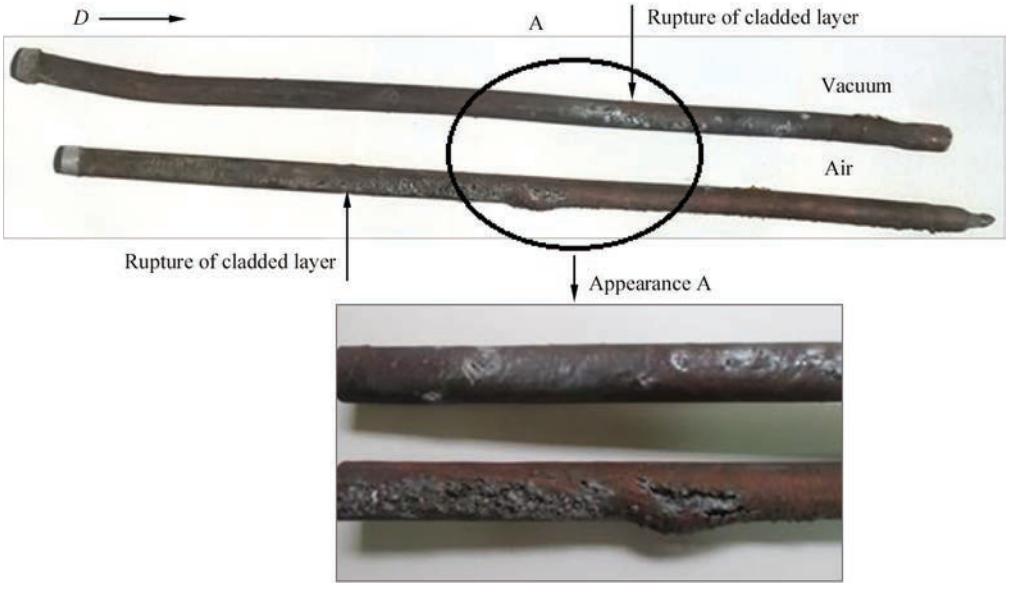

Figure 8. Coaxial workpiece after explosion welding. General appearance, above – with vacuum, below — without vacuum, detonation direction is from left to right. Appearance A — rupture of cladded layer, above — with vacuum, below — without vacuum

welding in air. This is explained by the fact that in welding on these conditions at a distance of 250 mm from the beginning of the process, a rupture of the cladded layer (Figure 8) occurs, which results in the leakage of a heated shock-compressed air. At the same time, on the workpiece, produced by vacuuming of the welded gap, the beginning of defects in the form of a rupture of the cladded layer is observed at a distance of about 500 mm from the closest to the point of initiation of the edge of the workpiece.

The dependence of the width of intermetallic layer on the conditions and the distance from the beginning of welding looks similar (Figure 7). It can be seen that at the initial area of the specimen the width of the intermetallic layer during welding in air at the conditions V_c = 2000 m/s is 35 μm, which is significantly (1.75 times) higher than during welding in vacuum of 20 μm. The width of the intermetallic layer during welding in air on the conditions V_c = 2600 m/s amounts to 45 μm, which can be compared with welding in vacuum — 40 μm. This indicates the fact that at the initial stage of welding, the main mechanism of transition of mechanical energy into heat energy is plastic deformation of the near-weld zone metal.

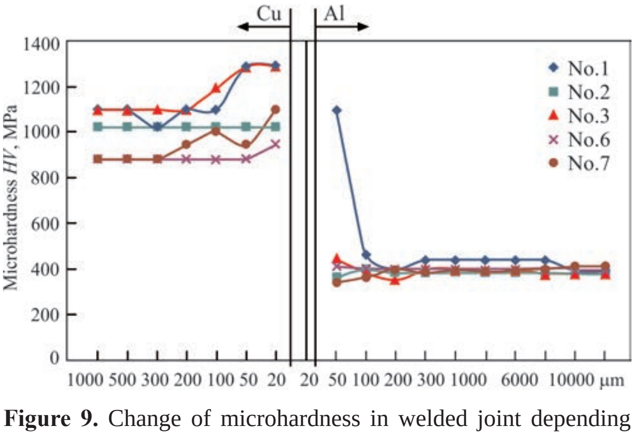

Figure 9. Change of microhardness in welded joint depending on welding conditions and presence of air in the gap (specimen numbers correspond to Figure 2)

In the middle area of the workpiece in welding on the conditions V_c = 2000 m/s, the width of intermetallic layer increases relative to the initial area during welding both in vacuum and in air. At this time the ratio of the width of the intermetallic layer produced in air to the width of the layer produced in vacuum, is up to 1.14 times reduced. At the end of the workpiece during welding in air on the conditions V_c = 2000 m/s a 1.25 times increase in the width of intermetallic layer is observed as compared to the middle area, and during welding in vacuum, an increase in the width is not observed.

Therefore, vacuuming of the welding gap in explosion welding of long-length coaxial joints allows reducing the width and volume of an intermetallic layer, but does not exclude the formation of intermetallics.

A smaller amount of intermetallics in vacuum welding indicates that the main energy input to the creation of intermetallics provides a channel effect, which is especially revealed in explosion welding of coaxial joints.

Studies of the microhardness of the welded joint zone of coaxial copper-aluminium workpieces (Figure 9), produced by explosion welding in vacuum and without it at different conditions (V_c = 2000 and V_c = 2600 m/s) showed that in the joint zone, the nature of microhardness distribution typical for explosion welding with the values of 946–1100 MPa is observed, which is by 10–15 % higher than the value of 860–940 MPa for a flat bimetal copper-aluminium [14].

A strengthening of the near-contact layers is observed, the microhardness of copper in explosion welding on the conditions V_c = 2000 m·s^{-1} in vacuum amounts to 1190 MPa, which is higher than the microhardness of the near-contact layers in welding on the same conditions in air by 150 MPa (specimens No.6 and No.3, respectively). The zone of maximum microhardness of copper (946–1100 MPa) reaches 0.05–0.15 mm. This is also a confirmation of the fact that the collision speed in vacuum welding exceeds the collision speed during welding in air.

The microhardness of aluminium in the near-contact zone is in the range of 336–413 MPa, which is by 5–12 % lower than the maximum microhardness of aluminium (400–460 MPa) for bimetal copper-aluminium produced by the two-dimensional circuit [14], while in the contact zone at a depth of 0.02–0.05 mm microhardness is lower than at a greater depth. This is probably associated with the fact that in explosion welding by a coaxial circuit a more intense heating of the surface layer occurs as compared to a parallel circuit and a thin layer of aluminium, which has a low melting point, is partially annealed and becomes softer.

Conclusions

1. It was experimentally established that in explosion welding of copper with aluminium according to the coaxial circuit with vacuuming of the welding gap, it is possible to produce a workpiece without cladding defects of up to 500 mm length with a diameter of 26 mm, and up to 200–250 mm with the same diameter in welding without vacuuming of the welding gap.

2. On the basis of metallographic examinations, it was established that vacuuming of the welding gap allows almost 1.4 times reduction in the width of intermetallic layer on average on the length on the conditions of V_c = 2000 m/s and in 1.2 times on V_c = = 2600 m/s and reducing the volume fraction of intermetallics by 1.1 times and 1.15 times in welding in the abovementioned conditions, respectively. This is explained by the fact that the main energy contribution to the formation of intermetallics provides a channel effect.

3. It was established that generation of vacuum (~ 20 kPa) in the gap during explosion welding of copper with aluminium, which were assembled coaxially, reduces the amount of intermetallics appearing after welding by 20 %.

1. Bryzgalin, A.G., Dobrushin, L.D., Shlensky, P.S. et al. (2015) Manufacture of coaxial copper-aluminium rods using explosion welding and drawing. *The Paton Welding J.*, **3–4**, 69–73.
2. Melikhov, V.P. (1979) About length of explosion welding stability of eccentrically located cylinders. In: *Explosion welding and cutting*. Ed. by V.M. Kudinov. Kiev, PWI, 25–28 [in Russian].
3. Tsemakhovich, B.D. (1987) Prospects of explosion welding in nuclear machine-building. In: *Proc. of 7th All-Union Meeting on Explosion Welding and Cutting (Kiev, 29–30 September, 1987)*, Kiev, PWI, 60–66 [in Russian].
4. Kovalevsky, V.N., Alekseev, Yu.G., Sagarda, E.V. (1985) *Cladding of thick-wall pipes by explosion energy.* In: *Application of explosion energy in welding engineering.* Ed. by V.M. Kudinov. Kiev, PWI, 103–108 [in Russian].
5. Kovalevsky, V.N., Alekseev, Yu.G., Senchenko, G.M. et al. (2001) *To the problem of theory of explosion welding of pipes.* In: *Welding and related technologies.* Minsk, Pepubl. Interdept. Transact., 37–39 [in Russian].
6. Atroshchenko, E.S., Rozen, A.E., Los, I.S. et al. (2000) Calculation of explosion welding parameters in throwing a cylindrical shell. In: *Explosion welding and properties of welded joints: Interuniv. Transact.* Ed. by V.I. Lysak, Volgograd, VolgGTU, 24–30 [in Russian].
7. Malakhov, A.Yu. (2019) *Explosion cladding of long-length cylindrical products by functional coatings*: Syn. of Thesis for Cand. of Techn. Sci. Degree. Chernogolovka [in Russian].
8. Deribas, A.A., Zakharenko, I.D. (1974) On surface effects in oblique collisions of metallic plates. *Fiz. Goreniya i Vzryva*, 10(**3**), 409–423 [in Russian].
9. Khansin, M., Andergo, K. (1962) *Structures of binary alloys.* Ed. by I.I. Novikova, I.L. Rolberg. Vol. 1. Moscow, Metallurgiya [in Russian].
10. Ishutkin, S.N., Kirko, V.I., Simonov, V.A. (1980) Study of thermal action of shock-compressed gas on surface of colliding plates. *Fiz. Goreniya i Vzryva*, **6**, 69–73 [in Russian].
11. Berdychenko, A.A., Zlobin, B.S., Pervukhin, L.B., Shtertser, A.A. (2003) On possible inflammation of particles ejected into the gap in explosion welding of titanium. *Ibid*., **2**, 128–136 [in Russian].
12. Pervukhin, L.B., Pervukhina, O.L., Denisov, I.V. et al. (2016) To problem about limit of size of sheets produced by explosion welding. *Izvestiya VolgGTU*, **10**, 76–86 [in Russian].
13. Dobrushin, L.D., Fadeenko, Yu.I., Illarionov, S.Yu., Shlensky, P.S. (2009) *Channel effect in explosion welding*, **11**, 16–17 [in Russian].
14. Trykov, Yu.P., Gurevich, L.M., Shmorgun, V. (2004) *Layered composites based on aluminium and its alloys.* Moscow, Metallurgizdat [in Russian].

Received 22.01.2021

https://doi.org/10.37434/tpwj2021.02.02

DEVELOPMENT OF BRAZING ALLOY, BRAZING TECHNOLOGIES AND CORRECTION OF CASTING SURFACE DEFECTS OF HEAT-RESISTANT NICKEL ALLOYS FOR SHIP GAS TURBINES

V.V. Kvasnytskyi[1], **M.V. Matviienko**[2], **H.P. Mialnitsa**[3], **I.H. Kvasnytska**[4] and **Ye.A. Buturlia**[5]
[1]National Technical University of Ukraine «Igor Sikorsky Kyiv Polytechnic Institute»
37 Peremohy Prosp., 03056, Kyiv, Ukraine. E-mail: kvas69@ukr.net
[2]Kherson branch Admiral Makarov National University of Shipbuilding
44 Ushakova Str., 73000, Kherson, Ukraine. E-mail: maksym.matvienko@nuos.edu.ua
[3]Gas Turbine Research and Production Complex «Zorya»–«Mashproekt»
42A Bogoyavlensky Prosp., 54000, Mykolaiv, Ukraine, Ukraine. E-mail: welding@nuos.edu.ua
[4]Physical and Technological Institute of Metals and Alloys of the NAS of Ukraine
34 Akademik Vernadsky Blvd, 03142, Kyiv, Ukraine. E-mail: kvasnytska@ptima.kiev.ua
[5]Admiral Makarov National University of Shipbuilding
9 Heroiv Ukrainy, 54000, Mykolaiv, Ukraine. E-mail: welding@nuos.edu.ua

The aim of the work was to develop brazing alloy and technology of brazing heat-resistant CM93-BI and CM96-BI nickel alloys, used in the production of new generation ship gas turbines. A prerequisite was to provide high-temperature strength of the brazed joints not lower than 80 % of the strength of the base metal. During the development of the brazing alloy, a two-stage procedure was used, where at the first (calculation) stage the required concentrations of alloying elements in the base of brazing alloy, noncompliance of γ- and γ′-phases structure parameters, critical temperatures, number of electron vacancies, physical and mechanical properties of alloys were determined. At the second (experimental) stage, the rational content of the number of depressant elements was determined. As a depressant, boron was chosen. It was established that when using a brazing alloy containing 1.0–1.2 wt.% of boron, the structure of the base metal and the weld are identical. After brazing and heat treatment, boride eutectics in the brazed joints were not revealed. It was established that within the determined limits boron does not reduce the resistance of brazed joints to high-temperature salt corrosion. The surface properties of the brazing alloy and its interaction with CM93-BI and CM96-BI alloys were studied. The developed SBM-4 brazing alloy showed high technological properties and allows raising the temperature of working gas in gas turbines. The developed technology of brazing CM93-BI and CM96-BI alloys provided the tensile strength σ_t at the level of the base metal. The long-term strength of the brazed joints at a temperature of 900 °C was equal to 314–321 MPa on the basis of 100 h, which amounts to 0.89–0.91 of a long-term strength of polycrystalline alloys. The technology of correction of blade defects by SBM-4 brazing alloy was developed. 12 Ref., 4 Figures.

Keywords: brazing alloy, heat-resistant nickel alloys, brazing technology, correction of casting defects, depressant elements, boron, gas turbines, blade

Ship and aircraft gas turbines operate on different fuels, so the chemical composition of heat-resistant alloys for ship and aircraft gas turbines (GT) is different, and the operating temperatures of aircraft turbines reach 1220 °C [1]. Global trends in the development of mechanical engineering indicate a widespread use of welding and related processes for manufacture of structures for different purposes [2]. The main method of joining heat-resistant nickel alloys is brazing [3]. Fusion welding of GT blades does not give positive results because of the hot crack formation of both during welding and heat treatment and leads to softening and destruction of directionally solidified and single-crystal structures [4].

The GT blades of ships are manufactured by precision vacuum casting, each one is produced separately. In the presence of surface defects, it allows correcting them by brazing. With the help of brazing, sign holes of the cooled blades for fixing inner rods are also closed. Taking into account the fact that the essence of brazing consists in reducing the melting point of the brazing alloy by using depressants, an important problem of braz-

B.B. V.V. Kvasnytskyi — https://orcid.org/0000-0002-7756-5179, M.V. Matviienko — https://orcid.org/0000-0002-1020-0415,
H.P. Mialnitsa — https://orcid.org/0000-0003-2144-4519, I.H. Kvasnytska — https://orcid.org/0000-0003-3790-2035,
Ye.A. Buturlia — https://orcid.org/0000-0003-2604-5664

ing is to increase the level of strength of brazed joints to the level close to the strength of the base metal. It is also necessary to provide the resistance of brazed joints against high-temperature salt corrosion (HSC) in the conditions of operation of offshore gas turbines. The most heat-loaded in GT are nozzle and working blades. Taking into account the difficult operating conditions of ship GT, turbines of a new generation were designed, new heat-resistant CM93-BI and CM96-BI nickel alloys (HNA) [5] were developed, which allow raising the operating temperature of the gas by 40–60 °C. To braze new HNA it is necessary to create new brazing alloys with higher melting and brazing temperatures, which provide the formation of joints with a high heat resistance and long-term strength. Solving these problems is very important for the development of ship gas turbine construction. The relevance of the development grows significantly during brazing of new generation materials, which provide higher operating temperatures and service life, in particular, CM93-BI and CM96-BI alloys for ship GT.

Analysis of scientific publications on brazing alloys and brazing technologies of HNA shows that almost all of them are devoted to the development of brazing alloys for HNA of aircraft turbines, for example, ZhS32 [4], ZhS36 [6, 7], ZhS6U [8]. In [8] VPr36 brazing alloy was used, and to reduce the temperature of brazing, NS12 brazing alloy based on the Ni-12Si system was added.

To braze the mentioned alloys, different brazing alloys were used, for example, VPr24, VPr27, VPr36, VPr37, VPr44 (Russia) [9], VN-2, VN-3 (PRC) [10]. VPr36, VPr37 and VPr44 brazing alloys are recommended by the document PO 13-2011 of BIAM for using in the experimental production of aircraft industry for the purpose of brazing heat-resistant alloys, in particular, also on the base of intermetallic Ni_3Al.

In [9], to braze VKNA-4U alloy based on Ni_3Al with EP975 alloy, complexly-alloyed VPr24, VPr27, VPr47, VPr48 and VPr36 brazing alloys were used to join the disc to the blades. The results presented in the work show that all brazing alloys except of VPr36 formed eutectic interlayers, which significantly reduce the strength of brazed joints.

In [10], to braze IS10 alloy at a temperature of 1250–1270 °C as a depressant, brazing alloy with boron was used. In [4, 9] for brazing of ZhS36 and ZhS32 alloys, VPr37 and VPr44 brazing alloys with the brazing temperature higher than 1260 °C were investigated, which are unacceptable for CM93-BI and CM96-BI alloys.

Recently, in [11] brazing alloys were developed, in which as a depressant Zr is used. According to the results of brazing, two brazing alloys with concentrations of 1.0–2.0 wt.% of Zr of the system Ni–Cr–Ti–Nb–Al–(Me)–Zr for brazing of intermetallic alloys at a temperature of about 1250 °C were selected. Brazing alloys using palladium are also being developed, which are still at the stage of studying. In the studied works the procedure of development of brazing alloys is not reflected. Analysis of the literature also showed that no publications on the development of brazing alloys for ship gas turbines were revealed.

The aim of the project is to develop brazing alloy and brazing technology for heat-resistant CM93-BI and CM96-BI nickel alloys for manufacture of new generation ship GT with a high temperature strength of brazed joints not lower than 80 % of the base metal. To achieve this aim it is necessary to solve the following problems:

- to propose a procedure of brazing alloy development using computer programs that determine the distribution of alloying elements in phases, structure stability and strengthening of HNA;
- to choose a rational alloying of the base of brazing alloy and effective depressants;
- to determine the brazing temperature and other important characteristics of brazing alloy;
- to investigate the surface properties of brazing alloy and its interaction with CM93-BI and CM96-BI alloys;
- to determine the structure, chemical composition and properties of brazed joints;
- to develop the technology of brazing of CM93-BI and CM96-BI alloys and correction of surface defects of castings with HNA.

To determine the composition of brazing alloy, it was proposed to use a procedure consisting of two stages [12]. At the first stage, the chemical composition of the base of brazing alloy is determined, taking into account the peculiarities of operating conditions of the blades of ship GT and the achievements of metals science of HNA. At this stage, computer programs are used available at developers and manufacturers of HNA. It was proposed to additionally introduce chemical elements into the brazing alloy base, which are more effective in strengthening it.

Subsequently, applying calculations by means of computer programs, the rational limits of the content of alloying elements in the base of brazing alloy were determined, taking into account their mutual influence on the number and structure of reinforcing phases, distribution of elements by phases, noncompliance of parameters of crystal structure of γ- and γ′-phases, number of electron vacancies, critical temperatures, physical and mechanical properties of alloys. One of the main criteria in choosing rational alloying limits is minimizing the susceptibility of alloys to formation of brittle topologically close-packed (TCP) phases.

As the base of the filler mertal, CM93-BI alloy was selected, which is alloyed by Re in the amount of 2.4–2.8 wt.% and Ta — 3.3–3.6 wt.%, as far as it is known that rhenium efficiently strengthens HNA, and tantalum improves thermal stability of γ′-phase.

According to the results of calculations, an excessive alloying of alloys with the elements, that increase the susceptibility to the formation of TCP phases, in particular, Cr, Mo, W, Re, was established. Since W has the largest number of electron vacancies, then in the base of the brazing alloy its content is reduced to 2.0–3.0 wt.%. In order to increase the resistance of the alloy to a high-temperature corrosion, the concentration of Cr was increased to 14.5 wt.%. Into the alloy up to 6.2 wt.% of Ti was introduced in order to reduce the liquidus and solidus temperatures and form a strengthening γ′-phase. Other elements have the concentrations, close to the initial CM93-BI alloy. The average content of the elements in the base brazing alloy amounts to (wt.%): 13.0 Cr; 7.0 Co; 4.0 Al; 4.5 Ta; 3.75 Re; 2.5 W; 1.5 Mo; 5.45 Ti; 0.25 Hf; 0.575 Zr 0.4 Nb; 0.07 C; Ni is the rest.

Having no alternative, as a depressant, boron was chosen. The amount of boron can be determined only experimentally by melting alloys with different concentrations of boron. The first brazing alloy was melted with a concentration of boron being 0.75 wt.%, but it spread poorly even at a temperature of 1230 °C.

To reduce the number of experimental melts, an alloy of five elements was melted, which was designated as 4D with the following chemical composition: 14 Cr; 9.5 Co; 2.5 Al; 2.4 V, the rest is nickel. 4D alloy was added to the first melt of SBM-4 brazing alloy in the amount of 10, 20 and 30 %, which provided a gradual change in the concentration of boron. With the introduction of 10–30 % of 4D alloy, the concentration of boron increases from 0.915 to 1.245 %.

To reduce the number of experimental studies and build a regression model, the method of experimental planning was also used. The coefficients of the model were checked through Student's criterion (*t*-criterion), necessary to determine the significance of the coefficients of the regression equation. For this purpose, a hypothesis was put forward, that a parameter or statistical characteristic of the equation coefficient is slightly different from zero. At the same time, an alternative hypothesis was put forward that a parameter or statistical characteristic is significantly different from zero. If the main hypothesis is incorrect, then the alternative is taken as the truth.

The adequacy of the mathematical model was verified through F-test, or by Fisher's test. According to Fisher's test, a null hypothesis was put forward, the fulfillment of which determines that the calculated mathematical expectation is equal to the known (experimental) expectation. To calculate the F-test, the dispersions of reproducibility and adequacy are used.

Based on the results of investigations, the concentration of boron in SBM-4 brazing alloy was taken equal to 1.0–1.2 wt.%. Based on the average values of boron concentration and the content of alloying elements of the brazing alloy base, SBM-4 brazing alloy for industrial application was melted. The content of chemical elements in SBM-4 brazing alloy is the following: wt.%: 12.5–14.5 Cr; 6.5–7.5 Co; 3.0–5.0 Al; 3.0–6.0 Ta; 3.0–4.5 Re; 2.0–3.0 W; 1.0–2.0 Mo; 4.7–6.2 Ti; 0.2–0.3 Hf; 0.45–0.7 Zr; 0.3–0.5 Nb; 1.0–1.2 B; 0.04–0.10 C; Ni is the rest.

When using the brazing alloy containing 1.0–1.2 wt.% of boron, the structure of the base metal and the weld is identical. According to the results of experimental studies of the interaction of brazing alloy with the base metal, it was found that at a brazing temperature of 1210–1235 °C, the brazing alloy has satisfactory technological properties.

After brazing and heat treatment, in the joints boride eutectics were not revealed.

Alloying of Ta allows increasing the resistance of alloys to oxidation and high-temperature corrosion. While studying embers, it was found that in addition to the protective oxides NiO, CoO and Cr_2O_3, there is also Ta_2O_3 oxide, which does not interact with sodium sulfate and forms a dense protective film that reduces the rate of high-temperature corrosion.

It is known that CM93-BI and CM96-BI alloys have a high resistance to HSC, so it was important to determine the effect of boron in SBM-4 brazing alloy on resistance to it. For this purpose, CM93-BI and CM96-BI alloys with the concentrations of boron being 1.0, 1.2, 1.5, 2.0 and 2.5 wt.% were melted. The tests were carried out at a temperature of 900 °C during 20 h in a melt of salts of 25 % NaCl + 75 % Na_2SO_4. It was found that at a boron concentration of 1.2 %, the resistance of alloys to HSC did not decrease. After melting of SBM-4 brazing alloy, cylindrical specimens were manufactured and investigations on their resistance to HSC were carried out.

Investigations of the structure and chemical composition of brazed joints were carried out on the specimens that were brazed in the same batch with the specimens for mechanical tests or on the specimens after mechanical tests. For mechanical tests, the specimens were brazed at a temperature of 1210–1215 °C with up to 15 min holding and subsequent cooling to 1070 °C and holding for 60 min.

CM93-BI and CM96-BI alloys are used for manufacture of blades with polycrystalline and directional structures. Since producing of several specimens with a directional structure requires special preparation, in the work polycrystalline specimens were used. The tensile strength σ_t of brazed joints was at the level of the base metal. Long-term strength for the joints of polycrystalline CM93-BI and CM96-BI alloys amounts to 0.91 and 0.89, respectively.

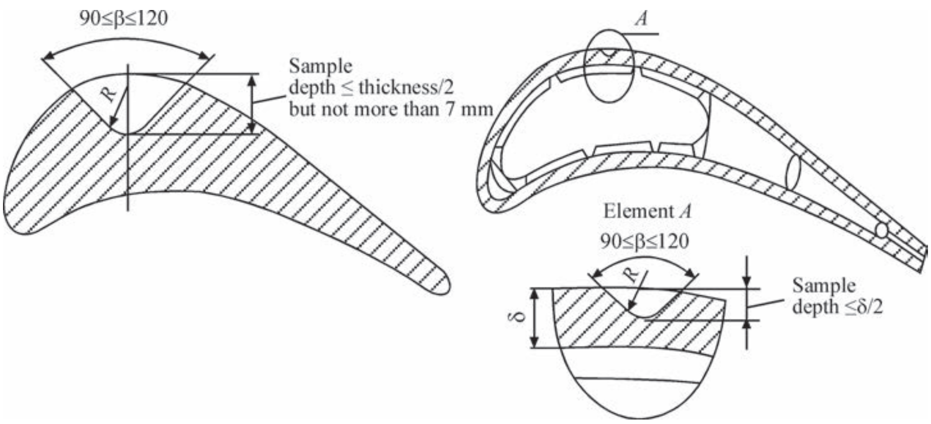

Figure 1. Development of surface defect such as cavity of the blade with a polycrystalline structure of CM93-BI alloy

Defects of the blades can be detected at different stages of their manufacture and operation. The most predictable are defects in castings of the blades. Despite a constant improvement in refractory mixtures for manufacture of ceramic molds, rods, crucibles, filters and casting technology, the yield of suitable blades does not reach 100 %.

Most of the casting defects are superficial. The most widespread are defects in the form of slag inclusions, «beads» and other contaminants of up to 3.0 mm size, have much less discontinuities, underfills and cracks. According to the technological instructions (TI) of NPKG «Zorya»–«Mashproekt», all defects are divided into those, for which corrections are not allowed and surface defects, the correction of which is carried out depending on location area on the blade, sizes of defects and distance between them. On the blades, areas and criteria are marked where correction of defects is allowed. For example, on inlet and outlet edges of the blades correction of defects is not allowed. The surfaces of power protrusions of the blades, radii of the blade feather transitions to the root, etc. are not corrected. Other defects are limited by depth, quantity, size, category of structures. In the course of brazing development, different supplements are introduced into technological documents (2019) and new instructions are agreed.

Depending on the size of a defect, its correction is performed with or without a filler. Small defects (determined according to TI) are corrected by SBM-4 brazing alloy without filler, such defects as cavities are prepared as shown in Figure 1 for blades with polycrystalline structure of CM93-BI alloy.

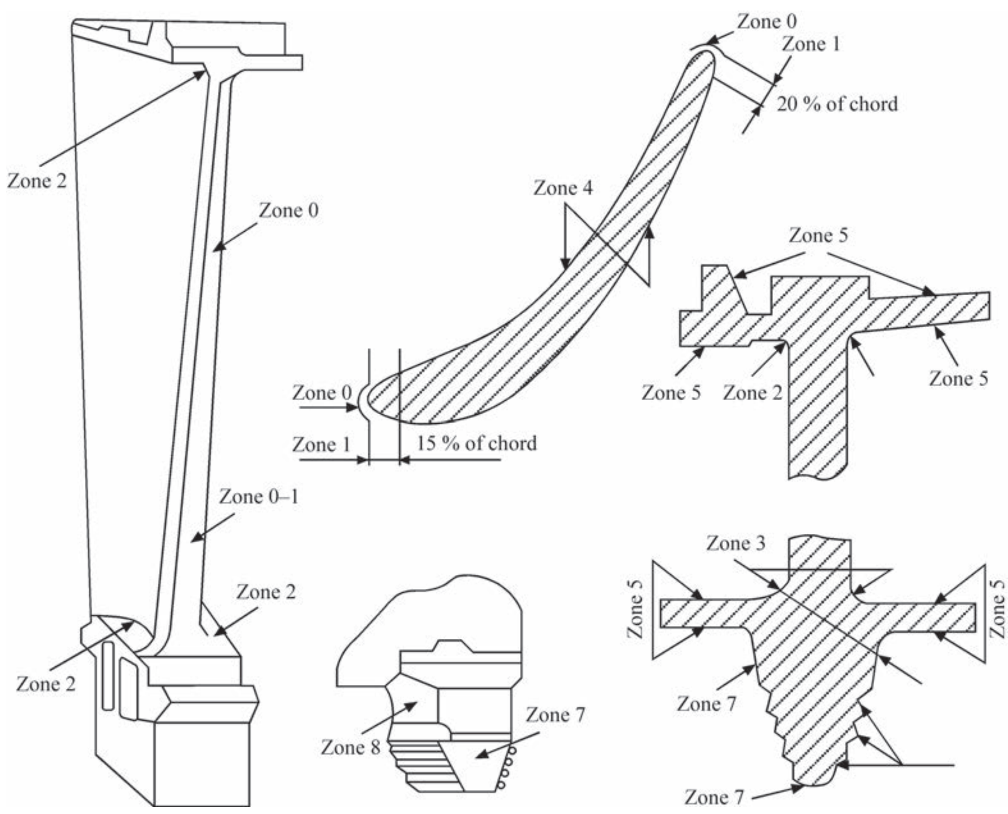

Figure 2. Scheme of working uncooled blade with a single-crystal structure of CM96-BI alloy

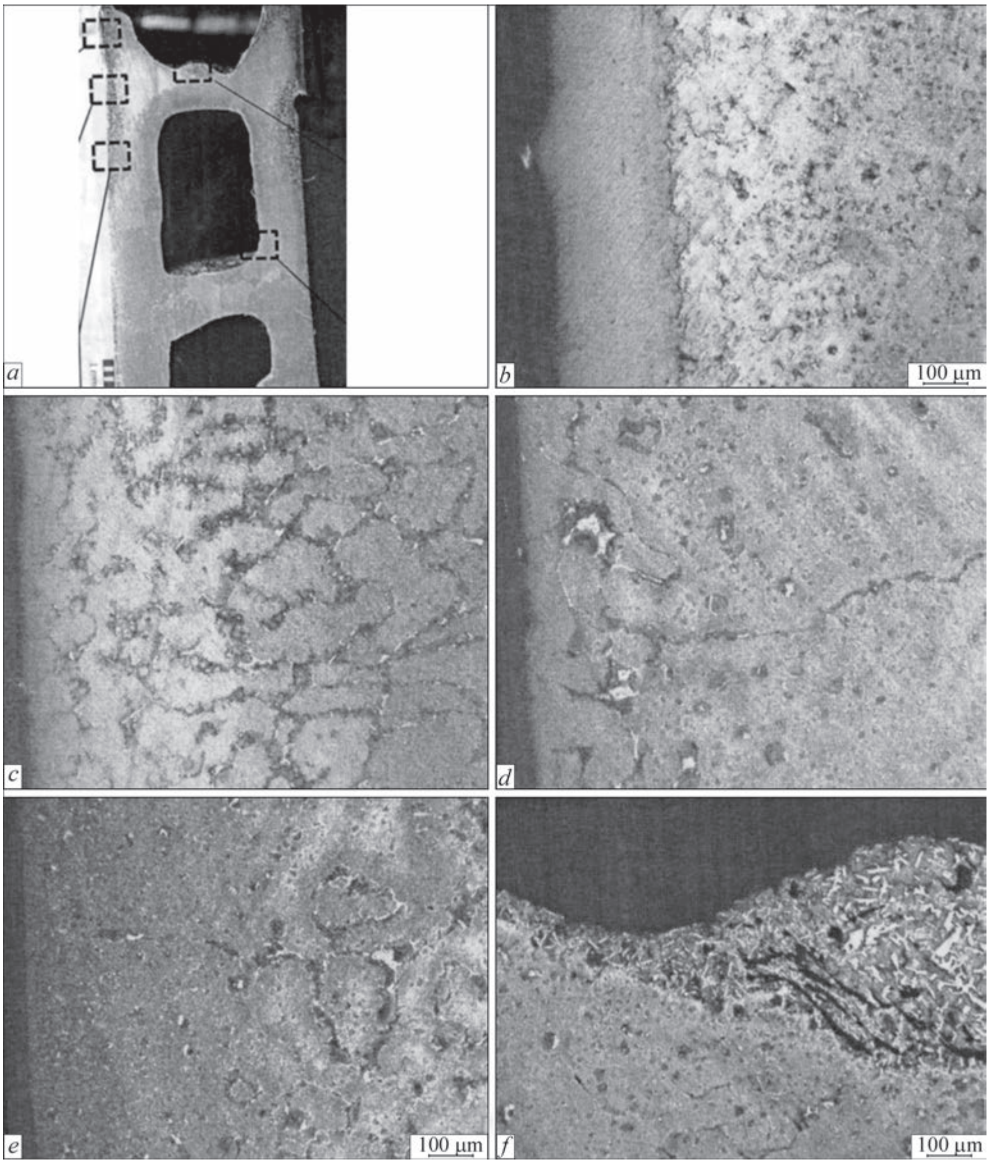

Figure 3. Macrosection of the blade (*a*), microstructure with corrected surface defects (*b*, *c*, *d*), base metal (*e*) and brazed sign hole (*f*)

Correction of casting defects begins at their detection after cleaning and bench work (inspection for defects). Before correction of defects, the blades should undergo the entire step cycle of heat treatment, including homogenization at a temperature of 1180 °C in accordance with the Technological Process. The sizes of defects to be corrected after preparation should meet the requirements of standard documents. The areas to be corrected should be prepared until a complete removal of a defect at an angle of $90° \leq \beta \leq 120°$ in accordance with Figure 1. The surface of the blade around a defect should be cleaned of oxides at a distance of less than 5 mm.

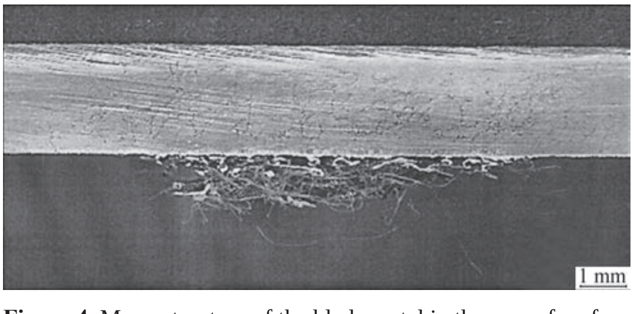

Figure 4. Macrostructure of the blade metal in the area of surface defect correction with a protective coating layer

Figure 2 shows a sketch of a working uncooled blade with a single-crystal structure of CM96-BI alloy and zones of defect location, in which the sizes of defects of GT blades acceptable for correction are regulated by the instructions of the enterprises. The location and sizes of defects on the blades acceptable for correction are regulated by the instructions of the enterprises.

Figure 3 shows the macrosection of the blade of CM93-BI alloy and the microstructure of the metal with corrected surface defects and remelted sign hole. The macrosection in the area of a surface defect correction on the «trough» of the blade with the applied protective coating is shown in Figure 4.

Before applying the correction powder, the surface of the defect should be degreased with alcohol or wiped with a lilac cloth soaked in acetone.

As a filler, the powder of SM88U-BI alloy of centralized production by Ukrspetsstal or high-temperature SBM-3 brazing alloy, developed at NUK and NVKG Zorya-Mashproekt are used. Filler and SBM-4 brazing alloy represent a mixture in a ratio of 1: 1. The powder mixture is fixed on the surface of the blade with a 5 % solution of BMK-5 resin in acetone. The amount of composite powder should be greater than the volume of the prepared defect by 40–50 %. Correction of defects is performed according to the same parameters of the modes as brazing.

SBM-4 brazing alloy fills the gaps well and does not affect the structure of the base metal. Cracks or microcracks during the correction of defects as a result of using brazing alloy are also not observed.

It should be noted that for the current generation of ship turbines for correction of surface defects, VPr11-40N brazing alloy with a melting point of 1020 °C and NS12 with a melting point of about 1150 °C are used, which leads to melting followed by destruction of the protective coating. CM93-BI and CM96-BI alloys allow increasing the brazing temperature to 1230 °C, using SBM-4 brazing alloy, and increasing the life and operating temperature of the gas in the turbine.

Conclusions

1. A two-stage procedure of brazing alloy development was used, according to which at the first (calculation) stage the rational limits of alloying elements in the base of brazing alloy, noncompliance of parameters of γ- and γ′-phases structure, critical temperatures and number of electron vacancies were determined. One of the most important criteria for rational content of alloying elements is to minimize the susceptibility to the formation of TCP-phases, in particular, brittle σ-phase. At the second — experimental stage, rational content of depressant elements is determined.

2. Duirng industrial research tests, SBM-4 brazing alloy showed high technological properties and it allows increasing the temperature of the working gas in the turbine.

3. Brazing and melting temperature of SBM-4 brazing alloy excludes its interaction with the protective coating of the Co–Cr–Al–Y and Y_2O_3 systems during its deposition and heat treatment.

4. For SBM-4 brazing alloy, Temporary technical conditions UKFA 360.107.002-VTU and Technological instruction on correction of surface defects applying the method of brazing in vacuum UKFA 387.341.002-TI were developed.

5. Brazing of polycrystalline blades of CM93-BI alloy is carried out at a temperature of 1200–1215 °C, and from CM96-BI alloy with single-crystal or directionally crystallized structures at a temperature of 1220–1230 °C during 15 ± 5 min. After brazing, the blades are cooled to a temperature of 1070 °C and kept for 60 minutes, then their cooling in vacuum is continued to a temperature of 200 °C.

6. To correct defects, as a filler the powder of CM88U-BI alloy can be used, of centralized production by Ukrspetsstal or high-temperature SBM-3 brazing alloy, developed at NUK and NVKG «Zorya»–«Mashproekt». Filler and SBM-4 brazing alloy represent a mixture in a ratio of 1: 1. The powder mixture is fixed on the surface of the blade with a 5 % solution of BMK-5 resin in acetone. The amount of composite powder should be greater than the volume of the prepared defect by 40–50 %. A defect correction is performed according to the same parameters of the modes as brazing.

1. Kablov, E.N. (2012) Strategic directions for the development of materials and technologies for their processing for the period up to 2030. *Aviats. Materialy i Tekhnologii*, **5**, 24–30 [in Russian].
2. Kryvov G.O., Zorykin K.O. (2012) *Production of welded structures: Manual for students of higher educational instit.*, Kyiv, KVITs [in Ukrainian].
3. Yermolaiev, H.V., Kvasnytskyi V.V., Kvasnytskyi, V.F. et al. (2015) *Brazing of materials: Manual.* Ed. by V.F. Khorunov, V.F. Kvasnytskyi. Mykolaiv, NUK [in Ukrainian].
4. Lukin, V.I., Rylnikov, V.S., Afanasiev-Khodykin, A.N. (2012) Features of brazing of single-crystal castings from ZhS32 alloy. *Svarochn. Proizvodstvo*, **5**, 24–30 [in Russian].
5. Mialnytsia, H.P., Maksiuta, I.I., Kvasnytska, Yu.H., Mykhnian, O.V. (2013) Selection of an alloying complex for a new corrosion-resistant alloy of GTE blades. *Metaloznavstvo ta Obrobka Metaliv*, **2**, 29–34 [in Ukrainian].
6. Lukin, V.I., Rylnikov, V.S., Afanasiev-Khodykin, A.N. (2010) Peculiarities of producing of the brazed joints of the alloy ZhS36. *Tekhnologiya Mashinostroeniya*, **5**, 21–25 [in Russian].
7. Afanasiev-Khodykin, A.N., Lukin, V.I., Rylnikov, V.S. (2010) Technology for producing permanent joints from ZhS36 alloy. *Svarochn. Proizvodstvo*, **7**, 27–31 [in Russian].
8. Malashenko, I.S., Mazurak, V.E., Kushnareva, T.N. et al. (2014) Vacuum brazing of cast nickel alloy ZhS6U with composite brazing fillers based on VPr-36 (Pt 1). *Sovrem. Elektrometallurgiya*, **4**, 26–42 [in Russian].
9. Lukin, V.I., Rylnikov, B.C., Afanasiev-Khodykin, A.N., Timofeeva, O.B. (2013) Features of diffusion brazing technology of EP975 heat-resistant alloy and VKNA-4U casting monocrystalline intermetallic alloy as applied to the «Blisk» design. *Svarochn. Proizvodstvo*, **7**, 19–25 [in Russian].
10. Yue, X., Liu, F., Chen, H., Wan, D., Qin, H. (2018) *Effect of bonding temperature on microstructure evolution during TLP bonding of a Ni_3Al based Superalloy IC10*. MATEC Web of Conferences, 206(**11**), 03004.
11. Maksymova, S.V. (2014) Brazing filler metal without boron and silicon for brazing heat-resistant nickel alloy. *The Paton Welding J.*, **8**, 15–21 [in Russian].
12. Kvasnytskyi, V., Korzhyk, V., Kvasnytskyi, V. et al. (2020) Designing brazing filler metal for heat-resistant alloys based on Ni_3Al intermetallide. *Eastern-Europ. J. of Enterprise Technologies*, 6, 108(**12**), 6–19.

Received 26.10.2021

https://doi.org/10.37434/tpwj2021.02.03

NEW ALGORITHMS OF HIGH-FREQUENCY WELDING OF BIOLOGICAL TISSUES*

G.S. Marynskyi[1], **K.G. Lopatkina**[1], **O.V. Chernets**[1], **S.E. Podpryatov**[1,2], **V.A. Tkachenko**[1], **I.O. Belousov**[2] and **V.A. Vasylchenko**[1]

[1]E.O. Paton Electric Welding Institute of the NAS of Ukraine
11 Kazymyr Malevych Str., 03150, Kyiv, Ukraine. E-mail: office@paton.kiev.ua
[2]Kyiv City Clinical Hospital No.1. 121 Kharkiv Highway, 02091, Kyiv. E-mail: KCRZ@ukr.net

Studies of the influence of new algorithms for welding biological tissues on the temperature parameters of the process in the weld zone and the biophysical and structural characteristics of the tissues being welded using the advanced control system of EKVZ-300 series apparatuses have been carried out. The effect of new experimental algorithms for high-frequency welding of biological tissues on the temperature parameters of the process and the characteristics of tissues of various types in the seam area was studied. 9 Ref., 6 Figures.

Keywords: high-frequency welding, biological tissues, EKVZ-300 «PATONMED» apparatus, welding algorithms, process temperature values, structural and biophysical changes in tissues, research complex

Beginning from 2002, the technology of high-frequency (HF) welding of biological tissues using the apparatuses developed at PWI has been extensively used in surgical practice in medical establishments of Ukraine. This technology offers significant advantages, compared to other processes during performance of even the most complicated operations [1–5].

At the same time, continuous improvement of the available and development of new algorithms of the process and appropriate equipment for their realization are required for further development, expanding the application areas and improvement of the effectiveness of high-frequency technology application in the surgical practice. In this connection, performance of integrated studies of structural and biophysical characteristics of the seam zone, as well as temperature values of the process of joining and treatment of biological tissues under the impact of high-frequency current supplied by different algorithms, is certainly timely.

Figure 1. PWI research complex

The objective of this work is studying the influence of new experimental algorithms of HF welding of biological tissues on temperature values of the process, change of tissue characteristics in the seam zone, as well as documenting and analysis of the advantages of application of the developed algorithms, compared to those currently used.

The objects of study were removed pig organs, namely small and large intestine, stomach, bronchi, etc.

Experiments were conducted in an all-purpose research complex (Figure 1) [6–8], which consisted of:

- upgraded apparatuses of EKVZ-300 type with enhanced technological capabilities — special control system and software, ensuring realization of both standard welding algorithms, and new ones, making a special kind of energy impact on the object of study;
- specialized research stand, fitted with different basic and experimental electrodes (Figure 2);
- working bipolar tools and their mockups;
- measuring and recording equipment.

*The following persons participated in the work: Yu.Z. Buryak[1], V.K. Serdyuk[1], S.S. Podpryatov[2], E.E. Matsas[1], N.A. Chvertko[1], V.O. Bysko[1], S.D. Grabovskyi[1].

G.S. Marynskyi — https://orcid.org/0000-0003-0753-0154, K.G. Lopatkina — https://orcid.org/0000-0002-7604-6174,
O.V. Chernets — https://orcid.org/0000-0001-8537-2302, V.A. Tkachenko — https://orcid.org/0000-0003-2983-778X,
S.E. Podpryatov — https://orcid.org/0000-0003-1350-7532, I.O. Belousov — https://orcid.org/0000-0003-1624-7019

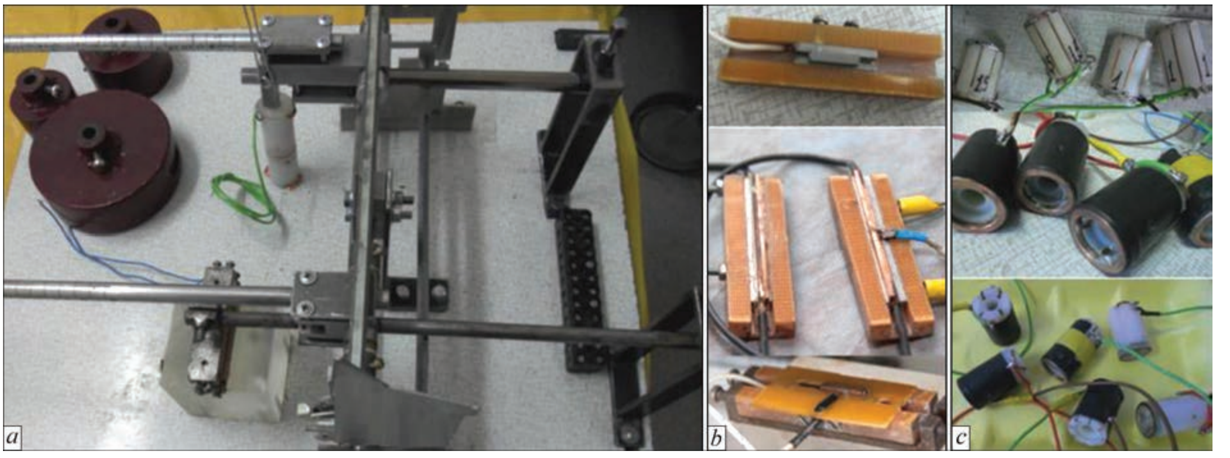

Figure 2. Specialized research stand (*a*), linear (*b*) and ring (*c*) electrodes

This complex, which is being continuously upgraded and improved, enables conducting extensive research of the process, in particular studying the impact of the following characteristics on its temperature values, biophysical and structural properties of different biological tissues in the seam zone:

- different welding algorithms;
- specific pressure of electrodes on the tissues being welded (in the range from 0 up to 4 N/mm^2);
- diverse tool designs with electrodes of different geometry (electrode area in the range from 2.0 to 270 mm^2).

During this series of experiments both the main electric and mechanical (specific pressure, etc.) characteristics of the process, and tissue temperatures directly in the seam zone, were recorded. Temperature measurement was performed by insulated thermocouples that were mounted into the electrode body and were in direct contact with the material being welded. At the same time, temperature was controlled by a contactless method with a thermovision camera.

Studies were conducted using both defined in previous work and new variants of the algorithms that should provide sound welded joints at shortening of the extent of the HAZ, lowering of process temperature, absence of charring in the seam zone and HAZ and absence of tissue «sticking» to the electrodes [9].

When testing the welding algorithms for evaluation of the joint quality and studying the biophysical and structural characteristics of the tissues, visual estimation, mechanical and hydraulic testing, as well as histological studies were performed. The results of experimental studies performed on removed small intestine and bronchi of a pig are partially presented below.

Testing of new welding algorithms was performed at linear welding of small intestine of a pig (0.6–0.8 mm wall thickness, 25–28 mm diameter) in an upgraded stand by an experimental bipolar clamp with electrodes of 45 mm^2 area; interelectrode gap of 0.05 mm, and specific pressure between the electrodes of 2.6 N/mm^2.

Given below are the results obtained when studying the impact of the developed new welding algorithms, according to which the set voltage was supplied as modulated pulses of a set duration, equal to 0.1 and 1.0 s. Here, the value of voltage and total duration of its feeding remained unchanged in both the cases.

During testing of both the variants of the algorithms a linear welded joint of small intestine formed between the bipolar electrodes without evolution of vapour or fumes, without «sticking» of tissues contacting the electrodes or of the tissues in the seam zone. By visual estimation and results of mechanical testing of the welded joints of studied tissues of small intestine, when using the above algorithms a sound, strong, elastic, continuous and sealed welded joint was produced. The tissue was of the same colour against the light over the entire area of the seam. There was no deformation, charring or spasm of the tissues in the seam zone and HAZ. The formed seam did not have any perforations, and consisted of a continuous homogeneous tissue.

The process of welding the experimental samples of small intestine using the above algorithms took place at temperature which was not higher than 60–70 °C under the experimental conditions and was significantly lower than that at application of earlier used algorithms.

Figure 3 gives the temperature values of the process at testing new experimental algorithms of small intestine welding (No.1 — duration of pulses and pauses of 0.1 s; No.2 — duration of pulses and pauses of 1.0 s) and standard (traditional) algorithms (No.3 —pulse duration of 1.0 s, pause duration of 0.2 s; No.4 — pulse and pause duration of 0.2 s).

It should be noted that increase of pulse length from 0.1 s (algorithm No.1) to 1.0 s (algorithm No.2)

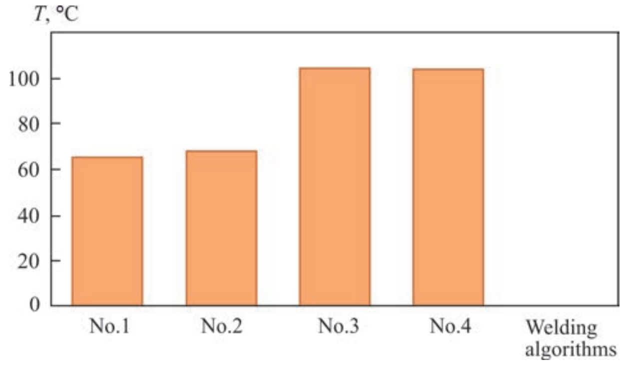

Figure 3. Average temperature values of the process of small intestine welding under the conditions of application of new experimental (Nos 1, 2) and traditional (Nos 3, 4) algorithms for small intestine welding

in experimental algorithms, at other conditions being equal, practically did not influence the temperature values under the experimental conditions.

Similar results were obtained at welding small intestine of a pig (wall thickness of 0.8–0.9 mm), using experimental algorithms with a standard bipolar clamp (electrode area of 70 mm^2 without interelectrode gap) at an essentially smaller (0.46 N/mm^2) specific pressure between the electrodes.

In this case a standard bipolar clamp, additionally fitted with an insulated thermocouple that was in direct contact with the tissue being welded, was used for experiments. Specified pressure was ensured using a system with a preset force.

Application of experimental algorithms, compared to standard ones, also allowed a significant lowering of the process temperature values. Temperature in the seam zone was not higher than 70 °C.

Based on visual estimate and mechanical testing results, against the background of lowering of temperature parameters of the process, the proposed algorithms provided sound and strong joints with improved biophysical characteristics of the tissue in the seam zone and reduced HAZ (Figure 4).

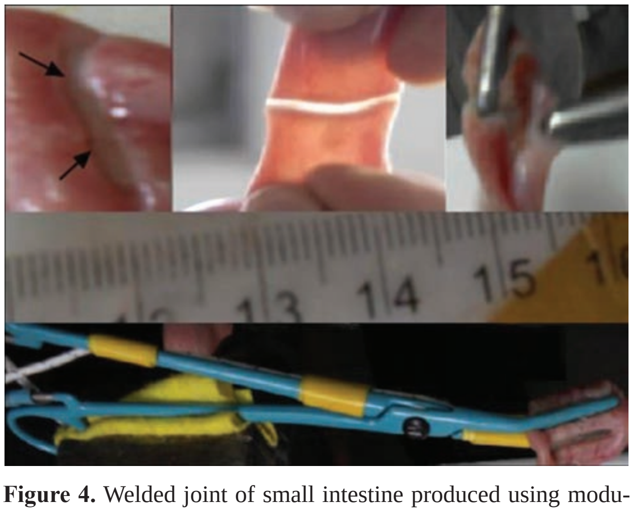

Figure 4. Welded joint of small intestine produced using modulated pulses. Welding was performed with standard bipolar clamp (electrode area of 70 mm^2, specific pressure between the electrodes of 0.46 N/mm^2, without electrode gap), additionally fitted with a thermocouple

Other experimental material used to conduct experimental work, were the removed bronchi of a pig (wall thickness of 0.5–0.7 mm, diameter of 6.0–6.5 mm). The area of stand electrodes and the clamp was 45 mm^2, interelectrode gap was 0.05 mm, and specific pressure between the electrodes was 2.6 N/mm^2.

The proposed algorithms allowed an essential shortening of the total time of HF current action on the tissue, obtaining sealed closure of the bronchi and lowering the temperature values of the process. Application of the new welding algorithms of the total duration from 0.1 to 2.0 s yielded better results of the process temperature values, compared with the results, obtained at application of earlier defined algorithms of a much greater duration (6–12 s). Temperature at the moment of bronchi closing at testing new algorithms did not exceed 40–70 °C that is almost two times smaller (Figure 5) than that recorded at application of the majority of earlier defined algorithms for bronchi welding.

Figure 5 shows the temperature values of the process with application of new algorithms of welding bronchi of the total duration of 0.1 s (No.1), 0.5 s (No.2), 0.8 s (No.3) and an algorithm of total duration of 8 s, that is currently used (No.4).

The most sound bronchi closure under the conditions of conducting this experimental stage, took place, by visual estimate, at process temperature of 47–65 °C with the total duration of impact of high-frequency current on the tissue of 0.5–1.5 s in the seam zone. No charring, spasm or «sticking» of the tissue to the electrodes under experimental conditions were observed. HAZ dimensions were within 0–0.1 mm. Selected samples with sound closure of the bronchi were used to conduct tightness testing (Figure 6, *a*) and mechanical and hydraulic tests (Figure 6, *b*).

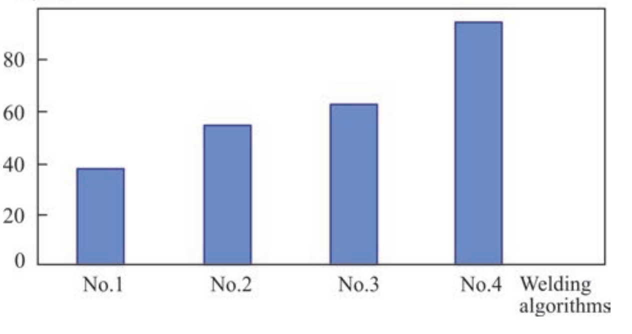

Figure 5. Temperature values of the process of bronchi closing under the conditions of application of new experimental (Nos 1–3) and currently available (No.4) welding algorithms

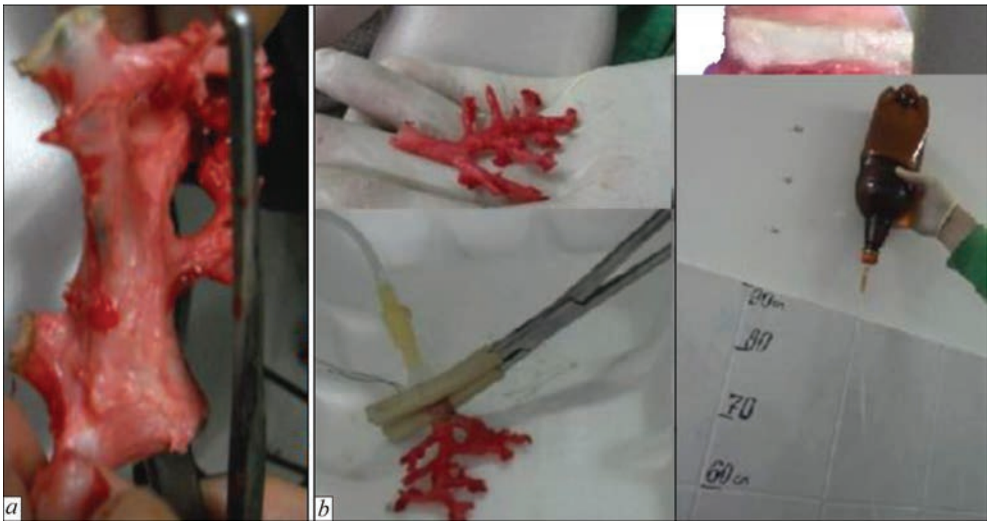

Figure 6. Testing of bronchi welds produced at application of special welding algorithms: *a* — vascular patency test; *b* — hydraulic testing

Visually determined sound closure of the bronchi obtained under the above-mentioned conditions, withstood 1000–1500 mm H_2O at hydraulic testing.

Results of studying the impact of new welding algorithms on the bronchi tissue demonstrated the good prospects for their application and the need to carry on the experimental work.

Conclusions

1. Results of the conducted experimental work showed that application of new experimental algorithms for welding biological tissues offers significant advantages, compared to earlier defined welding algorithms. These are producing sound seams at lower temperature values of the process and improvement of biophysical characteristics of the tissues in the seam zone and HAZ.

2. Based on visual estimate, mechanical and hydraulic testing of samples of different tissue type, it was established that new ingenious joining algorithms which can be realized at application of the developed control system of the apparatuses, allow producing sound joints of biological tissues at minimum specific pressure of electrodes, and ensure minimum temperature of heating of the tissues being joined and minimum length of the HAZ, that in its turn points to the good prospects for application of the proposed algorithms and continuation of experimental studies.

1. (2009) *Tissue-saving high-frequency electric welding surgery*: Atlas. Ed. by B.E. Paton, O.N. Ivanova. Kiev, PWI, IEW [in Russian].
2. Paton, B.E., Krivtsun, I.V., Marinsky, G.S. et al. (2013) Welding, cutting and heat treatment of live tissues. *The Paton Welding J.*, **10–11**, 135–146.
3. Podpryatov, S.E., Gichka, S.G., Podpryatov, S.S. et al (2012) Structure of electric weld as a basis of the new development of surgery. In: *Proc. of 7th Int. Sci.-Pract. Conf. on Welding and Heat Treatment of Live Tissues. Theory. Practice. Prospects (Kiev, 30 November 2012).* Ed. by G.S. Marinsky. Kiev, PWI.
4. (2018) In: *Proc. of 13th Int. Sci.-Pract. Conf. on Welding and Heat Treatment of Live Tissues. Theory. Practice. Prospects (Kiev, 30 November–1 December 2018).* Ed. by G.S. Marinsky. Kiev, PWI.
5. Nychytailo, M.Yu, Furmanov, Yu.O., Gutsulyak, A.I. et al. (2016) Formation of biliary-enteric and interintestinal anastomoses under the conditions of bile peritonitis using HF electric welding in the experiment. *Klinichna Khirurgiya*, **1**, 65–68 [in Ukrainian].
6. Marinsky, G.S., Chernets, O.V., Tkachenko, V.A. et al. (2016) Bench research of high-frequency electric welding of biological tissues. *The Paton Welding J.*, **12**, 41–45.
7. Marinsky, G.S., Podpryatov, S.E. Chernets, O.V. et al. (2018) Investigation of high-frequency welding of biological tissues in the specialized experimental complex of the E.O. Paton Electric Welding Institute. In: *Proc. of 13th Int. Sci.-Pract. Conf. on Welding and Heat Treatment of Live Tissues. Theory. Practice. Prospects (Kiev, 30 November–1 December 2018))*. Ed. by G.S. Marinsky. Kiev, PWI, 63–67.
8. Lopatkina, K.G., Marinsky, G.S., Chernets, O.V. et al. (2015) Research complex for experimental studies of HF welding of different types of tissues. In: *Proc. of 10th Int. Sci.-Pract. Conf. on Welding and Heat Treatment of Live Tissues. Theory. Practice. Prospects (Kiev, 27–28 November 2015*. Ed. by G.S. Marinsky. Kiev, PWI, 40–41.
9. Podpryatov, S.S., Marinsky, G.S., Chernets, O.V. et al. (2018) Investigation of the influence of parameters of supplying pulsed high-frequency voltage on the change of dielectric characteristic of biological tissues in the model of electrically-welded interintestinal anastomosis. *Medychna Informatyka ta Inzheneriya*, **2**, 37–43 [in Ukrainian].

Received 04.12.2020

https://doi.org/10.37434/tpwj2021.02.04

INFLUENCE OF HEAT TREATMENT ON THE PROPERTIES OF WELDED JOINTS OF V1341 ALLOY UNDER MODELED OPERATING CONDITIONS

L.I. Nyrkova, T.M. Labur, S.O. Osadchuk, M.R. Yavorska and **V.A. Koval**
E.O. Paton Electric Welding Institute of the NAS of Ukraine
11 Kazymyr Malevych Str., 03150, Kyiv, Ukraine. E-mail: office@paton.kiev.ua

The paper presents the results of comparative studies of corrosion-mechanical resistance of welded joints of V1341 alloy 1.2 mm thick, produced by manual argon-arc welding with free and constricted arc, after different types of heat treatment (HT) — artificial aging and complete cycle heat treatment (hardening and artificial aging). It was shown that artificial aging increases the strength characteristics of welded joints: those produced by free arc — by ~23 %, compared to the base metal, by constricted arc — by ~29 %, but reduces the relative elongation by ~82 % and ~84 %, and the strength coefficient — to 0.77 and 0.71 (0.81 and 0.83 in as-welded state), respectively. The complete cycle of HT provides increase in both strength and ductility. After artificial aging, as well as after a complete heat treatment cycle, the potential difference between the base metal and the HAZ does not exceed the permissible value of 0.05 V (according to GOST 9.005), which will not be dangerous at operation in nonaggressive environments. Artificial aging and full HT cycle do not impair the resistance of welded joints of V1341T alloy to exfoliating corrosion compared to as-welded state, which is assessed as value 2. An increase of resistance to intercrystalline corrosion (ICC) after artificial aging was demonstrated, the maximum depth of which was 0.301 mm for a joint produced by a free arc, and 0.233 mm — for a joint produced by a constricted arc (in as-welded state it was 0.350 mm and 0.47 mm, respectively). After a complete HT cycle, the ICC depth was 0.287 mm and 0.345 mm, respectively. Artificial aging reduces the corrosion-mechanical resistance of welded joints produced by free and constricted arc: the time-to-fracture of the samples was 9 and 12 days, respectively (compared to 45 days in as-welded state), but after a cycle of HT maximum time-to-fracture of welded joints increased to 54 and 31 days, respectively. Welded joints produced by a constricted arc had higher corrosion-mechanical resistance after a complete heat treatment cycle. 14 Ref., 5 Tables, 7 Figures.

Keywords: aluminium alloy, welded joints produced by free and constricted arc welding, mechanical properties, structure, intercrystalline corrosion, exfoliating corrosion, corrosion under constant strain, potentiometry, voltamperometry

Aluminium alloys of Al–Mg–Si–Cu alloying system combine a wide range of properties: high adaptability-to-fabrication, strength, weldability and corrosion resistance [1, 2]. Sheet alloy V1341 from this group is widely used to manufacture cylinders of different designs for storage of liquid substances [3]. During manufacture of such tanks their individual elements are joined by nonconsumable electrode manual argon-arc welding by a free or constricted arc [1, 2, 4]. However, the process of welding by a free arc takes place at its low penetrability in weld formation [2]. Application of constricted arc welding improves the weld shape and promotes lower softening of the joint after welding [1]. As the thermal cycle of nonconsumable electrode welding leads to welded joint softening, the items are heat treated before operation.

A lot of investigations are devoted to the influence of heat treatment operations on the change of properties of aluminium alloys, but they predominantly study the base metal behaviour [5, 6]. As the state of as-welded metal is unique for each thickness of the semi-finished product by material structure, and there is not enough such data in publications, the objective of this work was establishing the impact of different heat treatment modes on the set of service properties of the welded joints of sheet aluminium alloy V1341T (δ = 1.2 mm), produced by argon-arc welding by a free and constricted arc.

This paper is a continuation of a series of experimental studies, the results of which are presented in works [7–10].

Experimental procedure. Investigations were conducted on welded joints of aluminium alloy of V1341 grade of the following chemical composition (spectral analysis was performed in DFS-36 spectrometer), wt.%: Al — base, (0.45–0.9) Mg, (0.5–1.2) Si, (0.15–0.35) Mn, (0.1-0.5) Cu, (0.05–0.1) Ca, 0.25 Cr, 0.2 Zn, 0.15 Ti, 0.5 Fe, and not more than 0.1 of other

L.I. Nyrkova — https://orcid.org/0000-0003-3917-9063, T.M. Labur — https://orcid.org/0000-0002-4064-2644,
S.O. Osadchuk — https://orcid.org/0000-0001-9559-0151, M.R. Yavorska — https://orcid.org/0000-0003-2016-6289,
V.A. Koval — https://orcid.org/0000-0001-5154-1446

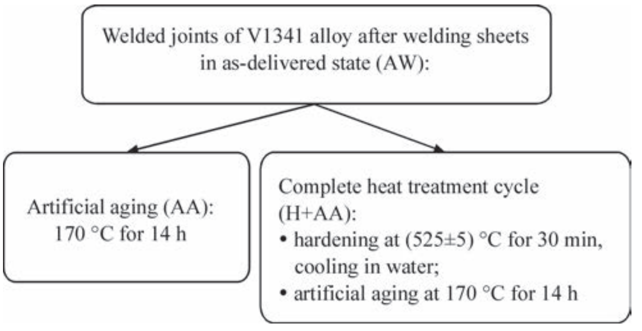

Figure 1. Scheme of conducting studies of V1341T alloy joint and applied modes of their heat treatment

elements. Wire of Sv2117 grade of 2 mm diameter was used for welding the alloy. Technological aspects of welding were discussed in detail in previous works [7–9]. In this work, joints welded along the rolling direction were investigated. The schematic of studying the joints and applied modes of their heat treatment are presented in Figure 1.

Features of structural transformations in welded joints produced with a free and constricted arc, were studied on metallographic sections, cut out normal to the weld axis. Sections were prepared by a standard procedure, and the microstructure was revealed by electrolytic etching in a solution of the following composition: 930 ml CH_3COOH + 70 ml $HClO_4$.

Electrochemical studies were conducted in a solution of 3 % NaCl by potentiometry and voltamperometry methods with application of PI-50-1.1 potentiostat and Pr-8 programmer. The nature of potential distribution over the welded joint surface was studied by the method of measuring the potential under the drop by PWI procedure. Pressure electrochemical cell was used to obtain polarization curves. The working electrodes were individual zones of the welded joint, the reference electrode was saturated chloride-silver electrode EVL-1M1, and additional electrode was platinum. Potential sweep rate in potentiodynamic mode was $5\cdot10^{-4}$ V/s. Before taking the polarization curves, the sample surface was prepared by a standard procedure.

Resistance to intercrystalline corrosion (ICC), exfoliating corrosion and corrosion cracking was assessed in keeping with the requirements of GOST 9.021 [11], GOST 9.904 [12], and GOST 9.019 [13]. Testing for corrosion cracking was conducted under the condition of continuous axial tensile stress in the metal on the level of 160 MPa at full immersion of welded joint samples into the solution of 3 % NaCl in «Signal» unit for not less than 45 days. The weld was located normal to the direction of tensile stress action.

Results and discussion. *Macro- and microstructure of welded joints.* Figures 2 and 3 show the macro- and microstructure of base metal of V1341T alloy and its welded joints, produced depending on the welding process and kind of applied heat treatment. The weld form factor of the joint produced by a constricted arc is approximately 4 % higher, compared to the welded joint, produced with a free arc (2.52 and 2.43, respectively) [9].

Analysis of the microstructure of welded joints of V1341T alloy in naturally aged condition revealed that under the conditions of action of the thermal cycle of welding, decomposition of oversaturated solid solution and dissolution of the strengthening phases take place, irrespective of the kind of the arc. Solidification of molten weld metal at cooling is accompanied by precipitation of secondary phases and coagulation of insoluble phases (Figure 3, *a*). It is due to a considerable number of the main alloying elements and additives in the alloy composition [3]. In keeping with the constitutional diagram of Al–Mg–Si–Cu–Fe system, the following binary phases can be in equilibrium with the solid solution in the alloy: Mg_2Si, $SiCuAl_2$, $FeAl_3$, Mg_5Al_8, as well as ternary phase: $CuFeAl_5$, $CuMgAl_2$, $FeSiAl_2$, $FeMg_3Si_6$. During weld solidification they form the same quanti-

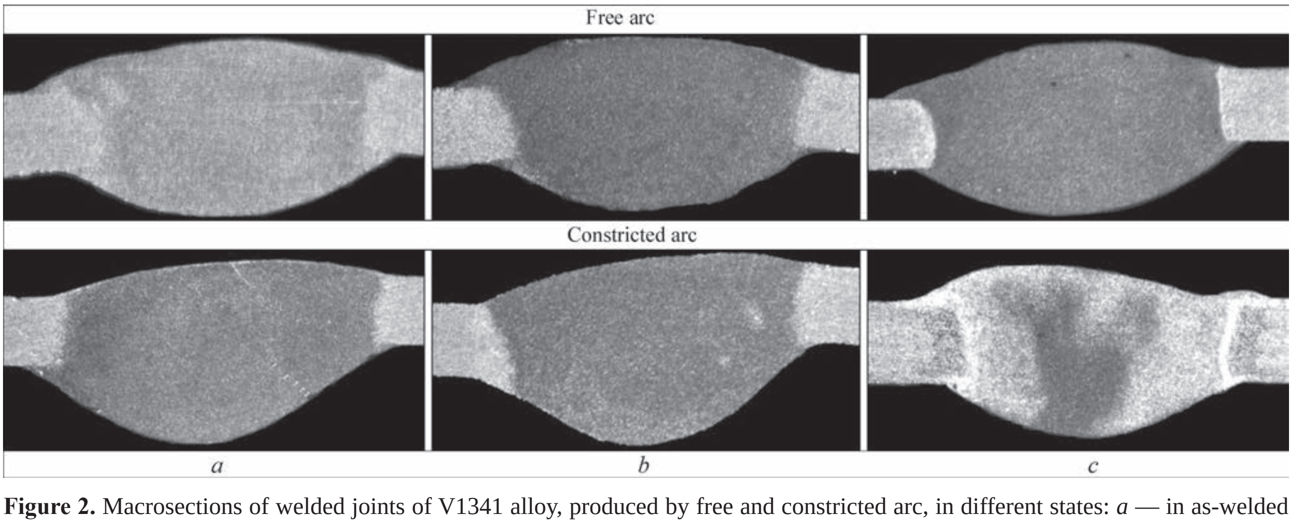

Figure 2. Macrosections of welded joints of V1341 alloy, produced by free and constricted arc, in different states: *a* — in as-welded state; *b* — after artificial aging; *c* — after a complete heat treatment cycle

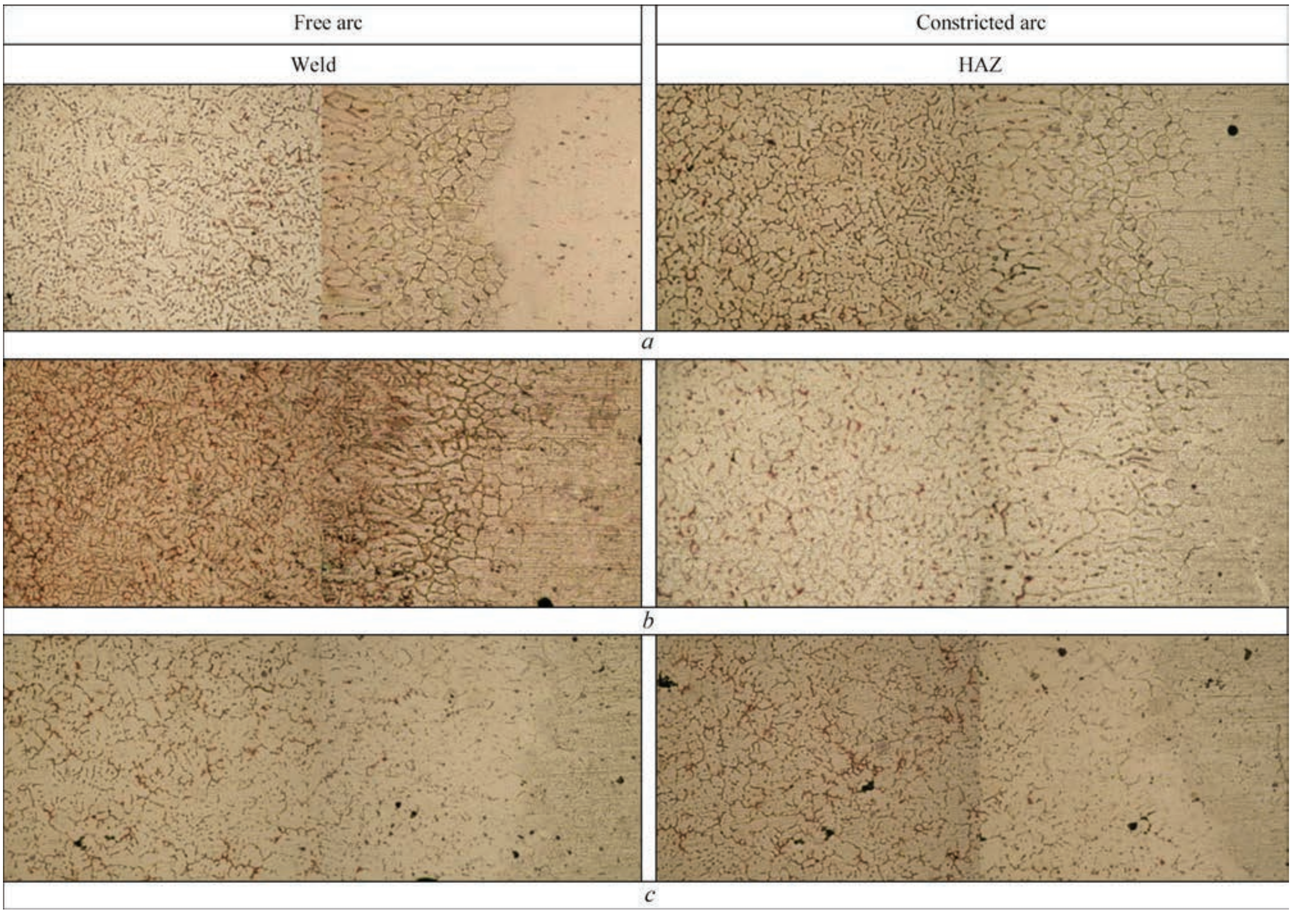

Figure 3. Microstructure (×320) of welded joints of V1341T alloy produced by constricted and free arc, in different states: *a* — as-welded state; *b* — after artificial aging; *c* — after a complete heat treatment cycle

ty of metastable phases, which are uniformly located, but differ by their shape and geometrical dimensions. Their characteristic feature is instability of decomposition within one grain [3]. Boundary areas of the crystallites are enriched in alloying elements, and their bulk is depleted in them, while thin eutectic interlayers form along the boundaries.

Microstructure of the zone of weld fusion with the base metal has melted-off grain boundaries, which formed under the action of heating at welding. Contact melting of the grains between each other or with eutectic phase Mg_2Si, which is located along the grain boundaries, results in their thickening. Fast removal of the arc, metal solidification and weld formation lead to formation of columnar crystals, oriented normal to the direction of the vector of arc movement, near the fusion boundary of the weld and base metal (Figure 3, *b*). From the base metal side, decomposition of oversaturated solid solution and simultaneous dissolution of earlier formed strengthening phases and precipitation of secondary phases proceed in the fusion zone. Coagulation of insoluble intermetallic phases of iron and silicon, which penetrate into the metal at the stage of metallurgical production of the alloy, and can cause higher stresses in the structure, also takes place [1].

In the HAZ area of V1341T alloy joints an increase of grain size and coagulation of insoluble phase inclusions, and complete or partial lowering of the strengthening effect after natural aging are observed, as well as local annealing and hardening of individual structural component areas (Figure 3, *c*). Interaction of boundary inclusions of intermetallics with the solid solution here causes formation of areas with liquid interlayers of low-melting eutectics along the grain boundaries. This is due to the features of structural and phase transformations in the metal under the impact of the thermal cycle of arc welding.

Performance of the operation of artificial aging of the joint samples leads to an increase of volume fraction of secondary phases and their density in the weld structure (Figure 3, *a, b*). The process is accompanied by thickening of grain boundaries as a result of their contact fusion with each other or with Me_2Si eutectic phase located near the grain boundaries. The above-mentioned microstructural transformations proceed as a result of solid solution decomposition, and strain hardening of phases that improves the strength of welded joint metal (Table 1).

Performance of a complete cycle of heat treatment of the joints (hardening and artificial aging) leads to a

Table 1. Mechanical properties of base metal and welded joints of V1341T alloy produced by free and constricted arc, after heat treatment by different modes

Sample state	σ_t, MPa	$\sigma_{0.2}$, MPa	δ, %	α, deg	WJ strength coefficient	σ_t, MPa	$\sigma_{0.2}$, MPa	δ, %	α, deg	WJ strength coefficient
	Welded joint produced by a free arc					Welded joint produced by constricted arc				
As-welded (AW)	195.0 / 250.5	130.11 / 87.6	2.6 / 18.9	56 / 180	0.83	200.32 / 50.5	144.31 / 87.6	1.7 / 18.9	66 / 180	0.81
After artificial aging (AA)	257.63 / 35.7	215.53 / 13.3	1.9 / 10.7	30 / 180	0.76	258.73 / 35.7	204.03 / 13.3	1.7 / 10.7	46 / 180	0.77
After hardening and artificial aging (H + AA)	241.53 / 21.1	288.6 / 282.0	6.9 / 10.7	35 / 158	0.75	323.03 / 21.1	294.32 / 82.0	3.3 / 10.7	43 / 158	1.00

Note. Values of welded joint properties in the respective state are given in the numerator, those of base metal —– in the denominator.

change of grain dimensions, width of interlayers between them and to presence of secondary phase inclusions in the structure, etc (Figure 3, *a*). Precipitation of additional secondary phase inclusions and uniform nature of their distribution over the entire weld volume has a positive impact on mechanical properties of welded joints (Table 1). On the boundary of weld fusion with base metal, formation of thinner boundaries of structural components is noted (Figure 3, *c*). They are associated with presence of small copper additives (0.3 %) in the alloy that by the data of work [3] limits the rate of precipitation of Guinier–Preston zones which are in a metastable equilibrium with the solid solution. The morphology of phase precipitates from the matrix is of a homogeneous nature, and phase dimensions are dispersed. It is determined by quick fixation of structural components at hardening of joint samples in water. Performance of artificial aging operation after hardening allows preserving the morphology of structural component location, as well as shape and dispersed dimensions of phase inclusions. Thickening of the boundaries of weld crystallites and base metal grains is noted in individual areas in the zone of fusion with the base metal. Their total thickness is smaller than in the structure of welded joints after artificial aging (Figure 3).

As was noted above, structural transformations, occurring in V1341T alloy during welding with a free and constricted arc and further heat treatment of the welded joints, influence their mechanical property values (Table 1). In keeping with the obtained data, the strength of joints welded by a free or constricted arc is equal to 195.0 and 200.3 MPa that is 22 and 20 % lower than base metal strength. Strength coefficients of the joints are equal to 0.83 and 0.81, respectively. The yield limit of welded samples, compared with base metal also decreases by 30 and 23 %, respectively (Table 1). Note that welding technology has a stronger impact on the level of ductility values, namely: relative elongation and bend angle decrease by 86 and 91 %, and by 70 and 63 %, respectively.

After artificial aging, the welded joint strength characteristics become higher compared to as-welded conditions. At application of a free arc, strength is equal to 257.6 MPa that is by ~23 % lower than that of base metal in the same condition, and with a constricted arc it is 258.7 MPa (by ~ 29 % lower). At the same time, lowering of the strength coefficient to the level of 0.76 and 0.77 is observed. Yield limit also rises, however, its numerical values remain smaller compared with base metal: by 31 % for joints produced with a free arc, and by ~35 % for joints produced with a constricted arc (Table 1). Performance of artificial aging operation causes further lowering of the values of ductility (bend angle and relative elongation), by ~83 and ~82 % for a joint produced with a free arc, and by ~74 and ~84 % for a joint produced with a constricted arc (Table 1), respectively.

Performance of the operation of complete heat treatment cycle causes a 25 % increase of strength in joints produced with a free arc (up to 241.5 MPa), compared to base metal. In joints, produced by a constricted arc, strength increased up to 323.0 MPa almost to base metal level (321.1 MPa). The value of strength coefficient of the joints was equal to 0.75 and 1.0 %, respectively. Positive impact of the heat treatment mode was observed in the values of yield limit, which rose and even somewhat exceeded the base metal level and was equal to 288.6 and 294.3 MPa for joints produced by a free and constricted arc. An increase of the level of relative elongation of the joints up to 6.9 to 3.3 % was also observed (Table 1). At the same time, the level of bend angle was smaller, compared to as-welded state and almost the same, compared to samples after artificial aging: 35 % (for a free arc) and 43 % (for a constricted arc).

Thus, after a complete heat treatment cycle an increase of strength characteristics to base metal level, was found in samples of welded joints produced by a

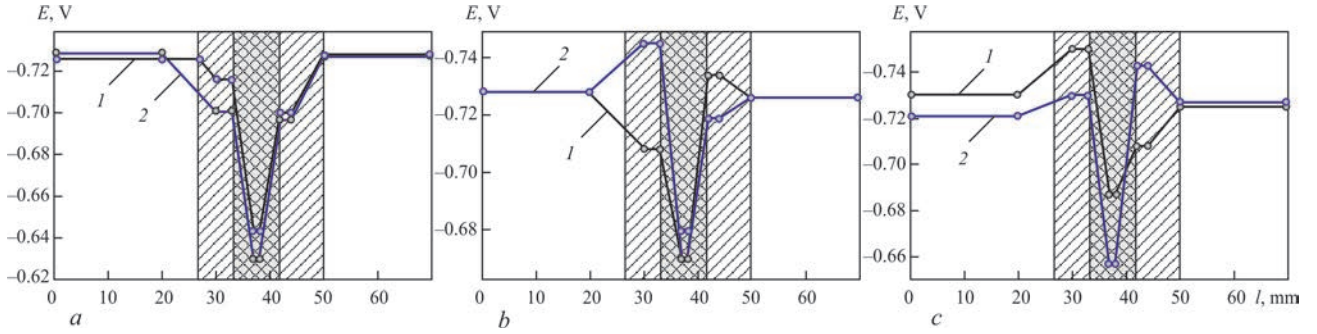

Figure 4. Nature of distribution of electrochemical potentials under the drop in different zones of welded joints of V1341T alloy, produced by a free (*1*) and a constricted (*2*) arc, as well as in different states: *a* — after welding; *b* — after artificial aging; *c* — after complete heat treatment cycle

Table 2. Difference of potentials between the zones of V1341T alloy welded joint in different states

Difference of potentials between welded joint zones, V	Welded joint state					
	Free arc			Constricted arc		
	AW	AA	H+AA	AW	AA	H+AA
Base metal — weld	0.099	0.042	0.041	0.117	0.066	0.044
Base metal — HAZ	0.030	0.015	0.010	0.068	0.013	0.032

constricted arc that is, probably, due to reduction of electrochemical heterogeneity of the joint structure, as a result of formation of a fine-grained structure and narrowing of the HAZ under the impact of a more concentrated arc energy due to its compression by argon [1].

Electrochemical studies. Measurement of corrosion potentials in the studied samples showed that the difference of potentials between the base metal and weld for as-delivered welded joints is equal to ~0.099 V (free arc) and ~0.117 V (constricted arc) (Figure 4, Table 2). Both kinds of heat treatment applied after welding, reduce the above difference, which after artificial aging was equal to ~0.042 V (free arc) and ~0.066 V (constricted arc), and after a complete heat treatment cycle: ~0.041 V (free arc) and 0.044 V (constricted arc), respectively. The difference of potentials between the base metal and HAZ for as-delivered welded joints was smaller compared to the weld, and it was equal to ~0.030 V (free arc) and ~0.068 V (constricted arc). After heat treatment of the samples the difference of potentials between base metal and HAZ became even smaller, namely after artificial aging it was equal to ~0.015 V (free arc) and ~0.013 V (constricted arc), and after a complete heat treatment cycle it was ~0.010 V (free arc) and ~0.032 V (constricted arc), respectively.

Thus, the operations of sample heat treatment reduce the difference of potentials between base metal and HAZ to admissible values, except for joints, welded by a free arc after artificial aging. The difference of potentials between base metal and HAZ after both the applied kinds of heat treatment did not exceed the admissible level (0.05 V), in keeping with GOST 9.005 [14].

Polarization curves of base metal and weld in joints produced by a free and a constricted arc in different states are given in Figure 5. Their analysis showed

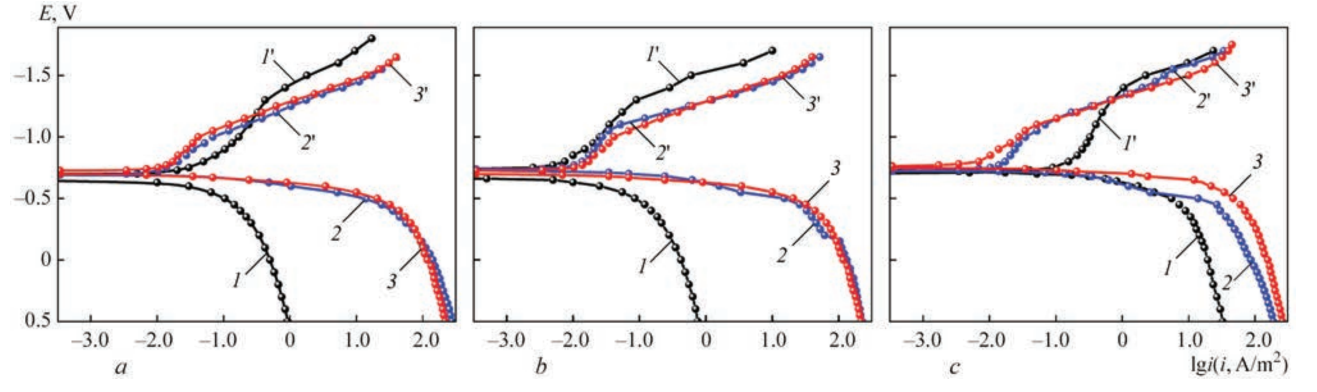

Figure 5. Anode (*1*, *2*, *3*) and cathode (*1′*, *2′*, *3′*) polarization curves of base metal (*1*, *1′*) and welded joints of V1341T alloy, produced by a free arc (*2*, *2′*) and constricted arc (*3*, *3′*) in different states: *a* — as-welded; *b* — after artificial aging; *c* — after hardening and artificial aging

Table 3. Electrochemical characteristics of base metal and weld of V1341T alloy joints produced by a free and a constricted arc in 3 % NaCl

Sample characteristic	Sample state	E_{cor}, V	i_a, A/m^2	i_d, A/m^2	E_{H_2}, V
BM	As-delivered (natural aging)	–0.728	0.03	2.95	–1.38
	AA	–0.724	0.015	0.026	–1.32
	H+AA	–0.715	1.79	0.33	–1.42
WJ produced by a free arc	As-welded	–0.699	1.07	0.023	–0.99
	AA	–0.726	1.09	0.023	–1.06
	H+AA	–0.729	1.80	0.026	–0.99
WJ produced by a constricted arc	As-welded	–0.708	3.37	0.016	–1.05
	AA	–0.736	1.09	0.022	–1.0
	H+AA	–0.737	21.88	0.02	–1.07

Note. i_a — anode dissolution current at –0.6 V potential; i_d — limit diffusion current; E_{cor} — corrosion potential; E_{H_2} — hydrogen evolution potential.

that the anode dissolution current (at –0.6 V potential) in the weld of samples of both the joints in as-welded condition (Figure 5, curves *2*, *3*) is higher than that in the base metal: 1.07 A/m^2 (free arc), 3.37 A/m^2 (constricted arc) and 0.03 A/m^2 — base metal (Table 3).

Heat treatment by artificial aging mode reduces the anode currents in the weld, which were 1.09, 1.09 and 0.015 A/m^2 (Table 3), respectively. After a complete heat treatment cycle, the difference between the anode dissolution current of base metal and the anode dissolution currents of the welds was equal to 1.79 A/m^2 for base metal, and 1.80 and 21.88 A/m^2 for joints produced by a free and constricted arc, respectively. Cathode curves for welds in as-welded state shift to the area of lower currents, compared with base metal (Figure 5, *a*). Limit diffusion current in welds of both the studied methods of joining V1341T alloy is smaller (0.023 and 0.016 A/m^2), than in base metal (2.95 A/m^2) that may point to inhibition of the cathode process in weld metal (Table 3).

After artificial aging a slight increase in boundary diffusion current is observed in the metal of welds of both the joints, compared to as-welded state (0.023 A/m^2 (free arc), 0.022 A/m^2 — constricted arc, 0.0263 A/m^2 — base metal) (Figure 5, *b*, curves *2′*, *3′*). It results in manifestation of the tendency to activation of the corrosion process in this area on the polarization curve. A complete cycle of joint heat treatment considerably inhibits the corrosion process in welds that is manifested in reduction of the values of limit diffusion current to 0.026 A/m^2 (free arc), and 0.0202 A/m^2 (constricted arc), compared with base metal (0.33 A/m^2) (Figure 5, *c*, curves *2′*, *3′*) (Table 3). It should be noted that no significant difference in weld metal behaviour was found in joints produced by a free and constricted arc. Since in aqueous media, as indicated by the shape of polarization curves, corrosion of V1341T alloy occurs with diffusion control, the corrosion rate can be evaluated by values of limit diffusion current [14].

Thus, it was determined that heat treatment of welded joints of V1341T alloy by artificial aging mode promotes a slight increase of corrosion rate, but at the same time, lowers the potential of hydrogen evolution from the HAZ metal with both the studied welding methods, compared to base metal. Performance of a complete heat treatment cycle reduces the limit diffusion current and potential of hydrogen evolution in welds, irrespective of the welding process, compared to base metal. One can expect that with such HT mode, the corrosion resistance of the alloy welded joint metal will increase.

Intercrystalline corrosion resistance (ICC). Maximum of depth of base metal ICC in as-delivered

Table 4. Generalized results of assessment of corrosion-mechanical resistance of welded joints of V1341T alloy, produced by different technologies of nonconsumable electrode welding

Sample characteristic	Sample state	ICC depth, mm	Exfoliating corrosion resistance, num	Time-to-fracture, days
Base metal	As-delivered	0.082–0.086	2–3	67–88
	After artificial aging	0.074–0.117		47–77
	After hardening and artificial aging	0.111–0.209		45–87
WJ produced by base arc	As-welded	0.245–0.350		10–45
	After artificial aging	0.123–0.301		3–9
	After hardening and artificial aging	0.214–0.287		4–54
WJ produced by constricted arc	As-welded	0.289–0.467		9– > 45
	After artificial aging	0.062–0.233		9–12
	After hardening and artificial aging	0.074–0.345		9–31

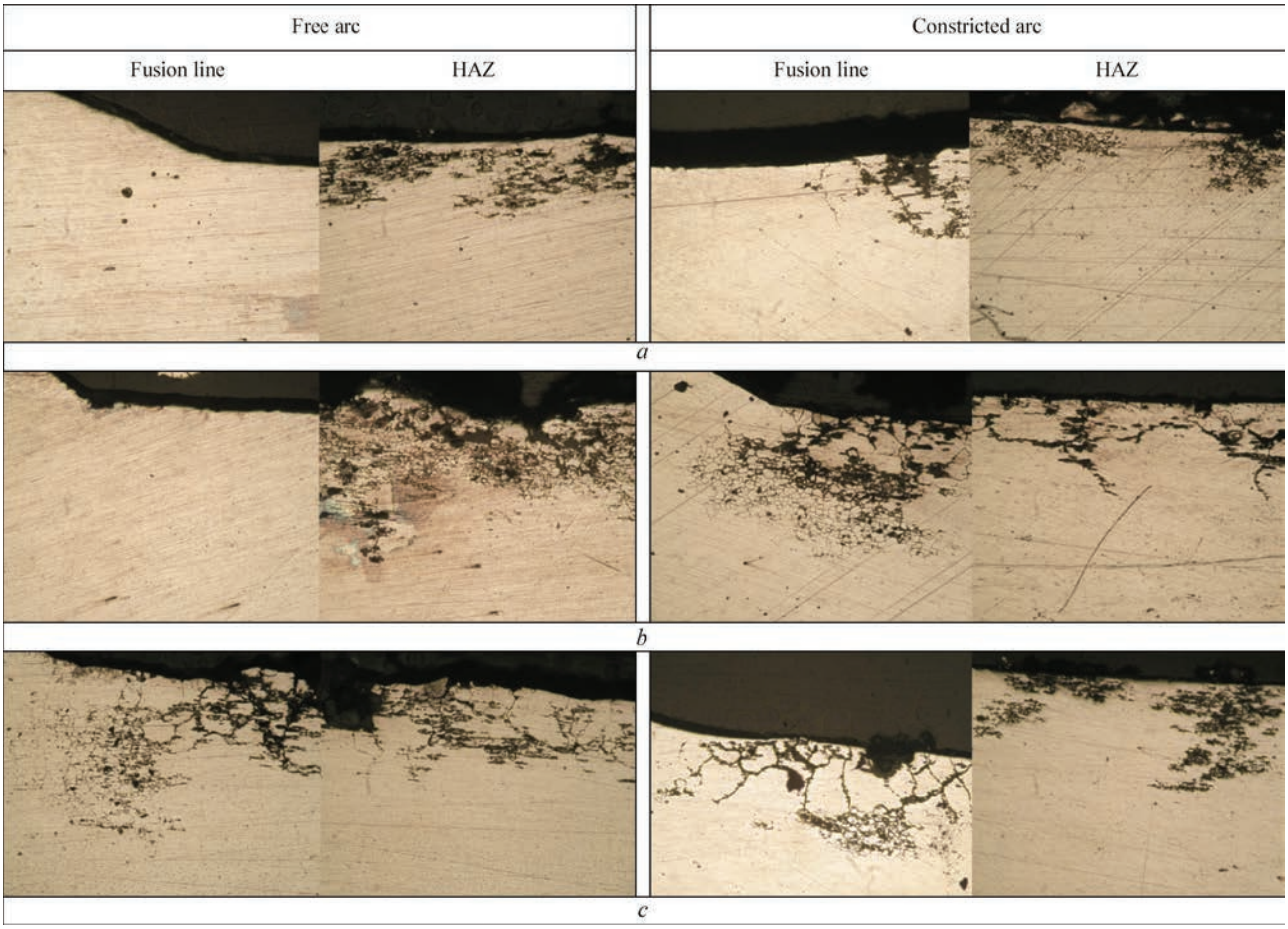

Figure 6. Appearance of samples in the fusion zone and HAZ of welded joints of V1341T alloy, produced by constricted and free arc, in different states, after testing for intercrystalline corrosion resistance, ×320: *a* — after welding; *b* — after artificial aging; *c* — after complete heat treatment cycle

condition is equal to approximately 0.086 mm. The intercrystalline fracture sites of welded joints produced with a free arc, were noted in the HAZ, and they developed to the depth of 0.350 mm (Table 4), and in those produced with a constricted arc they were found in the fusion zone and HAZ (Figure 6, *a*) to the depth of 0.506 mm. Artificial aging of joint samples caused a slight increase of metal sensitivity to ICC: intercrystalline cracks propagated in the HAZ of the joints produced by a free arc (Figure 6, *b*), to the maximum depth of 0.301 mm, and in the HAZ of joints produced by a constricted arc — to 0.233 mm. After a complete HT cycle intercrystalline cracks formed both in the HAZ and in the fusion zone of both the welded joints (Figure 6, *c*), ICC depth was 0.287 and 0.345 (0.533) mm, respectively (Table 5).

Thus, welding sheet alloy V1341 1.2 mm thick by a constricted arc causes a lowering of ICC resistance

Table 5. Results of assessment of exfoliating corrosion resistance of V1341T alloy welded joints produced by free and constricted arc in different states

Sample characteristic	Index description								Index value, number
	Nature of change in sample appearance	Largest delamination diameter, mm	Delamination area on each surface, %		Total length of cracked end faces, mm				
			A	B	1	2	3	4	
Welded joints produced by free arc									
AW	Delamination	<1.0	<1.0	<1.0	0	0	0	0	2–3
AA	Surface darkening	0	0	0	0	0	0	0	2
H+AA	Surface darkening	0	0	0	0	0	0	0	2
Welded joints produced by constricted arc									
AW	No changes	0	0	0	0	0	0	0	1
AA	Surface darkening	0	0	0	0	0	0	0	2
H+AA	Surface darkening	0	0	0	0	0	0	0	2

of welded joints, but well-chosen heat treatment mode can ensure increase of their intercrystalline fracture resistance.

Exfoliating corrosion resistance. Analysis of the surface of samples of welded joints produced by free arc (in as-welded condition) revealed delamination centers of almost 1 mm diameter, of the total area of not more than 1 %. No other indices reflecting a change in the appearance of studied sample surface were revealed (Table 5). Surface darkening was the main characteristic indication of a change in the properties of the joints after artificial aging or complete heat treatment cycle. Exfoliating corrosion resistance was evaluated by number 2. In welded joints produced by constricted arc, the value of exfoliating corrosion resistance in as-welded state was assessed by number 1, as no changes on the sample surface or end faces were found. After artificial aging or a complete cycle of joint heat treatment, a change of the sample surface colour was observed. Their exfoliating corrosion resistance was also assessed by number 2 to GOST 9.904. Thus, the surface colour change was found to be the only characteristic indicating a change in the properties of samples of both the kinds of welded joints after heat treatment, and exfoliating corrosion resistance was assessed as number 2.

Corrosion cracking resistance. Appearance of samples after testing for resistance to corrosion-mechanical cracking is shown in Figure 7. As revealed by visual analysis of the samples after welding and artificial aging, they failed in the base metal in the HAZ at 4–5 mm distance, and after conducting complete heat treatment of the samples — near the fusion zone with base metal. The time-to-fracture of welded samples produced by free arc decreased to 10–45 days (20 days on average), compared to base metal, for which it was from 67 to 88 days (almost 73 days) (Table 4).

Similar results were obtained for joints, welded by constricted arc. After artificial aging, the period of time to complete destruction of the samples was the shortest for both the studied methods of joining V1341T alloy. For joints produced by free arc, fracture occurred within 3–9 days, and for those produced by constricted arc it was 9–12 days. After a complete heat treatment cycle the maximum time-to-fracture of base metal was 87 days, of welded joints — 54 and 31 days, respectively.

Thus, heat treatment by the mode of hardening and artificial aging increases the corrosion-mechanical resistance of welded joints, both those produced by free and constricted arc. At the same time, mechanical property values after performance of a complete heat treatment are higher for joints, produced by a constricted arc. The highest level of corrosion-mechanical resistance as a result of conducting a complete heat treatment cycle is achieved in samples of welded joints produced by constricted arc.

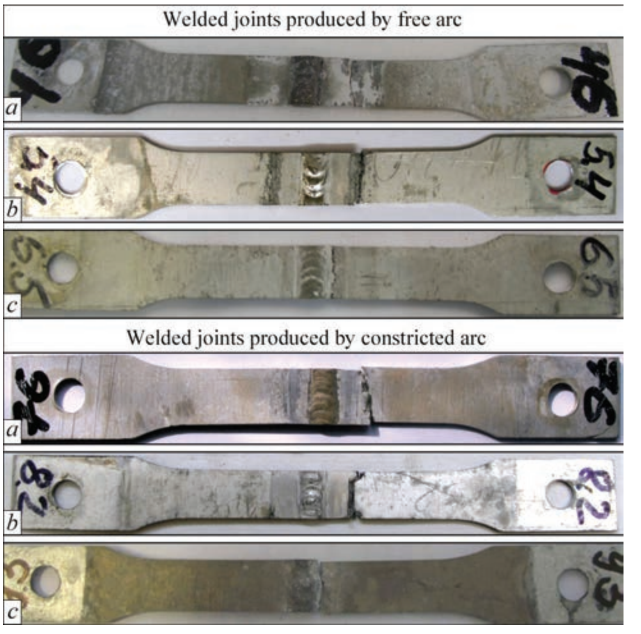

Figure 7. Appearance of samples of V1341T alloy welded joints produced by free and constricted arc, after testing for corrosion cracking resistance: *a* — as-welded state; *b* — after artificial aging; *c* — after complete heat treatment cycle

Conclusions

1. Conducting the artificial aging operation improves the strength properties of welded joints produced by free arc up to 257.6 MPa (by ~23 %, compared to base metal), by constricted arc — up to 258.7 MPa (by ~29 %). However, a lowering of the coefficient of strength of the joints to 0.76 and to 0.77 (0.81 and 0.83 in as-welded condition) is noted here. The value of relative elongation of the samples decreases by ~82 % for joints produced by free arc, and by ~84 % for joints produced by constricted arc. Performance of a complete heat treatment cycle ensures an increase of both strength and ductility values. The values of ultimate strength of the joints produced by free arc, rose by ~25 %, compared to base metal, and those of joints produced by constricted arc, increased to base metal level. The coefficients of strength of the joints were equal to 0.75 and 1.0, respectively. Relative elongation value also rose to the level of 6.9 and 3.3 %, respectively.

2. By the results of electrochemical investigations, it was determined that after heat treatment, both by the artificial aging mode, and after a complete cycle of heat treatment, the difference of potentials between base metal and HAZ did not exceed the admissible value (0.05 V), in keeping with GOST 9.005 that is not dangerous under the conditions of operation of V1341T alloy products in nonaggressive media.

3. Heat treatment by artificial aging mode promotes a slight increase of limit diffusion current (corrosion rate) of welded joints produced by free and constricted arc, but at the same time, it reduces the hydrogen evolution potential in welds of these joints, compared to base metal. A complete heat treatment cycle reduces the limit diffusion current and potential of hydrogen evolution in welds, produced by both the technologies of joining V1341T alloy that is indicative of an increase of corrosion resistance of welds.

4. It is found that conducting artificial aging or a complete heat treatment cycle of welded joints of V1341T alloy produced by a free or constricted arc, does not impair their exfoliating corrosion resistance, assessed by number 2.

5. Performance of artificial aging improves the intercrystalline corrosion resistance of V1341T alloy and its joints: cracks develop in the HAZ of the joint, produced by a free arc, to the maximum depth of 0.301 mm, and in the joint made by a constricted arc — to 0.233 mm (in as-welded state — 0.350 and 0.47 mm, respectively). After performance of a complete HT cycle, the depth of intercrystalline cracks is equal to 0.287 and 0.345 (0.533) mm, respectively.

6. Heat treatment by the artificial aging mode lowers the corrosion-mechanical resistance of welded joints produced by a free or constricted arc: time-to-fracture of the samples is reduced to 9 and 12 days, respectively (compared to as-welded state — 45 days). After a complete heat treatment cycle the maximum time-to-fracture of welded joints rises to 54 and 31 days, respectively. Higher corrosion-mechanical resistance after the complete heat treatment cycle was demonstrated by samples of welded joints, produced by a constricted arc.

The work was performed with the support of the NAS of Ukraine within the PWI departamental order program in 2017–2021 (State registration number 0117U001188).

1. Ishchenko, A.Ya., Labur, T.M. (2012) *Welding of modern structures of aluminium alloys.* Kyiv, Naukova Dumka [in Russian].
2. Krivov, G.A., Ryabov, V.R., Ishchenko, A.Ya. et al. (1998) *Welding in aircraft construction.* MIIVTs [in Russian].
3. Ovchinnikov, V.V., Grushko, O.E. (2005) High performance welded aluminium alloy V1341 of Al–Mg–Si system. *Mashinostroenie i Inzhen. Obrazovanie*, 3(**4**), 2–11 [in Russian].
4. Albert, D. (1993) Aluminium alloys in arc welded constructions. *Welding World Magazine*, 32(**3**), 97–114.
5. Pogatscher, S., Antrekowitsch, H., Leitner, H. et al. (2013) Influence of the thermal route on the peak-aged microstructures in an Al–Mg–Si aluminium alloy. *Scripta Mater*., **68**, 158–161.
6. Fridlyander, I.N., Grushko, O.E., Shamraj, V.F., Klochkov, G.G. (2007) High-strength structural alloy Al–Cu–Li–Mg of lower density doped with silver. *Metallovedenie i Termich. Obrab. Metallov*, **6**, 3–7 [in Russian].
7. Koval, V.A., Labur, T.M., Yavorska, T.R. (2020) Properties of joints of V1341T grade alloy under the conditions of TIG welding. *The Paton Welding J.*, **2**, 35–40.
8. Nyrkova, L.I., Labur, T.M., Osadchuk, S.O., Yavorska, T.R. (2020) Corrosion and mechanical resistance of welded joints of aluminium B1341 alloy, produced by argon arc welding using free and constricted arc. *Ibid*., **12**, 40–47.
9. Nyrkova, L.I., Osadchuk, S.O., Kovalenko, S.Yu. et al. (2020) Influence of heat treatment on corrosion resistance of welded joint of aluminium alloy of Al–Mg–Si–Cu system. *Fizyko-Khimich. Mekhanika Materialiv*, **5**, 131–138 [in Ukrainian].
10. GOST 9.021–74: *Unified system of corrosion and ageing protection. Aluminium and aluminium alloys. Accelerated test methods for intercrystalline corrosion.* Moscow, Izd-vo Standartov [in Russian].
11. GOST 9.904–83: *Unified system of corrosion and ageing protection. Aluminium and aluminium alloys. Accelerated test methods for exfoliation corrosion.* Moscow, Izd-vo Standartov [in Russian].
12. GOST 9.019–74: *Unified system of corrosion and ageing protection. Aluminium and magnesium alloys. Accelerated test methods for corrosion cracking.* Moscow, Izd-vo Standartov [in Russian].
13. GOST 9.005–72: *Unified system of corrosion and ageing protection. Metals, alloys, metallic and non-metallic coatings. Permissible and impermissible contacts with metals and non-metals.* Moscow, Izd-vo Standartov [in Russian].
14. Zhuk, N.P. (1976) *Course of theory of corrosion and protection of metals.* Moscow, Metallurgiya [in Russian].

Received 18.01.2021

https://doi.org/10.37434/tpwj2021.02.05

DEVELOPMENT OF NEW GENERATION FLUX-CORED WIRES FOR GAS-SHIELDED ARC WELDING OF JOINTS OF LOW-ALLOY STEELS WITH ULTIMATE STRENGTH OF 640–940 MPa

V.M. Shlepakov and O.S. Kotelchuk
E.O. Paton Electric Welding Institute of the NAS of Ukraine
11 Kazymyr Malevych Str., 03150, Kyiv, Ukraine. E-mail: office@paton.kiev.ua

The results of studying the properties of flux-cored wires with a metal core are considered, which were used as a base for suggesting approaches to development of compositions of flux-cored wires for gas-shielded arc welding of joints of low-alloy steels of higher and high strength. Application of dynamic thermal analysis of powder mixtures that model the wire cores, enabled obtaining information on kinetics of the processes which develop at heating and melting of flux-cored wire compositions that allows optimizing the core compositions. Recommendations were elaborated on selection and application of flux-cored wires for welding low-alloy high-strength steels. 10 Ref., 2 Tables, 3 Figures.

K e y w o r d s : arc welding, flux-cored wire, low-alloy high-strength steel

A stable tendency to increase the scope of application of high-strength low-alloy steels for fabrication of welded metal structures of engineering constructions (such as, for instance, main systems of transportation of gaseous and liquid products) and other facilities, particularly those operating under complex climatic conditions, provided the impetus for expansion of research and development in the sphere of creating new electrode materials for arc welding [1, 2]. Research and development of electrode materials for welding high-strength steels from the very beginning were aimed at controlling the microstructure in terms of optimizing the combination of particles of the bainite, ferrite and martensite components. Reaching the specified level of property values is made more difficult by a strong dependence of the dynamics of formation of microstructural components on welding mode parameters [3, 4]. The works devoted to the role of the composition of nonmetallic inclusions, their morphology and distribution along the grain boundaries in formation of the microstructure and properties of weld metal became an important step in development of ideas about the ways to control the visco-plastic properties of weld metal in high-strength steel joints [5–9]. Development of flux-cored wire for gas-shielded arc welding of joints of high-strength low-alloy steels was based on the results of research and development of flux-cored wires with a metal core [7], typical samples of which ensure optimal welding-technological properties. Numerous studies on selection and optimization of weld metal alloying system for welding high-strength low-alloy steels (HSLA) of different strength level formed the base for generalization of the recommended compositions of electrode materials by alloying system in the form of an international standard [10].

Application of the process of flux-cored wire arc welding in gas mixtures based on argon and carbon dioxide gas allows ensuring the stability of the process of transfer of the wire sheath metal and powder core materials which melt, into the weld pool within the limits of application of parameter ranges of the mode, characterized by spray or spray-droplet transfer, and which minimizes the electrode metal losses. Here, the process of melting of flux-cored electrode wire and running of the reactions of interaction of molten metal with the gas shielding atmosphere can be regulated by oxidizing capacity in a rather wide range without deterioration of welding-technological properties.

The objective of this work is research analysis and preparing recommendations on development of flux-cored wires for gas-shielded arc welding of joints of higher and high strength low-alloy steels.

Main research results and their discussion. Experience of application of metal-core type wires, where the powder core includes a complex powder mixture of low-melting mineral components for metallurgical processing and refining of weld pool metal, formed the base of research and development of

V.M. Shlepakov — https://orcid.org/0000-0002-8134-0685, O.S. Kotelchuk — https://orcid.org/0000-0002-5432-0232

flux-cored wires for welding high-strength steels. The materials used for fluxing, were low-melting salts of alkali-earth metals (fluosilicates, carbonates, aluminates, fluorides, etc.) with low hygroscopicity, the slag melts of which assimilate inclusions, forming as sharp-angled particles, film precipitates, spinels, which significantly lower the grain-boundary strength. Melt treatment by a fluxing mixture is designed for adjustment of the composition of nonmetallic inclusions and forms of their precipitation along the grain boundaries, as well as for lowering hydrogen content in the weld metal due to running of the reactions of its binding by fluorides. The composition of the refining slag system, is optimized in terms of the characteristics of powder mixture of the wire core. At manufacture of flux-cored wire for welding steels of a certain strength level it is recommended to conduct special control of the conformity of the mixture to the requirements, taking into account the possible change of raw material composition.

The refining mixture structure is based on application of a composition of element compounds from IIA (Mg, Ca, Ba), IIIA (A1) and IVA (Si) groups of the periodic system of elements. Metal-powder mixture is part of the salt composition that forms low-melting slags for refining, capable of removing nonmetallic inclusions from the weld pool metal before its solidification.

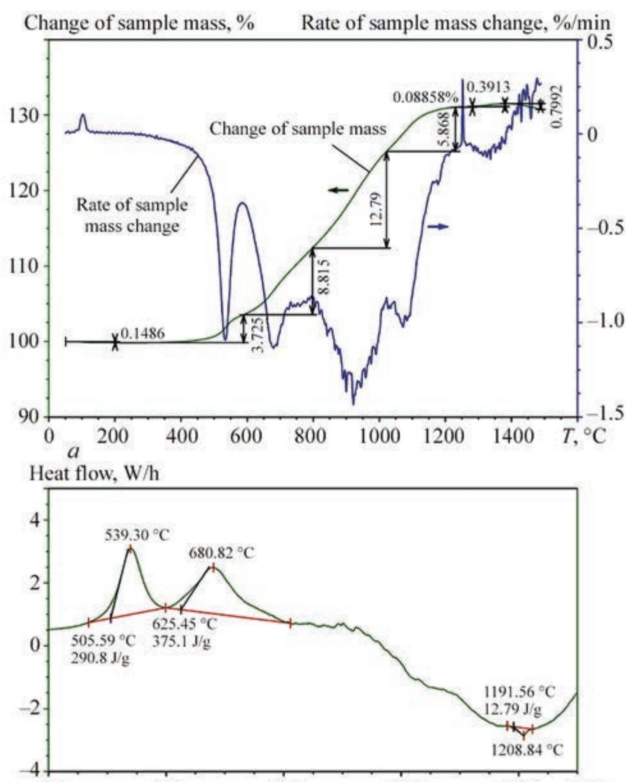

Figure 1. Results of thermogravimetric analysis (*a*) and analysis by the method of differential scanning calorimetry (*b*) of model core of flux-cored wire of oxide-fluoride type

Oxygen content in the weld metal is to a certain extent compensated by the total quantity of nonmetallic inclusions of oxide type, which affect the weld metal cold resistance. Oxygen content in weld metal within 0.25–0.35 wt.% is considered optimal. So, in welding with rutile type flux-cored wire in a mixture of Ar + CO_2, oxygen content decreases to 0.022–0.025 wt.%. Here, impact energy at –60 °C is equal to 50 J, compared to welding with the same wire in CO_2, when oxygen content can reach 0.05–0.06 wt.%, while impact energy values decrease and are close to 27 J at –40 °C.

Refining mixture compositions were designed proceeding from the results of dynamic thermal analysis of experimental powder mixtures, the composition of which was selected, taking into account the basic principles of weld metal alloying in welding high-strength steels of certain strength category. Complex thermogravimetric analysis in combination with differential scanning calorimetry allows determination of temperature ranges of formation of metal and slag melts, performing quantitative evaluation of the degree of development of thermochemical reactions of interaction of the studied compositions with the gas environment during dynamic heating (in particular, thermal destruction and evaporation of the components, as well as oxidation of metal components). Figure 1, *a* shows the results of thermogravimetric analysis of the model core of flux-cored wire of oxide-fluoride type, that contains Al-based master alloys (in particular, Al-Li and Al-Mg master alloys), and Figure 1, *b* presents the results of analysis of the same sample of flux-cored wire core by the method of differential scanning calorimetry together with calculation of total thermal effects of the reactions. The process of heating of the charge of flux-cored wires of oxide-fluoride type is characterized by exothermal effects of a high intensity at temperatures of about 600 and 800 °C, which are accompanied by increase of sample mass and lowering of oxygen content in the gas phase of the heating chamber, that is indicative of intensification of the processes of oxidation of powders of Al and Mg master alloys, iron powder and ferroalloys, respectively. The slag melt forms in the temperature range of 1190–1220 °C that is characterized by a respective endothermic effect, which reaches a maximum at the temperature close to 1200 °C.

Melt formation already at the stage of heating of the powder core in electrode wire extension, before melting of the wire sheath and evolution of gaseous products (CO, CO_2, SiF_4, etc.) determines the protective functions of the flux-cored wire and essentially influences the progress of the reactions of metal interaction with the gases at the drop and pool stages. Temperature ranges of thermochemical reactions (for instance, endothermic processes of moisture removal, destruction, melting and exothermic processes of oxidation and formation of complex compounds), which accompany the heating process, overlap, and their thermal effects are superposed one over the other, stimulating development of some processes and inhibiting other processes. Thus, control of these thermochemical reactions through correction of the core composition, allows regulation of its melting rate, achieving favourable characteristics of flux-cored wire melting, as a whole, as well as electrode metal transfer into the weld pool. Specific data on the heat flow magnitude at heating of powder compositions, enable assessment of heat losses for their heating and melting, allowing for mutual influence of exo- and endothermic reactions that develop in the flux-cored wire core.

Low-alloy welding consumables developed for welding high-strength steels, should satisfy higher requirements as regards their composition to ensure a low hydrogen content in the weld metal. High concentration of diffusible hydrogen in the welded joint can lead to formation of cold cracks. That is why, in welding of high-strength steels the quantity of hydrogen, penetrating into the weld pool, should be minimized. This is achieved due to initially low hydrogen content in the filler material and shielding gas, as well as due to ensuring welding conditions, preventing ingress of moisture and other hydrogen compounds into the welding zone from the environment.

In welding steels with the yield limit of up to 520 MPa, the admissible level of hydrogen content in the weld metal is limited by 5 cm^3/100 g of deposited metal, and in welding steels with the yield limit of 620 MPa and higher it can be up to 3 cm^3/100 g of deposited metal.

In order to manufacture flux-cored wires designed for welding high-strength steels, it is necessary to not only use initial raw materials with a low hydrogen content, but also ensure continuous monitoring of moisture content in all the raw materials and the ready charge during their storage and during wire manufacturing, and provide such conditions of storage and application of these consumables, which prevent their moisturizing. This is achieved by application of thermostatic containers at all the stages of flux-cored wire manufacturing. Cleaning of the steel strip should guarantee absence of moisture and remnants of conservation lubrication on the strip surface directly before its feeding for wire sheath forming and filling with the charge.

Flux-cored wire for high-strength steel welding is supplied to the user in hermetically sealed packing from aluminium foil, sealed under low vacuum. The term of use of flux-cored wire taken out of the sealed packing is limited by the documentation on producing welded joints of higher and high-strength steels.

Control of diffusible hydrogen content in raw materials which are used as components of flux-cored wire core and in charges for flux-cored wire core allows separating the components and compositions, application of which in the core of flux-cored wires for welding high-strength steels without special treatment should be limited. Thermal analysis of such materials combined with mass-spectrometry of the gas phase, is useful for achievement of this purpose. Considering possible oxidation of metal powders at heating up to high temperatures (700–1000 °C), thermal analysis is conducted in the flow of inert gas (usually, argon) for assessment of internal oxidation without the influence of air atmosphere.

Flux-cored metal materials (Fe·Mn, Mo, Fe·Si, Al, Al·Mg, Al·Ca) lose the adsorped moisture at heating in the temperature range of 110–240 °C. At further heating the structurally bound moisture is removed. This process is accompanied by development of internal oxidation processes. Results of thermal analysis allow determination of optimal conditions, under which the internal oxidation does not have any significant influence on removal of hydrogen and its compounds. It is rational to conduct heat treatment of the majority of materials in the temperature range of 200–400 °C, depending on the type of manufactured wire. A more complete removal of hydrogen and its compounds can be achieved by heat treatment of individual powders in a shielding atmosphere or in vacuum. However, even heat treatment of powder mixtures under regular conditions allows lowering the potential hydrogen content in the flux-cored wire core by 85 %.

Influence of strip cleaning and treatment of flux-cored wire surface to lower the diffusible hydrogen content in the weld metal was experimentally verified on test samples of flux-cored wires of carbonate-fluorite and metal-core types with comparable content of the core alloying part. Cold-rolled steel strip of 08Yu type of 0.8×12 mm dimensions was used for manufacturing such experimental flux-cored wires. The strip was cleaned from remains of conservation lubrication that is one of the greatest sources of diffusible hydrogen in flux-cored wires by two methods: mechanical

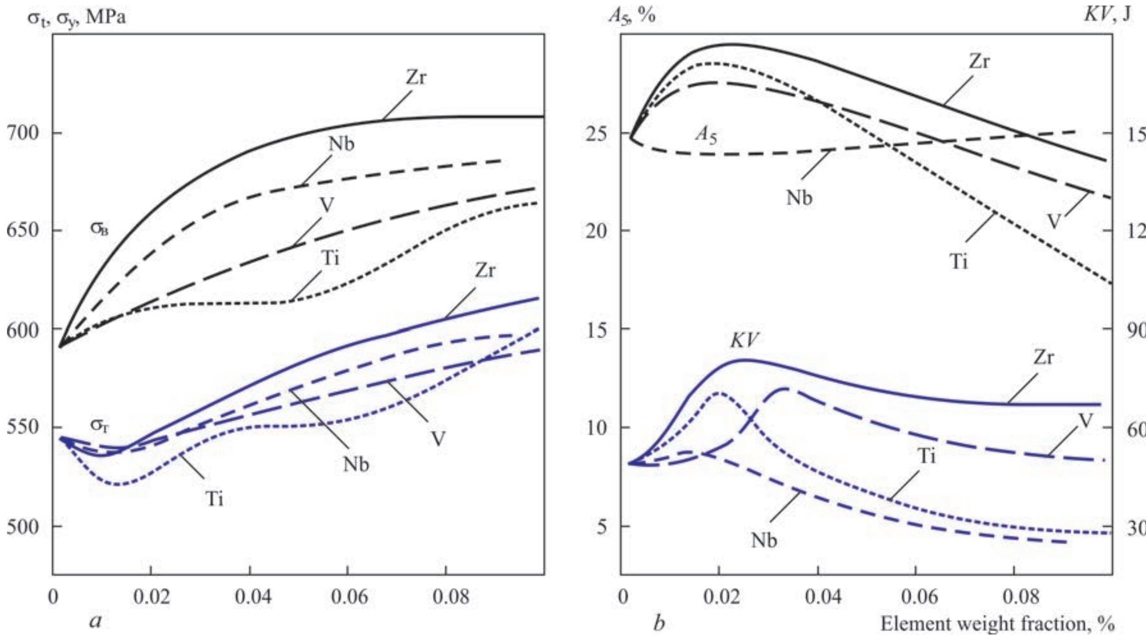

Figure 2. Mechanical properties of weld metal at microalloying by V, Ti, Nb and Zr: yield limit σ_y and ultimate tensile strength σ_t (*a*) and relative elongation A_5 and impact energy *KV* at testing temperature of –40 °C (*b*)

and rinsing in a degreasing solution. The results of analysis of diffusible hydrogen content in the strips cleaned by the first and second methods, turned out to be close and equal to approximately 1.2 cm^3/100 g of metal.

To prevent increase of hydrogen content in the flux-cored wire, it turned out to be useful to deposit an inhibiting coating on the wire surface after its cleaning. Wire packing in high-capacity containers of Marathon type is undesirable, because of the difficulties of ensuring the required sealing and the need to use the wire as soon as possible after opening the packing.

Development of core compositions of flux-cored wire for welding steels of different strength classes. Research and development of flux-cored wires for welding low-alloy high-strength steels in shielding gas atmosphere were conducted, taking into account the experience of producing steels of the respective strength class. In production of such steels the operations of refining and ladle treatment at the pouring stage, as well as heat treatment (hardening, tempering) at rolling are applied, as a result of which the rolled stock (steel) acquires a uniform microstructure of predominantly bainitic-martensitic class.

Regulation of the values of physico-mechanical properties of steels and electrode materials for their welding is achieved through microalloying by carbide- and nitride-forming elements (vanadium, niobi-

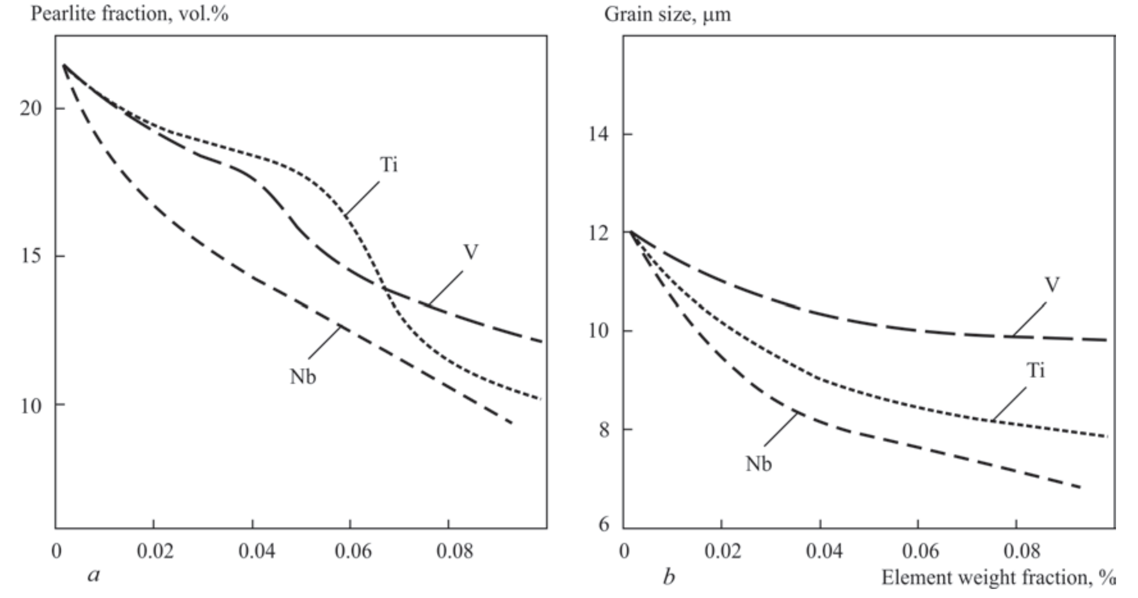

Figure 3. Influence of microalloying by V, Ti and Nb on metal microstructure: fraction of pearlite microstructural component in metal structure (*a*) and grain dimensions (*b*)

Table 1. Mechanical properties of weld metal of HSLA steels of different strength classes

Classification of flux-cored wire by EN ISO 18276 standard	Minimum value of yield limit of steel being welded, MPa	Values of properties of metal of the weld and welded joint			
		Yield limit, MPa	Ultimate tensile strength, MPa	Elongation, A_5, %	Impact energy ISO – V (J) at testing temperature
EN ISO 18276-A: T 55 5 Z M M 1 H5	550	> 550	640–820	> 22	> 47; –50 °C
EN ISO 18276-A: T 55 41 NiMo B M 2 H5 EN ISO 18276-A: T 55 61 NiMo B C 2 H5	–	> 550	640–760	> 23	> 60; –40 °C
EN ISO 18276-A: T 62 41 NiMo P M 1 H5	620	> 620	700–800	> 20	> 47; –40 °C
EN ISO 18276-A: T 62 5 Mn2.5Ni P M 1 H5	–	> 620	700–890	> 18	> 62; –40 °C > 47; –50 °C
EN ISO 18276-A: T 69 4 Z P M 1 H5	690	> 690	770–940	> 17	> 50; –40 °C

Table 2. Chemical analysis of the composition of weld metal of HSLA steels of different strength classes (typical values in wt.%)

Flux-cored wire classification by EN ISO 18276 standard	C	Mn	Si	P	S	Cr	Ni	Mo
EN ISO 18276-A: T 55 5 Z M M 1 H5	0.06	1.7	0.6	< 0.015	< 0.015	–	0.6	0.3
EN ISO 18276-A: T 55 41 NiMo B M 2 H5 EN ISO 18276-A: T 55 61 NiMo B C 2 H5	0.07	1.3	0.4	0.01	0.01	–	1.1	0.4
EN ISO 18276-A: T 62 41 NiMo P M 1 H5	0.07	1.40	0.40	< 0.015	< 0.015	–	0.9	0.4
EN ISO 18276-A: T 62 5 Mn2.5Ni P M 1 H5	0.08	1.35	0.35	< 0.015	< 0.015	–	2.2	–
EN ISO 18276-A: T 69 4 Z P M 1 H5	0.06	1.4	0.4	< 0.010	< 0.010	–	2.9	0.35
EN ISO 18276-A: T 69 4 Mn2NiCrMo M M 1 H5	0.05	1.5	0.5	0.01	0.01	0.4	2	0.4

um, zirconium, titanium) at lowering of carbon content and base alloying by manganese, silicon, nickel, molybdenum and chromium.

Analysis of the known systems of microalloying by vanadium, titanium, niobium and zirconium allowed selecting the system of microalloying through the flux-cored wire core, which is the most suitable for the tasks of welding high-strength low-alloyed steels and determining the optimum limits of such microalloying. The optimum is achieved (Figures 2 and 3) for microalloying by V — up to 0.08; Ti — up to 0.05; Nb — up to 0.02; Zr — up to 0.09 wt.%. Lowering of ductility (values A_5 and *KV*) is due to embrittlement of the grain boundaries. V, Ti and Nb are capable of forming film type carbonitrides.

Optimization of the composition of complex microalloying of weld metal through the flux-cored wire core was performed, allowing for adsorption activity of carbo- and nitride-forming and alkali-earth elements, and the influence of microalloying on the structurally-sensitive mechanical properties of the welded joint was experimentally assessed.

The main requirements to the properties of the metal of welds and welded joints of high-strength steels, made by gas-shielded arc fusion welding, are specified by international standard EN ISO 18276 «Flux-cored wires for gas-shielded welding of high-strength steels» [10]. As regards chemical composition, the limits were determined for weld metal alloying by the content of Mn, Ni, Cr and Mo, in keeping with the level of strength values; by impurity content: for carbon — 0.03–0.1 wt.%, sulphur — not more than 0.020 wt.% and phosphorus — not more than 0.020 wt.%; and by alloying elements — in keeping with the specified strength level. Recommended limiting of hydrogen content in the deposited metal is not more than 5 cm^3/100 g of deposited metal.

The compositions of flux-cored wires for gas-shielded welding were developed, taking into account the main requirements of the standard, in keeping with the flux-cored wire category by strength values.

Tables 1 and 2 give the values of the properties of flux-cored wires for arc welding of HSLA steels in shielding gases (82 % Ar + 18 % CO_2).

Conclusions

Obtained results were the base for development of flux-cored wires for welding HSLA steels and allowed formulating the main stages of such development:

- development of core compositions of flux-cored wires for welding high-strength steels in the shielding gas atmosphere of M21 type (Ar + CO_2 mixture), taking into account the strength class from 600 up to 800 MPa, which provide spray or spray-droplet transfer of electrode metal at 1.2 mm base diameter of the wire and when maintaining the recommended parameters of the welding mode;
- calculations of chemical composition of the deposited metal for welds, produced in arc fusion welding proceeding from the basic recommendations, included into EN ISO 18276 standard for welding steels

of the appropriate strength level that determines the fraction of disperse bainite component of weld microstructure, which forms at austenite-ferrite transformation during weld metal cooling;

• experimental confirmation of the conformity of microstructural composition of weld metal to the requirements made at maintenance of the recommended parameters of the welding process;

• conducting the full testing cycle, and verifying the compliance of these test results with technical requirements, made of the property values for joints of steels of the respective strength level.

1. Karlsson, L., Bhadeshia, H.K.D.H. (2007) Novelty in welding consumables. *Australian Welding J.*, **56**, Third Quarter, 44–49.
2. Malyshevsky, V.A., Grishchenko, L.V., Baryshnikov, A.P. (1999) Welding consumables and technology of welding of high-strength steels. *Voprosy Materialovedeniya*, 20(**3**), 46–62 [in Russian].
3. Widgery, D.J., Karlsson, J., Murugananth, M., Keehan, E. (2002) Approaches in the development of high strength steel weld metals. In: *Proc. of 2nd Intern. Symp. on High Strength Steel Weld Metals (Norway, Brussels, Belgium)*. The European Coal and Steel Community, 1–10.
4. Wang, W., Lin, S. (2002) Alloying and microstructural management in developing SMAW electrodes for HSLA-100 steel. *Welding J., Research Supplement*, **81**, 132–145.
5. Keehan, E., Karlsson, L., Andron, H.-O. Svensson, L.-E. (2006) New developments with C–Mn–Ni high strength steel weld metals properties. *Ibid*., **85**, 211–218.
6. Keehan, E., Karlsson, L., Thuvander, M., Bergquist, E.L. (2007) Microstructural characterization of as deposited and reheated weld metal — high strength steel weld metals. *Welding in the World*, **51**, 44–49.
7. Shlepakov, V.N., Kotelchuk, A.S. (2019) Improvement of technological and sanitary-hygienic characteristics of gas-shielded arc welding process. *The Paton Welding J.*, **6**, 29–33. DOI: https://doi.org/10.15407/as2019.06.05
8. Koseko, T., Thewlis, G. (2005) Inclusion in welds. *Material Sci. and Technol.*, **21**, 867–869.
9. Baryshnikov, A.P., Grishchenko, L.V., Malyshevsky, V.A. et al. (1996) Effect of oxygen content on impact toughness of weld metal produced in shielding gas medium. *Progressivnye Materialy i Tekhnologii*, **2**, 221–227 [in Russian].
10. (2005) DSTU EN ISO 18276:2015 (EN ISO 18276:2006, IDT; ISO 18276:2006, IDT): *Welding consumables. Tubular cored electrodes for gas-shielded and non-gas-shielded metal arc welding of high-strength steels. Classification.* ISO Office, Switzerland.

Received 02.12.2020

https://doi.org/10.37434/tpwj2021.02.06

INFLUENCE OF TECHNOLOGICAL AND METALLURGICAL FACTORS ON COPPER WELDED JOINT FORMATION IN ELECTRON BEAM WELDING

V.M. Nesterenkov, L.A. Kravchuk and **M.O. Rusynyk**
E.O. Paton Electric Welding Institute of the NAS of Ukraine
11 Kazymyr Malevych Str., 03150, Kyiv, Ukraine. E-mail: office@paton.kiev.ua

The influence of technological and metallurgical factors on welded joint formation in electron beam welding of M1 copper grade with the thickness δ = 18 mm by a vertical electron beam in the flat position in a one pass was studied. The system of a computer control of the process of electron beam welding in the UL-209M installation allows performing cleaning of the adjacent butt zone from the remnants of contaminants and oxides using a low-power electron beam focused on the metal surface in a single technological cycle. The use of high-speed local electron beam scanning in a circle allowed a significant reduction in the temperature in the central part of the welding pool and, thus, eliminated burnouts and splash of weld metal. It was established that the optimal welding speed at an accelerating voltage U_{acc} = = 60 kV is in the range v_w = 6–8 mm/s. Metallurgical treatment of welding pool with the help of inserts of aluminium and titanium foil eliminates the susceptibility to pores formation in the weld metal. 16 Ref., 1 Table, 5 Figures.

Keywords: electron beam welding, electron beam, computer control, circular scanning, penetration depth, input energy, welding speed, facial bead width, porosity

In electron beam welding (EBW), copper has a number of difficulties, which are mainly predetermined by its high thermal conductivity, high fluidity, intense evaporation in vacuum during heating above the melting point, as well as significant activity of the metal in interaction with oxygen and hydrogen in the molten state. A high thermal conductivity leads to increased cooling rates of the weld metal and the weld zone and to a short time of when the welding pool remains in the liquid state, which leads to a deterioration of the weld formation and the need in additional investigations to reduce weld porosity.

An increased fluidity of copper does not allow performing one-sided butt welding with a full penetration of edges in the flat and vertical positions. For satisfactory weld formation, on the reverse side backings are applied which densely adjoin to metal being welded, or are limited by a lock joint at non-through penetration.

The use of electron beams with normal (Gaussian) power density distribution in welding copper leads to overheating of the metal in the near-axial zone, its intensive evaporation and, as a consequence, spattering and unsatisfactory weld formation [1]. Thus, in electron beam welding of copper with a thickness δ > > 4 mm electron optical systems are used that provide uniformity of current across the cross-section of the beam, or systems in which the maximum current density is displaced outside the near-axial zone [2, 3].

The content of impurities in EBW copper has a great influence on the quality of welded joints [4]. The most harmful impurity that reduces the mechanical, technological and anticorrosion properties of copper is oxygen, the content of which should be limited and minimized by deoxidation [5].

In connection with the abovementioned, a set of studies was conducted on EBW M1 copper with a thickness of δ = 18 mm in order to determine the optimal energy, time and geometric parameters of the electron beam, as well as the influence of the preparation of the welded edges, and metallurgical methods for the formation and quality of welded joints.

Research procedure. EBW of plane specimens of M1 copper with the thickness δ = 18 mm of the size 200×80×18 mm was performed in the flat position by means of a vertical electron beam in the UL-209M installation with a computer control of all parameters and systems (vacuum, movement and rotation of electron beam gun (EBG), welding current, welding speed, focusing and deflection of electron beam, local scanning), created at the PWI [6]. The UL-209M installation is equipped an power complex based on ELA-60/60 and EBG, which moves inside the vacuum chamber along the linear coordinates *X*, *Y*, *Z* and also rotates around the *Y*–*Y* axis at an angle of 0–90°. At an accelerating voltage U_{acc} = 60 kV, EBG with a tungsten metal cathode with 3 mm diameter provides

V.M. Nesterenkov — https://orcid.org/0000-0002-7973-1986, M.O. Rusynyk — https://orcid.ord/0000-0002-7591-7169

Chemical composition of copper, wt.%

Grade of copper	Content of impurities, not more than											
	Bi	Sb	As	Fe	Ni	Pb	Sn	S	Zn	P	Ag	Composition of copper
M1*	0.0003	–	0.0007	0.004	0.0001	0.0013	0.0001	–	0.0017	–	0.0055	99.98
M* — chemical composition of copper was determined by emission spectral method.												

the current range of the electron beam I_b = 0–500 mA, as well as realization of technological scanning of the beam in the EBW process. The accuracy of EBG positioning on the coordinates not worse than 0.1 mm is provided. The alignment of the electron beam with the butt is provided by the RASTR system with an accuracy of not less than 0.1 mm [7].

The working distance from the end face of EBG to the surface of welded specimens was 200 mm, the residual pressure in the welding chamber reached $1\cdot10^{-2}$ Pa. Immediately before welding, the specimens were degreased with aviation gasoline (GOST 1012–72) or white spirit (GOST 3134–52), and then the ends and adjacent areas of 10 mm width were scraped by hand. The electron beam was focused on the surface of butt welded specimens, and the value of the welding current was set in such a way that at the optimal input energy, through penetration in a one pass with a guaranteed formation of the facial bead of the weld and point punctures on the back side of the weld was provided.

Mechanical tensile tests of round (type II) specimens of welded joints and base metal were performed in a rupture machine of type TsDM-10R (Germany) according to GOST 6996–66. In the manufacture of round specimens for tension, the middle part of the weld was chosen according to the penetration depth. Plane specimens with a V-shaped notch (type XI) for impact toughness determination were also manufactured.

The structure of welded joints was examined in the optical microscope of Neophot-32 type at a magnification of ×20–500. The nature of decrease in the

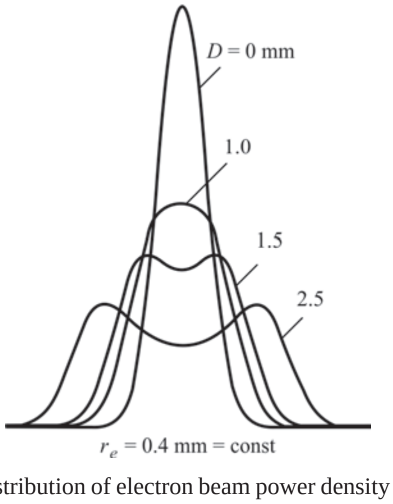

Figure 1. Distribution of electron beam power density while measuring the diameter of a circular scanning D and a constant effective beam radius r_e

strength of the base metal in HAZ was determined by measuring the hardness on the cross-sections in a microhardness tester of M-400 type of COMPASS Company at a load of 1N (application time is 10 s) at three levels of penetration depth (top, middle, bottom).

The chemical composition of M1 copper, given in Table, was determined by the method of emission spectral analysis in the ICAP6500 DUO installation («Thermo Electron Corporation», UK). Gas analysis performed in the RO-316 installation (LECO, USA) and the RH-402 installation (LECO, USA) showed that the content of oxygen and hydrogen in the investigated M1 copper is lower than the values admissible by GOST and amounts to O_2 = 0.0028 wt.%, H = = 0.0012 wt.%, respectively.

Evaluation of the results of EBW of M1 copper with a thickness δ = 18 mm was performed according to the following criteria: process stability, reproducibility of results, formation of a set penetration geometry, density and strength of welded joint, minimum porosity and absence of cracks.

Results of technological investigations. Deprivation of a high-temperature axial part of the heating spot at EBW of M1 copper was achieved by a high-velocity electron beam scanning in a circle, when the distribution of the resulting heat flux represents a rectangular pulse with a plane top and sloping edges or curves with two maximums [8, 9]. In this case, the power of electron beam is distributed along the scanning trajectory almost uniformly at frequencies f_{scan} > 1000 Hz [8]. As is shown in Figure 1, by changing the diameter of electron beam rotation, it is possible to significantly reduce the temperature in the central part of the welding pool and, thus, to eliminate burnouts and splashes of weld metal.

However, due to thermophysical properties of copper, which lead to high cooling rates of weld metal, it was found that at electron beam current I_b > 150 mA, welding speed $v_w \geq 5$ mm/s and a circular scanning diameter D > 1.5 mm, it becomes impossible to form a weld without craters and spattering of weld metal (Figure 2). Experimental penetrations on copper to a depth h_p = 18 mm and at D = 1.5 mm showed that the position of electron beam focus relative to the surface of the specimen within ± 5 % does not lead to elimination of the mentioned defects. Further investigations on the selecting conditions of EBW of M1 copper was carried out with a diameter of circular scanning D = 1.5 mm.

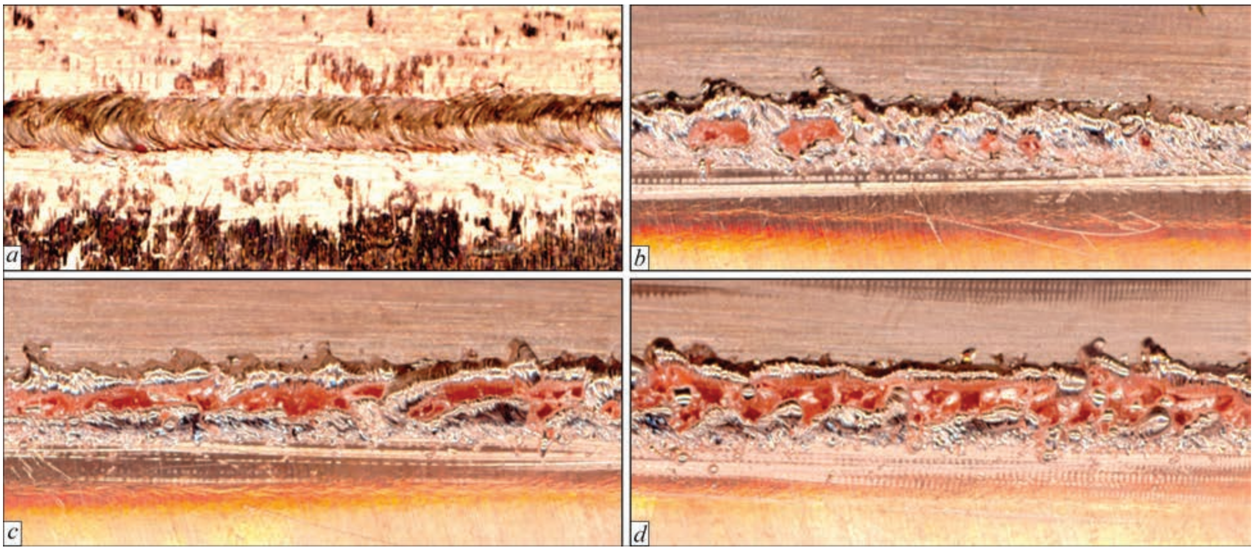

Figure 2. Formation of facial bead in the EBW weld of M1 copper with a thickness δ = 18 mm and different diameters of circular scanning: *a* — D = 1.5; *b* — 2.0; *c* — 2.5; *d* — 3.0 mm. EBW conditions: U_{acc} = 60 kV, I_b = 190 mA; v_w = 7.5 mm/s; ΔI_f = 0 mA; l_w = = 200 mm (×2)

The choice of the optimal value of welding speed is determined, on the one hand, by the condition of the minimum intensity of fluid dynamic excitations in the welding pool [10], on the other hand, by the condition of the minimum weld width for reduction of deformations, increase in crack resistance and minimizing the porosity of welded joint. Welding speed significantly affects the penetratability of electron beam and the amount of input energy of welding. In [11, 12] it was shown that in EBW of M1 copper of 12.5 mm with an accelerating voltage U_{acc} = 28 kV, the optimal range of welding speeds is 6–8 mm/s, and at increased welding speeds the instability of penetration depth and the value of lack of fusion at the weld root increases. To specify the effect of welding speed on the amount of input energy, we conducted investigations to determine the nature of the dependence $q/v = f(v_w)$ in the range of welding speed v_w = 5–10 mm/s at an accelerating voltage U_{acc} = 60 kV. As is shown in Figure 3, the value of the input energy in the studied range of welding speed varies significantly: at first it decreases quite sharply in the dependence q/v, and starting from the welding speed v_w = 7.5 mm/s, the decrease slows down. Similarly, the dependence $B_1 = f(v_w)$ varies and at a welding speed v_w = 7.5 mm/s the width of the facial bead of the weld is $B_1 \approx 2.5$ mm/s. Taking into account the data of the work on the porosity of the weld metal [11] and on the basis of the dependences obtained by us, the further investigations were performed at a welding speed v_w = 7.5 mm/s.

The main defect of the weld metal in EBW of copper is porosity. To prevent pores, at first it is necessary to remove oxides, adsorbed moisture and grease films from the surface of welded edges. In a single process cycle of EBW in the UL-209M installation, the adjacent joint area can be additionally cleaned from contaminants and oxides with the help of an electron beam focused on the metal surface with a power that does not lead to melting of the joint edges. In the conditions U_{acc} = 60 kV, I_b ~ 10 mA, v_w = 7.5 mm/s, $D \approx 10$ mm the pass was produced along the entire length of the joint before producing the main welding pass [6].

Metallurgical treatment of the welding pool to eliminate the susceptibility to pore formation in the weld metal and near the fusion line, as well as crystallization cracks in EBW of M1 copper was carried out by inserting foil of aluminium (AD0 alloy, 0.04 mm thickness) and titanium (VT1-00 alloy, 0.05 mm thickness) into the butt, acting as active deoxidizers and nitride-forming elements [13, 14]. By changing the width and thickness of the foil, the problem of dosed supply of these elements to the welding pool was solved. As is shown by experimental welding, the process of EBW of copper using alloying inserts of aluminium and titanium is characterized by a high hydrodynamic stability of welding pool and absence of

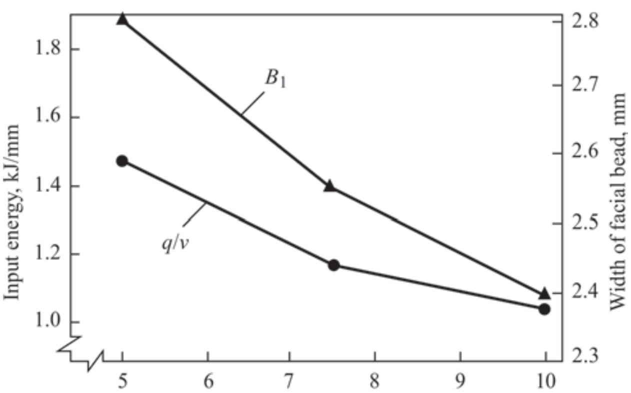

Figure 3. Dependence of the amount of input energy q/v and width of the facial bead in the weld B_1 on the speed of EBW of M1 copper with a thickness δ = 18 mm. EBW conditions: U_{acc} = = 60 kV; ΔI_f = 0 mA; l_w = 200 mm; D = 1.5 mm

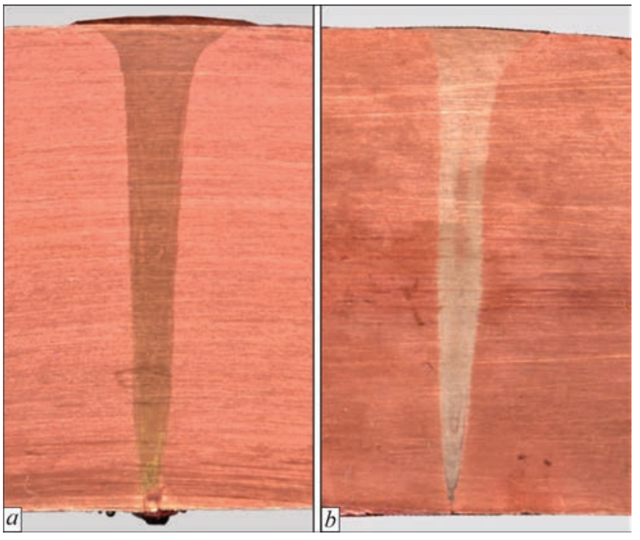

Figure 4. Formation of the weld cross-section with alloying inserts at EBW in the flat position by means of a vertical electron beam of M1 copper (×5): *a* — aluminium foil of AD0 grade with a thickness $\delta = 0.04$ mm; *b* — titanium foil of VT1-00 grade with a thickness $\delta = 0.05$ mm. EBW conditions: $U_{acc} = 60$ kV; $I_b = 197$ mA; $v_w = 7.5$ mm/s; $\Delta I_f = 5$ mA; $l_w = 200$ mm; $D = 1.5$ mm

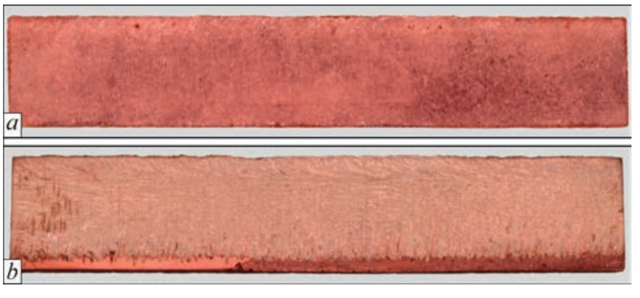

Figure 5. Formation of weld metal in the longitudinal section along the axis of M1 copper with 100 mm length during EBW in the flat position along the butt (×1.5): *a* — without an insert; *b* — with an insert with VT1-00 thickness $\delta = 0.05$ mm. EBW conditions: $U_{acc} = 60$ kV, $I_b = 197$ mA; $v_w = 7.5$ mm/s; $\Delta I_f = 5$ mA; $l_w = 200$ mm; $D = 1.5$ mm

liquid metal spattering, which provides a satisfactory facial bead formation in the weld and the stability of penetration depth along the weld length (Figure 4).

When the composition in the weld metal of aluminium or titanium is in the range of 0.1 wt.% and higher, the porosity can be reduced to a minimum value (lower than 10 mm^2 on the length of the weld being 100 mm), and the welds along the entire length will have a dense macrostructure (Figure 5).

It should be noted that microalloying of the weld, which occurs at this time, on the one hand, allows improving the mechanical properties of welded joints, and on the other hand, it leads to a decrease in thermal [15] and electrical conductivity [16].

Conclusions

1. The use of circular electron beam scanning with a diameter of up to $D = 1.5$ mm in EBW of M1 copper with the thickness $\delta = 18$ mm at an accelerating voltage $U_{acc} = 60$ kV provides the formation of a weld without craters and metal spattering in the near-axial zone.

2. It was established that at EBW of M1 copper with a thickness $\delta = 18$ mm, the optimal welding speed is in the range $v_w = 6$–8 mm/s.

3. Metallurgical treatment of welding pool with inserts of aluminium and titanium foil in EBW of M1 copper with a thickness $\delta = 18$ mm eliminates the susceptibility to pores formation in the weld metal.

1. Kajdalov, A.A., Nazarenko, O.K. (1973) Some problems of theory of electron beam welding. Elektron. *Obrab. Materialov*, **3**, 9–13 [in Russian].
2. Shilov, G.A., Akopyants, K.S., Kasatkin, O.G. (1983) Influence of frequency and diameter of electron beam circular scan on metal penetration in EBW. *Avtomatich. Svarka*, **8**, 25–28 [in Russian].
3. Ryzhkov, F.N., Bashkatov, A.V., Zakomoldin, A.F. et al. (1973) Welding of bronze Br.Kh0.8 and steel EI811 with oscillating electron beam. *Ibid*., **5**, 56–58 [in Russian].
4. Johnson, L.D. (1970) Some observation on the electron-beam welding of copper. *Weld. J.*, 49(**2**), 55–60.
5. Anoshin, V.A., Ilyushenko, V.M., Bondarenko, A.N. et al. (2014) Integrated evaluation of effect of main impurities on weldability of copper. *The Paton Welding J.*, **11**, 24–27.
6. Paton, B.E., Nazarenko, O.K., Nesterenkov, V.M. et al. (2004) Computer control of electron beam welding with multi-coordinate displacements of the gun and workpiece. *Ibid*., **5**, 2–5.
7. Nesterenkov, V.M., Kravchuk, L.A., Arkhangelsky, Yu.A. et al. (2015) Electron beam welding of medium-pressure chamber of gas turbine engine. *Ibid*., **12**, 29–33.
8. Nazarenko, O.K., Kajdalov, A.A., Kovbasenko, S.N. et al. (1987) Electron beam welding. Kiev, Naukova Dumka [in Russian].
9. Skryabinskyi, V.V., Nesterenkov, V.M., Rusynyk, M.O. (2020) Electron beam welding with programming of beam power density distribution. *The Paton Welding J.*, **1**, 49–53. DOI: https://doi.org/10.37434/as2020.01.07
10. Nesterenkov, V.M. (2003) Special features of capillary waves in the vapour-gas channel in electron beam welding of thick metal. *Ibid*., **4**, 7–12.
11. Agarkov, V.Ya. (1980) Electron beam welding of copper (Review). *Avtomatich. Svarka*, **11**, 42–43 [in Russian].
12. Nazarenko, O.K., Agarkov, V.Ya., Ikonnikov, V.I. (1986) Influence of method of edge preparation on weld pore formation in electron beam welding. *Ibid*., **2**, 21–25 [in Russian].
13. Goncharov, A.N., Krivosheya, V.E. (1980) *Effect of alloy additives on weldability of copper. In: Current problems of welding of nonferrous metals*. Kiev, Naukova Dumka, 221–225 [in Russian].
14. Ilyushenko, V.M., Anoshin, V.A., Bondarenko, A.N. et al. (1980) Investigation of influence of additives and a number of alloying elements on crack formation in welding of copper. *Ibid*., 217–221 [in Russian].
15. Kolachev, Ya.L., Livanov, V.A., Elagin, V.I. (1981) *Metals science and heat treatment of nonferrous metals and alloys*. Moscow, Metallurgiya [in Russian].
16. Si, L., Zhou, L., Zhu, X. et al. (2016) Microstructure and property of Cu–2.7Ti–0.15Mg–0.1Ce–0.1Zr alloy treated with a combined aging process. *Mater. Sci. Eng.: A650*, 345–353.

Received 30.11.2020

https://doi.org/10.37434/tpwj2021.02.07

SURFACING PARTS IN UNLOADING DEVICE OF CENTRIFUGAL PUMPS

O.S. Kostornoi, M.O. Laktionov and **K.Yu. Kholosha**
Joint-Stock Company «Research and Design Institute for Atomic and Power Pump Building»
2, 2nd Zaliznychna Str., 40003, Sumy, Ukraine. E-mail: laktionov@vniiaen.sumy.ua

Leveling of axial forces on the shaft of centrifugal pumps depends on characteristics of end slotted rings of the unloading device that determine the stability of a slotted gap between them. This paper presents the methods to improve wear resistance of surfaces mating between a slotted rings by their surfacing with coatings from a composite alloy reinforced by tungsten (relit) carbides. The advantages and disadvantages of electric arc, plasma-powder and furnace surfacing of slotted rings are shown, and a significant improvement in the process at a replacement of chipped tungsten carbide by spherical one is noted. 6 Ref., 4 Figures.

Keywords: *slotted rings, tungsten carbides (relit), wear resistance, arc surfacing, plasma-powder and furnace surfacing*

A feature of the centrifugal pump is the presence of axial force acting on the impeller shaft. In high-pressure multistage centrifugal pumps, one of the ways to balance the large axial forces acting on the rotor is to use a self-regulating automatic unloading device — hydraulic balancing device. It consists of two combined units: rotating unloading disc on the rotor shaft and «pad» fixed in the pump housing. Balancing of axial forces occurs in the process of self-regulation of a slotted end gap between the unloading disc and the «pad» of hydraulic balancing device. The principle of its operation is as follows: during axial movement of the rotor, a slotted end gap between the discharge ring and the «pad» of hydraulic balancing device changes, which entails a change in fluid flow in the hydraulic balancing device and appearance of fluid pressure on the rotor in the opposite axial direction. Thus, the axial forces on the rotor are equalized and its location is restored.

The functional reliability of hydraulic unloading device depends on the stability of dimensions of the end slotted gap between the surfaces of unloading disc and the «pad» of hydraulic balancing device. The optimal gap (0.06–0.10 mm) provides a minimal flowing of the pumped fluid and a slight reduction in the efficiency of the pump [1].

During operation of pumps, a slotted gap and the quality of surfaces connected in a gap zone are influenced by the following factors:

- at starts and stops of the pump, the gap can decrease to zero, that will lead to wear of contact surfaces;
- probability of contact of the rotor with the stator because of a high level of vibrations or deformations of the rotor during operation, especially in the transient conditions, can lead to tear or seizure of the metal of contact surfaces;
- presence of suspended particles in the pumped fluid leads to erosive wear of slotted gap surfaces;
- specific medium in fluid can cause corrosion wear on the surfaces of parts in the area of a slotted gap.

The wear of parts in the area of an end slotted gap caused a need in replacing the units of hydraulic balancing device. Therefore, a rational designing solution was the use of so-called slotted rings in the area of an end slotted gap, which are attached to the unloading disc and the «pad» of hydraulic balancing device.

In order to minimize the influence of these factors on the end gap of hydraulic balancing device in pump building, a special attention is paid to the choice of materials for manufacture of slotted rings. These materials should have a high resistance to tear and possible seizure of contact surfaces. The loss of metal in the gap zone as a result of corrosion or erosion corrosion should be insignificant during operation to avoid increase in the gap, reduction in the efficiency of the pump and rotor damping.

The hardness of rings in the area of a slotted gap can be adjusted in a wide range, using not only different base materials, but also using different methods of surfacing wear-resistant surface layer [2, 3]. The joint-stock Company «Research and Design Institute for Atomic and Power Pump Building» (JSC «VNDIAEN») in its developments of centrifugal pumps for the oil industrial complex used mainly arc surfacing of slotted rings with alloys based on cobalt type Stellite 6. For example, such surfacing was used in manufacture of serial centrifugal pumps of TsNS-180 type for pumping water into oil pools in order to maintain a pool pressure. However, in many fields, where quite aggressive and contaminated reservoir waters with solid particles are used, the rings of hydraulic balancing device, which were manufactured of steel 12Kh18N12M3T and deposited with Stellite 6, had a limited service life during operation.

It is known [4] that during the work with fluids containing abrasive particles, rings of tungsten carbide are successfully used. Also during surfacing of drill pipes operating in the conditions of intensive wear, a high efficiency was shown by a composite alloy based on cast tungsten carbides (further relit). Because of the growing requirements to the reliability of hydraulic balancing devices of pumps, the studies on surfacing of slotted rings of end sealing with a composite alloy reinforced by relit (further relit) were performed.

The process of surfacing with relit has two stages: dilution of welding pool on the basis of chromium-nickel alloy (matrix) and at the same time supply of relit grains to the welding pool. Relit grains have high hardness, high melting point values and specific weight. Slotted rings of end sealing are deposited in the flat position, which significantly simplifies the reinforcement of the matrix.

Initially, the works with relit surfacing were performed in relation to the pumps TsNS-180 on the rings of steel grade 12Kh18N12M3T with a diameter of 250/150 mm and a thickness of 27 mm. For experiments and implementation of the process of electric arc surfacing, the robotic complex Limat-RT280 was used, as a matrix material, welding wire Sv-07Kh25N13 with a diameter of 1.6 mm, as a reinforcing phase, chipped relit of grade «Z» according to TS U 322-19-005–96 were used.

In the process of testing the technology of electric arc surfacing, the following issues were solved:

• dosing device to supply chipped relit was designed;

• place and angle of supplying relit to the welding pool were determined;

• amount of relit in the composite alloy was optimized;

• optimal surfacing conditions were selected.

The influence of different factors on the quality of surfacing was evaluated on macrosections by the amount of relit on the working surface of slotted rings and by the absence of defects in the deposited metal (Figure 1).

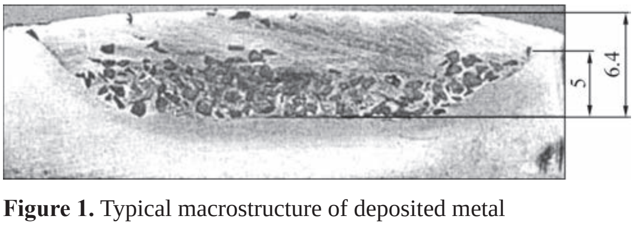

Figure 1. Typical macrostructure of deposited metal

The performed experimental works allowed providing:

• by more than 40 % higher content of relit in the deposited metal after mechanical treatment of deposited layer to a height of 2–3 mm;

• good wettability of relit grains with chromium-nickel metal in the welding pool;

• absence of cracks and other defects in the deposited metal.

The developed technology was successfully implemented and provided a significant increase in wear resistance of slotted rings in unloading device of centrifugal pumps in terms of providing the content of relit on working surfaces of at least 40 %.

However, chipped relit has a number of disadvantages associated with the technology of its production. A significant part of relit grains is characterized by heterogeneity of composition, nonequiaxiality and sharpness of shapes, as well as the presence of cracks. Ultimately, this negatively affects the serviceability of deposited composite layers [5]. This problem was solved after industrial development of the technology for producing a spherical shape relit. Such relit has a spherical shape of a set grain-size composition, which provides maximum flowability and, accordingly, reliable operation of dosing devices relit. Stable stoichiometric composition and fine-globular structure foster an increase in hardness and strength of spherical tungsten carbide granules [5]. These factors led to a widespread use of spherical relit for plasma-powder surfacing of different wear-resistant parts.

Plasma-powder surfacing of slotted rings in unloading device of pumps was performed in robotic specialized equipment of the Plasma-Master Company (Figure 2). Surfacing was performed on a ring of steel 08Kh21N6M2T with a diameter of 358/278 and a thickness of 30 mm. Welding materials: spherical tungsten carbide of grade KVS-1 according to TSU 24.1-19482355-001, matrix binding is the powder of grade PG-SR2 according to GOST 21448–75. The self-fusing alloy PG-SR2 on nickel base has a low melting point (1000–1100 °C), well moistens relit grains and has a high wear resistance [6].

In the process of testing the surfacing technology, the optimal process conditions, scheme of supplying relit and matrix powder were determined. The content of relit in the mixture was maintained at about 50 vol.%. According to data of [6], exceeding the specified optimal content of relit causes a significant increase in the surfacing current, which causes a marked dissolution of relit particles, embrittlement of matrix and, as a consequence, a reduced wear resistance. The microhardness of undissolved relit particles is 180–190 MPa, for semi-dissolved relit par-

Figure 2. Installation PM-302 for plasma-powder surfacing

ticles it is 130–160 MPa [6]. The macrohardness of surfacing after grinding of its surface to the working height (2–3 mm) is within *HRC* 50–56. The content of relit on the working surface of depsoited metal is more than 50 vol.% (Figure 3). The developed technology provides a high quality of deposited rings (Figure 4) and is successfully realized in pump building.

The abovementioned surfacing technologies allow producing composite layers with the reinforcement by tungsten carbides in the amount of 40–60 vol.% on the working surface of slotted rings. In addition to these methods of surfacing, while producing composite layers, the furnace method of surfacing is currently used. During furnace surfacing, relit grains are uniformly distributed in the composite layer and their partial melting is almost absent. For furnace surfacing of slotted rings, grain relit according to TS U 322-19-005–96 was used, and as a binder, chromium-nickel powders according to TS U 323-19-004–96 were used. The working thickness of the coating is 1.5–2.0 mm. The volume fraction of relit grains in a wear-resistant coating is in the range of 80–90 %.

In the domestic pump building, all three methods of applying a composite layer to slotted rings reinforced with relit are used: electric arc, plasma-powder and furnace surfacing. The choice of surfacing method is determined by production capabilities, operating conditions of pumps and economic factors. In the technological process of electric arc surfacing of slotted rings mainly universal welding equipment is used: small-sized manipulator, welding head with oscillating mechanism and dosing device for relit supply. Plasma-powder surfacing was initially introduced in the equipment of the Plasma-Master Company with

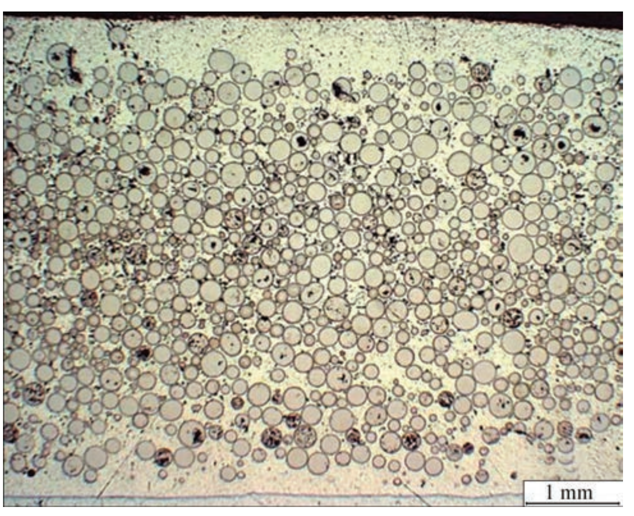

Figure 3. Microstructure of metal deposited by plasma-powder method using spherical relit

Figure 4. Slotted ring deposited by plasma-powder method

the use of spherical relit. The cost of spherical relit is much higher than chipped one, but in general, the advantages of using this process are obvious:

- stability, high manufacturability of surfacing process;
- uniform distribution of relit grains on the working surface of slotted rings;
- significant reduction in the amount of melted grains of relit;
- matrix binder on nickel base by itself has a high wear resistance;
- absence of defects inherent in the grains of chipped relit.

A composite wear-resistant layer reinforced with a spherical relit in the amount of not less than 50 vol.% in plasma-powder surfacing of slotted rings increases service life of pumps also in the conditions of growing loads and increase in corrosion and erosion influence.

Furnace surfacing is a rather complex technological process, but as to the advantages of the plasma-powder method it adds an important property of a composite deposited metal — it provides a more dense packing of relit in the matrix melt. The presence of more than 80 % of spherical relit on the working surface of slotted rings significantly improves their wear resistance and allows them to be successfully used during operation of pumps in rigid conditions.

Under the same operating conditions of pumps, the service life of end slotted rings have a successive significant growth when using surfacing with alloys based on cobalt of type Stellite 6; composite alloys reinforced by relit — electric arc, plasma-powder and furnace method. In this case, much better results were obtained when as a solid phase spherical relit was used.

1. Maliushenko, V.V., Mikhailov, O.K. (1981) *Energy pumps:* Refer. Book. Moscow, Energoizdat, 23–29 [in Ukrainian].
2. Ryabtsev, I.O., Senchenkov, I.K. (2013) *Theory and practice of surfacing works*. Kyiv, Ekotekhnologiya [in Ukrainian].
3. Kostornoy, O.S., Laktionov, M.O. (2020) Arc and plasma-powder surfacing of sealing surfaces of pump impellers. *The Paton Welding J.*, **1**, 57–60. DOI: https://doi.org/10.37434/as2020.02.10
4. Gulich, J. (2008, 2010) *Centrifugal Pumps*, Second Ed.
5. Zhudra, A.P. (2014) Tungsten carbide based cladding materials. *Ibid*., **6–7**, 69–74.
6. Som, A.I. (2004) Plasma-powder surfacing of composite alloys based on cast tungsten carbides. *Ibid*., **10**, 43–47.

Received 10.12.2021

https://doi.org/10.37434/tpwj2021.02.08

HYGIENIC CHARACTERISTICS OF WORKING ZONE AIR IN ARC WELDING OF COPPER AND ITS ALLOYS (Review)

O.M. Bezushko[1], **O.G. Levchenko**[2], **T.B. Maidanchuk**[1], **A.O. Lukyanenko**[1] and **O.M. Goncharova**[1]

[1]E.O. Paton Electric Welding Institute of the NAS of Ukraine
11 Kazymyr Malevych Str., 03150, Kyiv, Ukraine. E-mail: office@paton.kiev.ua
[2]National Technical University of Ukraine «Igor Sikorsky Kyiv Polytechnic Institute»
37 Peremohy Prosp., 03056, Kyiv, Ukraine. E-mail: mail@kpi.ua

A literature review of harmful substances formed in arc welding of copper and its alloys is presented. Literature data on studying emissions of welding aerosols in welding of copper and copper alloys are considered. It is shown that to create new grades of welding materials that would satisfy not only their welding technology, but also sanitary and hygienic characteristics, it is necessary to continue the study of chemical composition and levels of emissions of welding aerosols using modern standardized international procedures. 13 Ref., 1 Table.

K e y w o r d s : *copper, copper alloys, welding, brass, bronzes, welding aerosol, harmful substances, toxicity*

In terms of world production and consumption, copper and its alloys rank third after iron and aluminium. Such a wide demand is associated with the properties of this metal and its alloys [1]. Copper is a ductile metal with a high thermal conductivity and a low electrical resistance, copper alloys have high antifriction properties, as well as high corrosion resistance, including in seawater. This determines a widespread use of copper and its alloys in electrical and chemical industries, in shipbuilding and cryogenic engineering, in instrument making, metallurgical and other industries. The most widely used methods of welding and surfacing of copper and its alloys are arc welding methods (manual arc welding with coated electrodes (MMA), TIG and MIG welding in shielding gases, submerged-arc welding (SAW). The use of these processes is associated with harmful and dangerous production factors affecting welder.

Despite the significantly lower emissions of harmful substances [2] during TIG, MIG and especially submerged-arc (SAW) welding in shielding gases, in industry most often the process of manual arc welding with coated electrodes (MMA) is used, which is accompanied by a considerable emission of welding aerosol (WA) into the zone of welder's breathing (in manual arc welding using electrodes coated with aluminium bronze, specific aerosol emissions are 2–4 times higher, and the content of manganese oxides is higher by 1.5–2.0 times than during mechanized welding in argon [3]). In WA such chemical elements as copper, manganese oxides, fluorides, aluminium, zinc oxides, lead, phosphorus, ammonia and other may be present. WA has an irritating effect on human body and in some cases may cause oncology diseases. In particular, fluorides and oxides of manganese cause inflammation of mucous membrane and nervous disorders, lead provokes nausea, gastric, intestinal, nervous and kidney diseases, copper causes metal fume fever, aluminium oxides are accumulated in lungs, nickel oxides cause cancer of breathing passages [4].

The aim of the work is to analyze the existing data on harmful substances that contaminate air of industrial premises during arc welding and surfacing of copper and its alloys using coated electrodes.

The implementation of measures to improve the labor conditions of welding production workers is based on the analysis of data on chemical composition, emission levels and toxicity of WA. For this purpose, the primary sanitary and hygienic evaluation of welding materials applying the method of WA capture and determination of their quantity and chemical composition is carried out. At the same time, such sanitary and hygienic indices are used as intensity of formation (g/min) and specific emission of WA (g/kg of welding material). In addition, to evaluate the toxicity of WA or degree of impact on human body the following indices are used: threshold limit value (TLV) of harmful substances, the required volume of

O.M. Bezushko — https://orcid.org/0000-0002-6148-1675, O.G. Levchenko — https://orcid.org/0000-0002-9737-7212
T.B. Maidanchuk — https://orcid.org/0000-0002-2826-8514, A.O. Lukyanenko — https://orcid.org/0000-0002-0632-4984
O.M. Goncharova — https://orcid.org/0000-0002-5213-6300

TLV of harmful gases and aerosols in the air of welding workshops in arc welding of copper and its alloys [7]

Number	Description of substance	TLV, mg/m^3	Predominant condition in the production environment	Hazard category	Peculiarities of effect on human body
1	Nitrogen dioxide	2	f	3	O
2	Nitrogen oxide	5	f	3	O
3	Ozone	0.1	f	1	O
4	Salts of hydrofluoric acid (according to F): fluorides of Al, Mg, Ca, Cu and Sr	2.5/0.5	a	3	
5	Manganese in WA at its content: a) up to 20 % b) from 20 %	 0.2 0.1	 a a	 2 2	
6	Oxides of manganese (in terms of MnO_2): a) disintegration of aerosol b) condensation of aerosol	 0.3 0.05	 a a	 2 1	
7	Nickel, nickel oxides, sulfides and mixtures of nickel compounds	0.05	a	1	K, A
8	Hydrogen fluoride (in terms of F)	0.5/0.1	f	1	O
9	Copper	1/0.5	a	2	
10	Magnesium oxide	4	a	4	
11	Zinc oxide	0.5	a	2	
12	Aluminium and its alloys (in terms of Al)	2	0	3	F
13	Beryllium and its compounds (in terms of Be)	0.001	a	1	K, A
14	Lead and its inorganic compounds (in term of lead)	0.01/0.005	a	1	

Note. 1. If in the column «TLV» two values are given, it means that in the numerator TLV is the maximum and in the denominator it is the average variable. 2. Symbols: f — fumes and/or gases; a — aerosol; a + f — mixture of fumes and aerosols. 3. O — substances with a sharply directed mechanism of action that require automechanical control of their content in the air. A — substances that may cause allergic diseases in the working conditions. K — carcinogens. F — aerosols of mainly fibrogenic action.

air to dilute to TLV, expressed in m^3/h (per a unit of time) according to the international procedure [5]. In domestic practice, the index of air exchange of general exchange ventilation (i.e. the volume of air that should be supplied to the production room to dilute harmful WA substances to TLV) is used, expressed in m^3/kg of welding material.

The information on emissions of WA and gases in arc welding of copper, bronze, brass, and also copper-nickel alloys is very limited, and generalized data are absent. TLV of some harmful chemical elements, that may be in the composition of WA, formed during arc welding of copper and its alloys, are given in Table. These data are necessary for calculations of necessary air exchange of mechanical ventilation.

Coated electrodes for welding copper are manufactured of elongated (cold-deformed) wire or round elongated and pressed rods. The chemical composition of welding wire and rods of copper and copper-based alloys, regulated by the standard [6], depending on the grade may have a different amount of alloying elements and impurities (Si, Mn, Ag, Cr, Bi, Sb, As, Fe, Ni, Pb, Sn, Zn, S, P, O_2). In welding copper, electrodes Komsomolets-100 are the most widely used. The main toxic component of WA, which determines the required air exchange, is manganese. According to the degree of impact on human body, manganese belongs to the 2nd hazard category, i.e. it is highly toxic. The content of manganese oxides (in terms of Mn) in WA during melting of electrodes Komsomolets-100 is 3.9 g/kg, and the threshold limit value in the air of the working zone is 0.3 mg/m^3. According to the hygienic regulations of chemical substances in the air of the working zone [7], the threshold limit value of copper and its oxides in the air at the level of respiratory organs should not exceed 1 mg/m^3. The amount of air required to dissolve the aerosol to TLV in welding using electrodes Komsomolets-100 should be at least 13000 m^3/kg.

In industry the following bronzes are widely used: aluminium (4.0–11.5 % of Al), tin (2–10 % of Sn) [8, 9], manganese (4.5–5.5 % of Mn), silicon (0.5–3.5 %

of Si), beryllium (1.9–2.2 % of Be) and chromium (0.4–1 % of Cr).

In [3], the results of tests of electrodes for welding complexly-alloyed bronzes of the Cu–Al–Ni–Mn–Fe system are presented. Two grades of electrodes LKZ-AB and LKZ-ABN were tested. Electrodes of grades LKZ-AB and LKZ-ABN differ in the feature that the first are manufactured with the rods from the rolled bars of BrANMtsZh8-3-4-1 bronze and the second are with the rods from the wire BrAMts9-2. In this case, alloying of the deposited metal with nickel and iron is performed through the coating. The specific emissions of aerosol during alloying of the deposited metal through the coating (electrodes LKZ-ABN) are 2 times higher than without alloying (electrodes LKZ-AB). Therefore, in terms of sanitary and hygienic properties, the use of electrodes with alloying coatings in welding and surfacing of bronze is not rational. Two grades of electrodes such as Nicolium (BrANZhMts9-5-4-1.5) for welding bronze and Superston (BrAMtsZhN8-12-3-2) for welding bronze were also tested. The electrodes were manufactured of rods of the same composition as the base metal (respectively), and on the rods the coating of the base type was deposited. It should be noted that despite the differences in the composition of the electrode rods BrANMtsZh8-3-4-1 and BrANZhMts9-5-4-1,5 and the applied welding conditions, approximately the same average values of the total emission of WA (21.3 and 25.0 g/kg) were obtained.

Investigations of sanitary and hygienic characteristics of the electrodes designed by the Saint-Petersburg State Institute of Technology, which are used for welding of aluminium complexly-alloyed bronzes (grades LPI-73, LPI-48-AB2, LPI-13, LPI-LKZ-ATs and LPI-LKZ-ATsK), were carried out by the Laboratory of Occupational Health and Ergonomics of the Research Institute for Labor Protection [3]. It should be noted that the specific emissions of WA during welding using all tested grades of electrodes are 18–25 g/kg, i.e. vary within relatively low limits despite significant differences in the composition and type of coatings, as well as used welding conditions. Exceptions are the electrodes of grade LKZ-ABN in which alloying of the deposited metal by nickel and iron is carried out through the coating. In this case, specific emissions of aerosol reach 40 g/kg, i.e. they increase by 1.5–2.0 times. In [3] the need in alloying metal of welds and deposits through the rods of electrodes instead of coatings is recommended to reduce the formation of welding aerosol and improve the sanitary characteristics of electrodes for manual arc welding of not only nonferrous but also ferrous metals.

The obtained results of hygienic evaluation of electrodes for welding of aluminium bronzes with unalloying coating allow concluding that the average value of specific emissions of aerosol is 20 g/kg of consumed electrodes. Large differences in the concentration of welding aerosol (WA) are predetermined by different sampling points (in front of the welder face shield and under the welder face shield), which makes them incompatible.

According to the results of hygienic evaluation of LPI-73 electrodes concerning justification of the hygienic certificate, the following data on the concentration of welding aerosol in the working zone are given (mg/m^3):

- during switched off ventilation in front of the welder face shield it is 111.1, and under the welder face shield it is 54.6;
- during operation of local exhaust ventilation in front of the welder face shield it is 15.7, and under the welder face shield it is 3.1.

Comparison of the results of the concentration of aerosol emitted during welding using bronze Superston and Nicolium electrodes, allows suggesting that the dust samples were taken under the welder face shield during the switched off exhaust ventilation. In this case the results are approximately the same (mg/m^3): 54.6 for LPI-73 electrodes; 39.0 for Superston electrodes; 41.0 for Nicolium electrodes.

Arc welding of brasses using coated electrodes is characterized by particularly unfavorable sanitary and hygienic conditions because of evaporation of zinc. According to the degree of impact on human body, zinc oxide belongs to the 2nd category of hazard, i.e. it is a hazardous substance. According to the requirements, the threshold limit value of ZnO in the air of the working zone should not exceed 0.5 mg/m^3. At the same time, the specific emissions of aerosols and gases in arc welding of brasses are much less studied than in welding of other nonferrous metals (for example, bronze and aluminium alloys) and such data are almost absent in the reference and technical literature. It was noted that a total emission of aerosol in welding using brass electrodes, the rods of which are made of brass LMtsZh55-3-1 reaches 211 g/kg of molten electrodes (coatings and welding conditions are not specified). This is 5 times higher than in welding of steels with the most toxic electrodes with acidic type coatings (up to 40 g/kg) and 10–20 times higher than in welding using electrodes with the coatings of basic, cellulose and rutile types (10–20 g/kg). It is quite obvious that this is mainly predetermined by evaporation of zinc, the boiling point of which (907 °C) is close to the melting point of brass.

A high fraction of zinc oxides in the composition of WA, which is formed during arc welding of brass, is confirmed by the data of [3]. Even in nitrogen-arc welding of L90 brass with M3r copper by a nonconsumable tungsten electrode using filler wire BrKMts3-1, the total amount of emitted aerosol was 48 g/kg, and the content of zinc oxide (ZnO) in it was 13.9 g/kg, i.e. 30 %. It should be taken into account that such a large amount of ZnO in the aerosol was formed in melting only the base metal. Based on the calculations of the authors, in order to bring the content of toxic elements to the threshold limit value, the specific air exchange in this case should be 27 200 m^3/kg. During melting of brass electrodes and the base metal, the total amount of the formed aerosol and the content of ZnO in it grow by several times. Therefore, respectively, it is necessary to increase the required air exchange of supply and exhaust ventilation to provide TLV.

Studies of sanitary and hygienic characteristics of electrodes of grades LPI-LKZ-ATs and LPI-LKZ-ATsK, designed for welding bronze of the system Si–Al–Zn (BrATsKZh8-6-0.3-0.3) with a high damping capacity, were carried out. The rods of LPI-LKZ-ATs electrodes are manufactured of rods of the same composition with the base metal, which contains in average 6 % of zinc. The rods of LPI-LKZ-ATsK electrodes are manufactured of BrAMts9-2 bronze, on which a unalloyed coating is deposited, and zinc is introduced into the deposited metal through spiral or shell made of L63 or LK62-0.5 brass, put on the coated part of electrode. Hygienic evaluation of aerosols of both grades of electrodes was performed on the content of copper and zinc oxides (total dust level was not determined).

Relatively low melting and boiling points of zinc during arc welding using coated electrodes (420 and 907 °C, respectively) lead to its losses on WA and spattering at the drop stage from 30 to 60 %. This is predetermined by a high content of formed zinc oxide in WA (9–11 g/kg). In this case, the content of copper oxides in WA during welding using electrodes of grades LPI-LKZ-ATs and LPI-LKZ-ATsK is 6.1–6.5 g/kg, i.e. it is at the level of the content of copper oxides in the emitted aerosol during welding using electrodes of grades LKZ-AB and LKZ-ABN (5.25–7.55 g/kg).

In the technical literature, not enough information is available concerning sanitary and hygienic characteristics of arc welding of tin bronzes. At the PWI, the electrodes of grade ANBO were designed [10–12]. Their coating has a specific composition, associated with the presence of chemically active components of sodium salts (hexafluorosilicate, hexafluoroaluminate and fluorides) relative to the binder (liquid glass), as well as nontraditional metal components (tin, copper-phosphorus powders). For the study, standard (sodium, potassium and mixed sodium and potassium) experimental lithium-containing samples of liquid glass were prepared, which provide unique properties to some types of electrodes [10, 13]. Sanitary and hygienic characteristics of the electrodes were evaluated according to the intensity of V_a formation and the specific emission of G_a WA. Determination of the intensity of formation and specific emission of WA was performed applying gravimetric method. The lowest levels of WA emission are achieved in welding with electrodes manufactured using sodium-lithium glass (V_a = 0.393 g/min, G_a = 8.71 g/kg). The electrodes close to them in terms of WA emission are manufactured of sodium-potassium and lithium binders. In terms of sanitary-hygienic indices, electrodes on potassium and potassium-lithium binder are the most favorable. Thus, for example, the intensity of formation and specific emissions in electrodes manufactured on potassium binder are, respectively, 22.0 and 23.6 % higher than in the electrodes on sodium-potassium glass. In terms of sanitary and hygienic properties, the electrodes manufactured on K-Na and Na binders, occupy intermediate positions between two extreme groups of electrodes [4].

Sanitary and hygienic characteristics of electrodes for welding copper-nickel alloys are absent in the technical literature.

In beryllium bronze the most toxic element is beryllium: its TLV amounts to 0.001 mg/m^3, and its hazard category is –1. Therefore, it can be welded only in closed chambers with exhaust ventilation at an air velocity in the working hole of the chamber not lower than 1 m/s, and the outlets of vacuum pumps should be connected to local ventilation. After welding of beryllium bronze, the chamber is cleaned with a 5 % hydrochloric acid solution with a switched on local exhaust ventilation and with the use of Lepestok respirator.

To reduce the concentration of WA in the zone of welder's breathing, local dust and gas receivers should be placed directly at the workplace, and the capacity of stationary or mobile ventilation devices should be at least 1000 m^3/h [2].

As the literature review showed, arc welding of copper and its alloys is accompanied by a significant emission of welding aerosol into the working zone of welder. The data on investigation of WA toxicity for arc welding methods are almost absent.

Comparative hygienic evaluation of welding methods was performed according to the value of ventilation air exchange (m^3/kg). But this value is not objective and does not provide us a complete picture of WA toxicity.

According to the international standards DSTU ISO 15011, welding consumables should be constantly inspected for compliance with the indices of labor safety (chemical composition, level of emissions, toxicity and hygienic class of welding aerosols). Therefore, to create new grades of welding consumables, that would satisfy not only their welding technological, but also sanitary and hygienic characteristics, it is necessary to continue the study of chemical composition and levels of emissions of welding aerosols with the use of modern standardized international procedures DSTU ISO 10882-1:2008, DSTU ISO 10882-2:2008, DSTU ISO 15011-1:2008, DSTU ISO 15011-2:2008 and DSTU ISO 15011-4:2008.

1. Osintsev. O.E., Fedorov, V.N. (2004) *Copper and copper alloys. National and foreign grades: Refer. book.* Moscow, Mashinostroenie [in Russian].
2. Bykovskyi, O.G. (2011) *Welding and cutting of nonferrous metals: Refer. book.* Kyiv, Osnova [in Ukrainian].
3. Zaks, I.A. (1999) *Electrodes for arc welding of nonferrous metals and alloys.* Saint-Petersburg, Strojizdat [in Russian].
4. Levchenko, O.G., Lukianenko, A.O., Demetska, O.V., Arlamov, O.Y. (2018) Influence of composition of binder of electrodes coating on cytotoxicity of welding aerosols. *Mat. Sci. Forum*, **927**, 86–92.
5. (2011) DSTU ISO 15011-4:2008. *Health and safety in welding and allied processes. Laboratory method for sampling aerosols and gases.* Pt 4: Form for recording data on aerosols. Ed. by O.Bezushko, Yu. Bondarenko et al. Valid from 2008.08.15. Kyiv, Derzhspozhyvstandart Ukrainy [in Ukrainian].
6. (1979) GOST 859–2014: *Copper. Grades.* Valid from 1979.01.01. Group V51. Moscow, Interstate standard [in Russian].
7. (2020) *Hygiene chemicals regulations in the air of the working zone. Law 1596 of 14.07.2020,* Ministry of Health of Ukraine. URL:https://zakon.rada.gov.ua/laws/show/z0741-20#Text.
8. Ponomarenko, O.I., Shinsky, I.O., Morgun, N.N. (2004) Casting by consumable patterns of bronze alloys. *Litejnoe Proizvodstvo*, **11**, 30 [in Russian].
9. Ponomarenko, O.I., Lysenko, T.V., Stanovsky, A.L., Shinsky, O.I. (2012) *Control of casting systems and processes.* Kharkov, NTU KhPI [in Russian].
10. Majdanchuk, T.B., Skorina, N.V. (2014) Improvement of adaptability to fabrication and welding properties of electrodes for tin bronze welding and surfacing. *The Paton Welding J.*, **6–7**, 176–181.
11. Ilyushenko, V.M., Anoshin, V.A., Skorina, N.V., Majdanchuk, T.B. (2013) Selection of slag-forming base of electrode coating for arc welding and surfacing of cast tin bronzes. In: *Proc. of 7th Sci.-Techn. Conf. of Young Scientists and Specialists on Welding and Related Technologies (22–24 May 2013, Kiev, Ukraine)*. Kiev, PWI, 155.
12. Ilyushenko, V.M., Anoshin, V.A., Bondarenko, A.N. et al. (2013) Development of electrode materials for welding and surfacing of complexly-alloyed bronzes. In*: Proc. of Abstracts of Int. Conf. on Welding and Related Technologies – Present and Future (25–26 November 2013, Kiev. Ukraine)*. Kiev, PWI, 72–73.
13. Skorina, N.V., Kisilev, M.O., Paltsevich, A.P., Levchenko, O.G. (2011) Properties of lithium-containing liquid glasses for production of welding electrodes. In: *Proc. of 4th Int. Conf. on Welding Consumables of CIS countries.* Krasnodar, 75–82.

Received 03.12.2021

https://doi.org/10.37434/tpwj2021.02.09

ACOUSTIC EMISSION METHOD AT EVALUATION OF THE STATE OF WELDS AND THEIR SERVICE PROPERTIES. PART 1. EFFECT OF WELDED JOINT TYPE ON ACOUSTIC EMISSION

S.A. Nedoseka, A.Ya. Nedoseka, M.A. Yaremenko, O.I. Boichuk and **M.A. Ovsienko**
E.O. Paton Electric Welding Institute of the NAS of Ukraine
11 Kazymyr Malevych Str., 03150, Kyiv, Ukraine. E-mail: E-mail: inpat59@ukr.net

The majority of existing structures have welded joints. It is of considerable interest to determine the differences in acoustic emission for various types of welded joints and change of the properties of materials in operating structures, which have welded elements, after long-term service, taking into account the time and probable violation of service conditions. The data of testing samples from such materials demonstrate the high sensitivity of acoustic emission method to welded joint type, and to changes of weld service properties. 9 Ref., 2 Tables, 14 Figures.

Keywords: welds, service properties, acoustic emission (AE), AE activity, damage, material destruction, loading, prediction

Service properties of the material are characteristics, which are revealed at material operation directly in the real structures. They are much more diverse that those, which are determined for the material at standard laboratory testing of the samples.

Note that the welded joints always are a source of initiation and development of defects, due to introduction of a great part of the defects into the material directly during welding, as well as generation of residual stresses.

Part 1 deals with the features and differences in AE parameters for welded joints of different types.

Irrespective of the kind of defects in welded joint area and causes for their appearance, be those pores (Figure 1), cracks, lacks-of-penetration or another factor, they are potential sources of material destruction. In this connection, the welded joint area requires priority control at performance of technical diagnostics. Determination of the real residual life of the material and its load-carrying capacity should be also based on assessment of the life and load-carrying capacity of the welded joint. Comparison of base metal properties and those of welded joint metal allows a more accurate estimate of the controlled product condition than just monitoring the base metal state. This work deals exactly with these important issues in the following order:

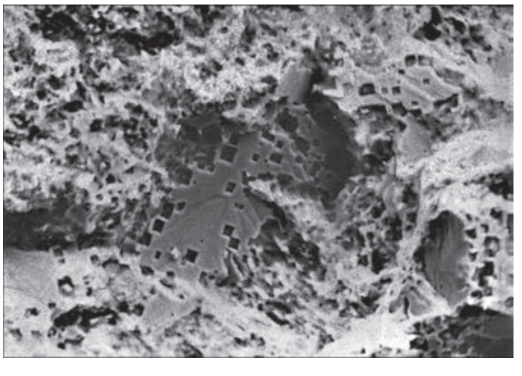

Figure 1. Pores in the weld, formed because of poor welding quality

1. Determination of the differences in AE at rupture testing of samples with welded joints of different types and selection of the most informative parameter that characterizes damage accumulation during deformation.

2. Determination of differences in AE for samples from metal with welded joints from AE for metal without them. Defining the parameter, which will allow determination of presence of welded joints in the tested sample.

3. Checking the efficiency of algorithms for prediction of the destruction, incorporated into the software of EMA type systems, on samples with different types of welded joints.

It should be noted that this paper generalizes the results of testing performed in different years using EMA systems from the 1st to the 3rd generations, which have such differences in presenting the amplitude and noise characteristics of AE signals, as application of the linear and logarithmic amplification modes, respectively. Despite that, the objectives set forth in the paper, have been reached, in particular, due to the fact that, as shown by the conducted research, the absolute values

S.A. Nedoseka — https://orcid.org/0000-0002-3239-381X, A.Ya. Nedoseka — https://orcid.org/0000-0001-9036-1413,
M.A. Yaremenko — https://orcid.org/0000-0001-9973-4482, O.I. Boichuk — https://orcid.org/0000-0001-5800-1549,
M.A. Ovsienko — https://orcid.org/0000-0002-2202-827X

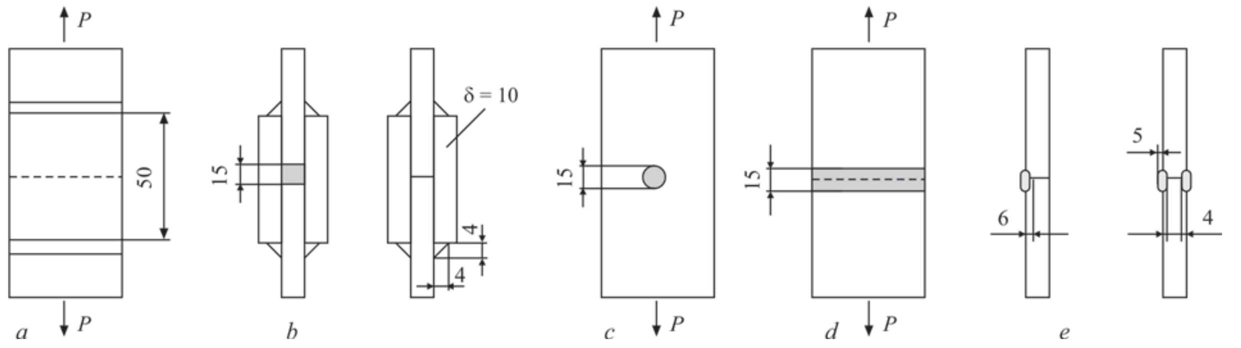

Figure 2. Schemes of welded joints testing (for *a*–*e* description see the text)

of AE signal amplitudes are not of principal importance for evaluation of the state of materials and prediction of their fracture. Somewhat more important, although not decisive, either, is the nature of their relative change during deformation and damage accumulation.

In order to solve the posed tasks, it was proposed to conduct a number of tests of 17GS steel samples, in order to reveal the differences in AE parameters, which develops at fracture of material with different welded joints. Series of samples with a transverse cut and several types of welded joints were prepared (Figure 2):

- *a* — with a transverse weld and two-sided cover plates welded to the sample surface;
- *b* — with two-sided cover plates welded to the sample surface;
- *c* — with a spot welded joint;
- *d* — with one-sided transverse weld;
- *e* — with two-sided transverse weld.

Welded joints were made by manual electric arc welding, with 3 mm UONI-13 electrode type.

Standard samples of the first type [1] were used for AE testing, in order to study the state of pipe materials (Figure 3). A tensile testing machine R-20 with a hydraulic drive was used for sample testing.

AE system EMA-2 with linear layout of a four-transducer array on the sample was used (Figure 3). Data processing was performed, using modern EMA-3.92 program. The distance between the transducer centers was equal to 110 mm, controlled zone was 140 mm (70 mm to the left and right from the sample center). Data were processed using cluster analysis during testing and at post-experimental processing. AE events that passed screening by the coordinate characteristic were combined into clusters. The cluster radius was 20 mm that allowed tracing AE localization centers along the sample length within the controlled zone. AE signals were recorded in the range of 100–1000 kHz.

The most typical test results are presented in the form of graphs in Figures 4–8. In them blue lines were used to plot a bar graph of AE event amplitudes (*A*, mV), red lines — a linear graph of loading on the sample (*P*, kg), black — point chart of «Rise time» parameter (*R*, μs), which characterizes the time of the signal rising to a maximum, violet — a linear graph of the total number of AE events (*N*, dimesionless). The abscissa shows the time from the start of the test.

Testing showed that the highest breaking load of 70–95 kN (7000–9500 kg) is characteristic for samples of *d* series, and the lowest of approximately 26 kN (≈2600 kg) — for *e* series. This is quite natural, as the material cross-section area in the working part in such a welded joint is smaller than for other samples. Moreover, off-center tension and bending are realized simultaneously during sample loading. The number of AE signals for samples of this series is small that can be clarified by the following factors:

- less damage introduced by welding;
- occurrence of the majority of AE events already during the cracking process, that is indicated by AE appearance at loads close to breaking ones and high, close to 500 mV amplitudes that are maximum for AE instruments of EMA-2 type.

A characteristic feature is absence of the same acoustic pattern for samples within each of the series, except for samples with a welded spot in *c* series and samples with a two-sided weld of *e* series.

Samples in *b* series are the most different. They failed first in one weld, then in another one. Testing was interrupted after breaking of one of the welds. The number of events for these samples differs 4.5 times, and maximum amplitudes —– by 2 times.

For samples with the welded spot (series *c*) and samples with a two-sided transverse weld (series *e*) acoustic emission was observed in an area of rounding-off

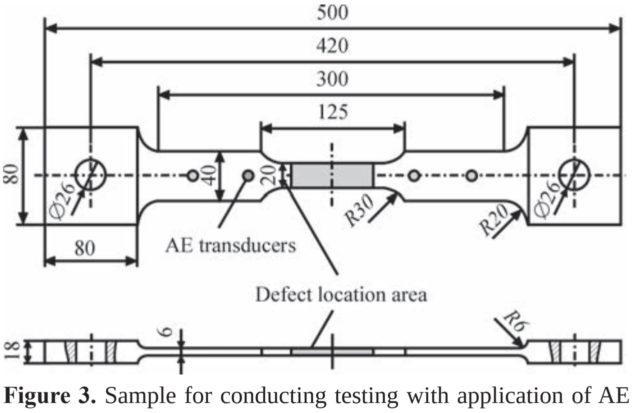

Figure 3. Sample for conducting testing with application of AE technology

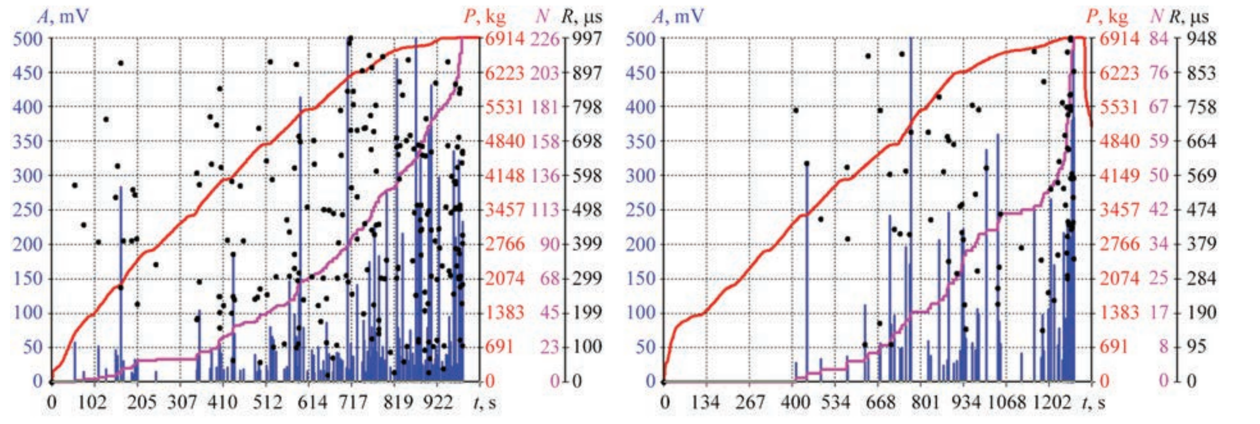

Figure 4. Diagrams of testing sample series *a*

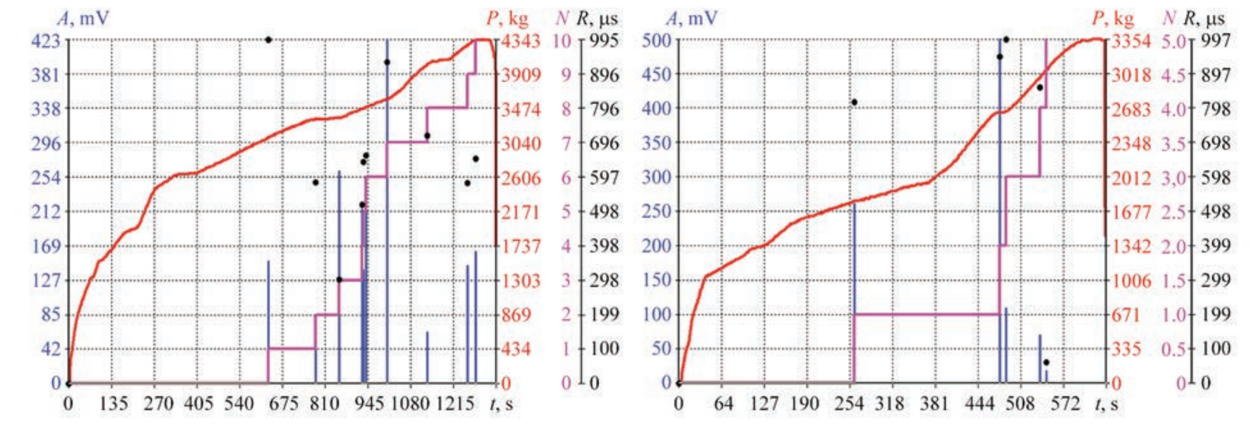

Figure 5. Diagrams of testing sample series *b*

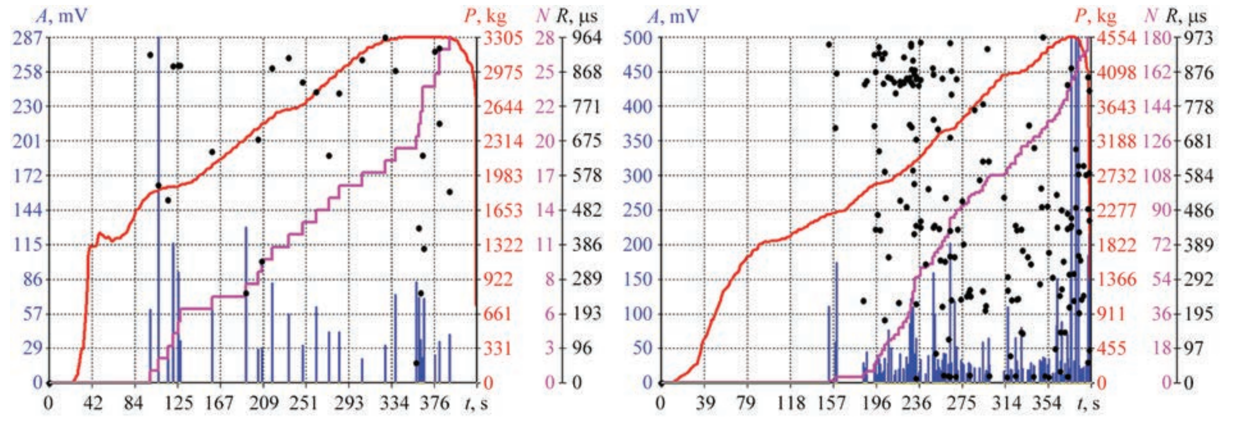

Figure 6. Diagrams of testing sample series *c*

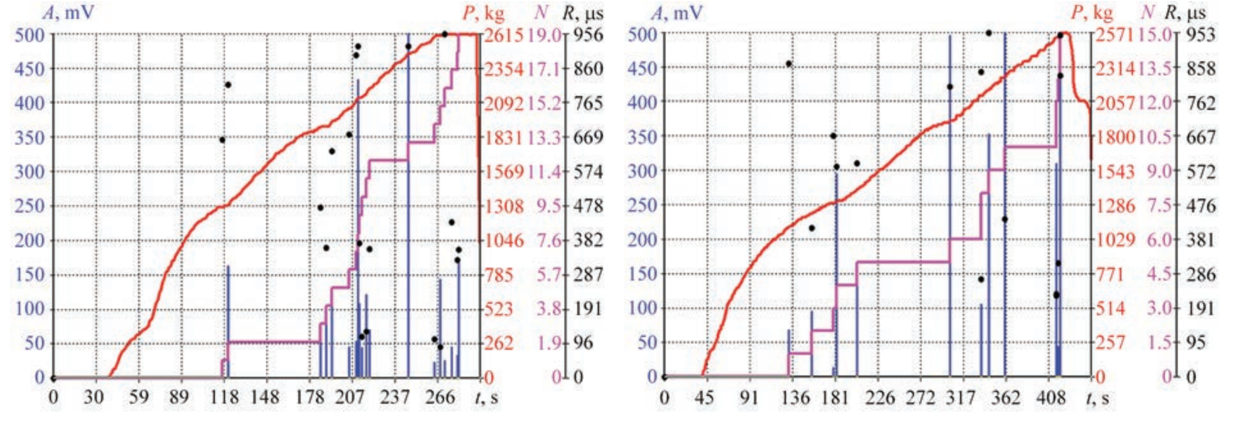

Figure 7. Diagrams of testing sample series *d*

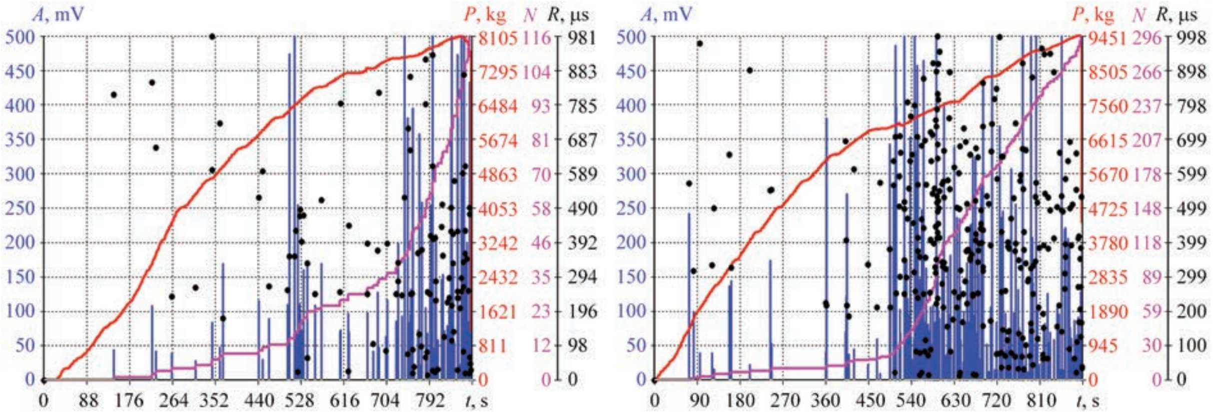

Figure 8. Diagrams of testing sample series *e*

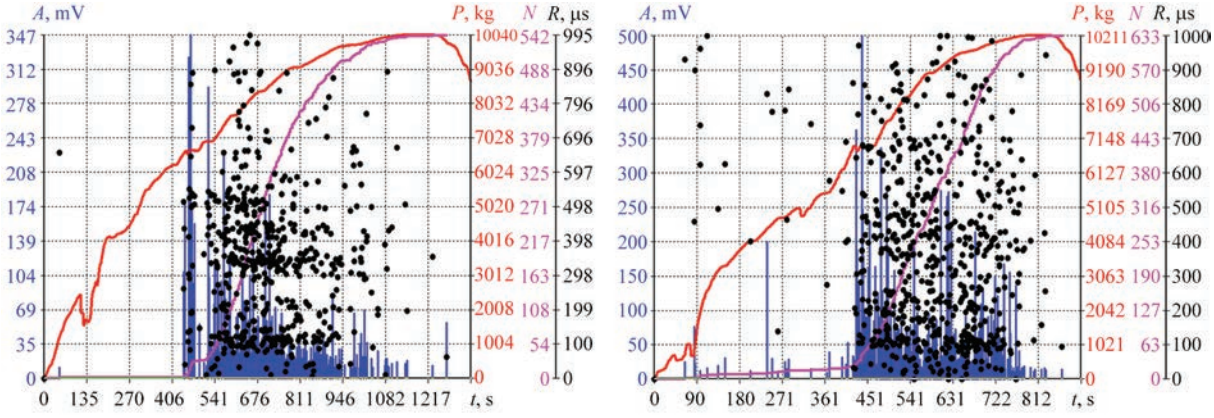

Figure 9. Diagrams of testing samples of monolithic metal from 17 GS steel

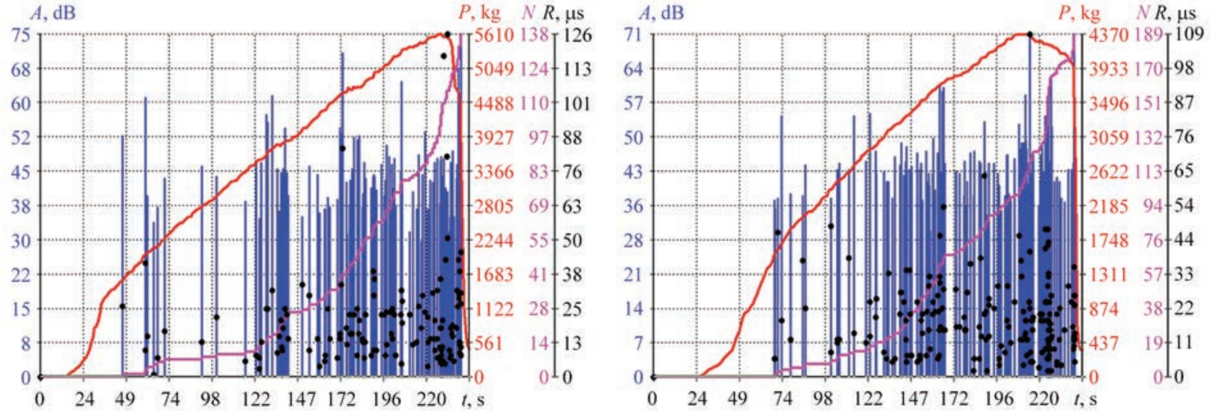

Figure 10. Diagrams of testing samples with two-sided welded-on elements

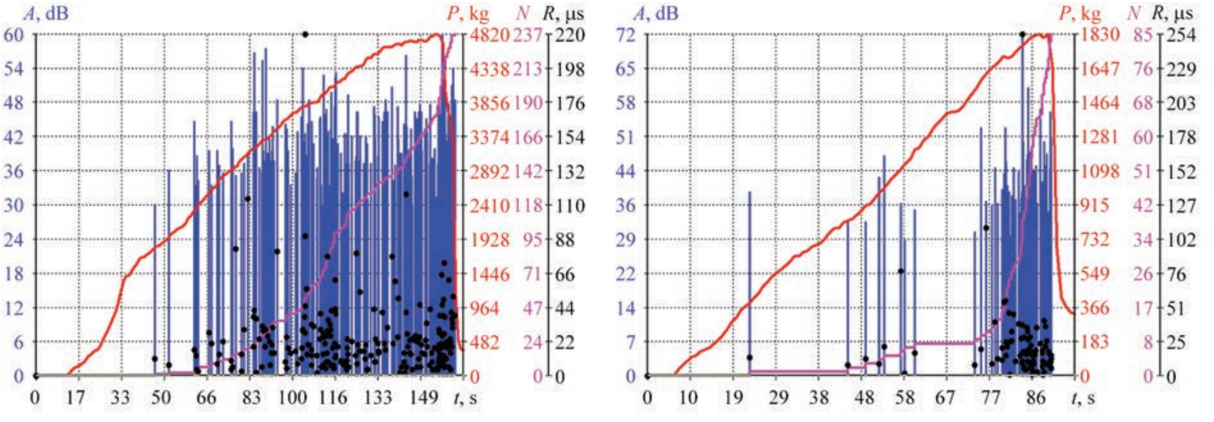

Figure 11. Diagrams of testing samples with randomly performed weld

radii on the working part thickening. It is obvious that for such kinds of welded joints stress concentration in the weld area was the lowest, resulting in more uniform deformation of the sample. This led to appearance of plastic strain zones and beginning of the process of damage accumulation in the area of rounding-off radii, and, eventually, caused occurrence of AE signals.

A characteristic feature is formation of destruction in the near-weld zone. As a rule, several centers of AE radiation in the welded joint zone were observed for all the samples, one of which coincided with the location of the weld or spot, while others were at a distance of 5–25 mm from the weld center in the HAZ (Figure 12).

Acoustic signals arriving from the zone of rounding-off radii, differ significantly from signals coming from the welded joint. They are smaller by amplitude and are associated primarily with plastic strain of the sample, so that they are more uniformly distributed in time. AE signals in the welded joint zone are caused predominantly by defects arising in welding. Their amplitude is higher, and the nature of their occurrence is more random. That is why both AE amplitude and activity allow clearly distinguishing between acoustic emission from the welded joint area and that in the plastic strain area.

On the whole, one can see that the nature of AE signal accumulation in the welded joint material during sample deformation is the most fully reflected by such a parameter as total number of AE events (denoted by N in the graphs).

In particular, note the change of the slope of the graph of the above-mentioned parameter for samples with welded joints that is clearly seen in the graphs, and can be related to the start of fracture zone formation. If we compare the shape of N curve of the sum of AE events for welded joints and for monolithic metal of the same grade (Figure 9), the difference immediately becomes obvious: for material with welded joints in the area of regular AE activity, i.e. when AE events are not isolated and rather uniformly arise in time, N curve is concave, and for monolithic material it is convex, on the contrary.

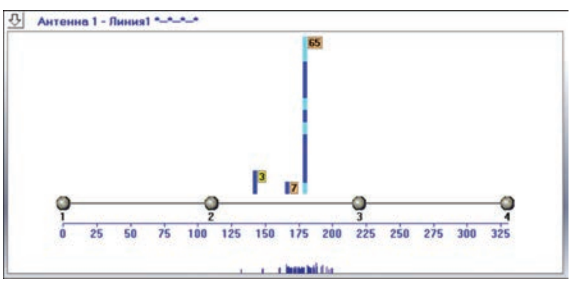

Figure 12. Screen of EMA-3.92 program with typical results of AE event location at welded sample testing. Bars with flags show clusters formed on the base of AE events, colour of strips on the bars corresponds to a certain amplitude range. AE events proper (coordinates along the horizontal, and amplitudes along the vertical) are represented by vertical lines below on the location scheme

Thus, the slope at the turning point of the curve of AE event accumulation is criterial. It allows distinguishing the material with the welded joint from the material without it. This is confirmed by numerous available data of testing various materials.

In particular, studied were the welded samples prepared by the following procedure: samples after rupture testing (without the welded joint) were welded in the rupture site. Welded joint quality was chosen to be arbitrary on purpose, as the samples were used further to check the fracture loading prediction, so that it is not known beforehand. 20 samples with both joint types: two-sided weld and welded spot were prepared. Further-on samples were tested by the same procedure, as others. Testing samples of this type is interesting in that AE can be unambiguously identified as related to welded joint fracture, as, allowing for the Kaiser effect, the base metal during deformation should emit a minimum number of AE events. The difference from the previous test series consists in that measurements of AE parameters were taken by EMA-3 system, and AE amplitude is expressed in decibels, in keeping with application of a logarithmic mode of signal amplification, unlike EMA-2 system.

Diagrams, shown in Figures 10, 11, represent the parameters, similar to those given in Figures 4–8, and the designations are the same, respectively.

The amount of damage increases with time (curve N — in the graphs), but in samples without the welded joint this growth slows down at a certain moment of time [2–6]. The difference in testing the welded samples consists in that no decrease in AE activity is observed for them at the final section of loading that, actually, gives rise to a change in the shape of curve N. At the same time, a significant scatter of such a parameter as «Rise time» suggests that it cannot serve as a criterial one for the tested samples. Now, the amplitude of AE events does not always correlate with the processes of damage accumulation at fracture, so that it cannot be used as a versatile criterion either.

The above data relate to steel samples. At some time, already with application of AE systems EMA-1 based on «Defectophone» instruments, such studies were conducted for aluminium alloys AMtsS and AMtsN (main properties of these two materials are very close). Tested were small-sized samples with different types of raisers (Figure 13, *a*) and wide flat samples AR-02 (Figure 13, *b*) with special frame structure, designed for equilibrium deformation [7, 8] of their central part (it allows obtaining the complete diagram of deformation during testing with the loading branch dropping to zero), with two types of welded joints — two-sided weld and welded spot (automatic arc welding with 1.8 mm AMts electrode, 360 A current, 380 V voltage). Small-sized samples without the welded joint demonstrated extremely low acoustic activity of 1 or 2 AE events during the entire testing period, and these events occurred directly during sample destruction. Even presence of a stress raiser did not affect the low AE activity. Wide samples without the welded joint demonstrated somewhat higher AE activity than the small-sized ones. But it was still essentially lower than in the majority of the tested steels.

However, presence of the welded joint led to an essential increase of the number of AE events, which can be unambiguously related to the volume of material, included into the HAZ. Table 1 gives brief summing-up of testing aluminium samples with maximum number of registered AE events.

The results of all the described tests show that the welded joint is the main source of AE that is recorded during loading, while the number of events depends on the volume of the material included into the HAZ. Another feature is absence of AE up to the moment, when the process of sample destruction starts concentrating in the welded joint zone.

During testing the prediction of breaking load of welded samples by EMA-3.92 software was verified. A typical fragment of program window with hazard indicator, which displays the prediction results, is shown in Figure 14. Explanations for the location array screen are given in the description for Figure 9. Elements of testing control and timer are shown above the location screen, and indicator strip with predicted breaking load is displayed below.

Hazard indicator gives the number of location AE array (No.1 in this case), number of AE event cluster, for which the prediction was made (No.1) and its center coordinates (182 mm), which are calculated from No.1 transducer from left to right. Furtheron, fracture prediction is shown in kg, in keeping with the tensile testing machine scale, as well as the calculated damage level of the sample material expressed in percent, at the moment of issuing the maximum warning No.3 — «Hazard».

Table 2 gives the selected results of breaking load prediction for samples without the welded joint and with joints of different types. It does not seem possible to present all the obtained data in view of the large amount of them. The necessary regularities can be quite clearly seen, analyzing those data, which were included into Table 2.

As one can see from Table 2, for the majority of the samples, the real breaking load falls within the prediction range. Samples of series *b*, *c*, and *d* are an exception, for which the prediction is higher than the real values of breaking load. And even though the lower limit of the prediction falls within the deviation of ±15 % admissible for EMA type systems, the upper limit significantly exceeds it. Let us analyze why such a phenomenon is in place exactly for samples of the mentioned series. The most obvious conclusion is that the samples of these series during testing are subjected to off-center tension. At the same time, the prediction algorithms, incorporated into EMA system software, were based on standards, which envisage the traditional uniform loading of rod samples or tube-shell structures [9]. Thus, in order to adjust the destruction prediction for cases of off-center tension, additional study is needed, which

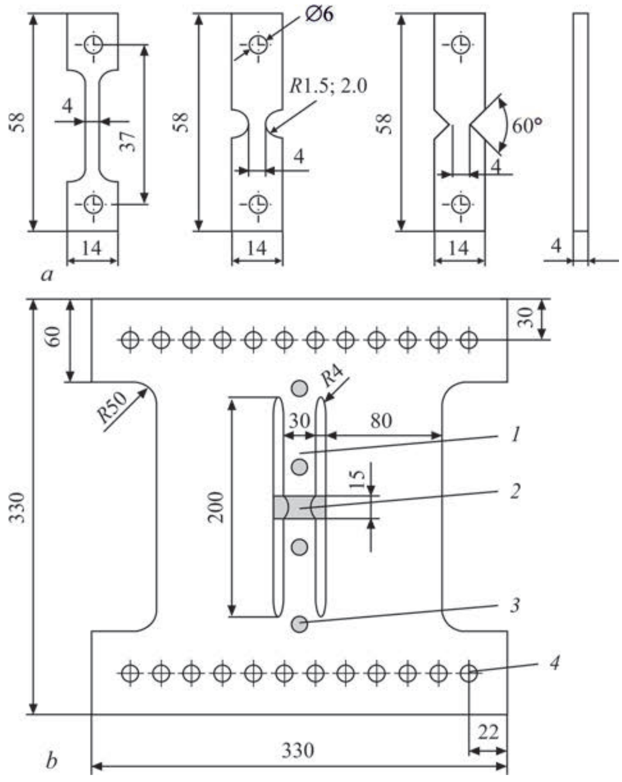

Figure 13. Samples for aluminium alloy testing: *a* — samples with different types of raisers; *b* — wide flat samples (*1* — spring dynamometer; *2* — welded joint area; *3* — AE transducer; *4* — 12 openings of 12 mm dia with 26 mm distance between them)

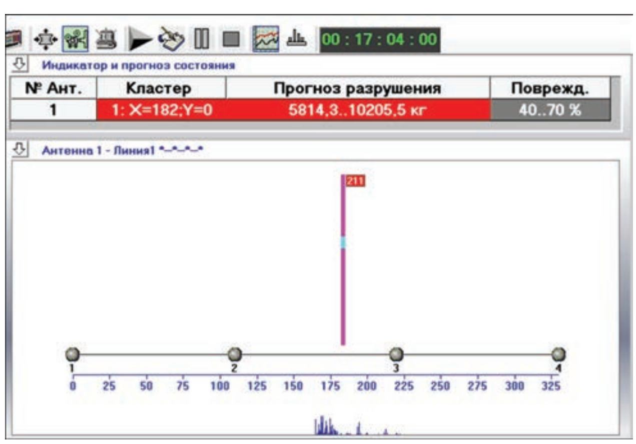

Figure 14. Screen of EMA-3.92 program with the results of AE event location and prediction of breaking load at testing one of the samples

Table 1. Final results of testing aluminium alloys AMtsS and AMtsN

Sample type	Small-sized	AR-02		
		Unwelded	With welded spot	With two-sided weld
Number of AE events	2	28	398	438

Table 2. Results of prediction of breaking load of steel samples

Sample type and number	Time of predicted fracture, s	Time of fracture start, s	Number of AE events, used in prediction	Current load, at which prediction was made, kg	Level of hazard warning	Fracture prediction — lower limit, kg	Fracture prediction — upper limit, kg	Actual breaking load, kg
Without WJ No.1	352	1153	27	5907	1	8787	15424	10039
Without WJ No.2	249	836	12	4738	1	6857	12036	10211
Series a No.1	402	991	11	4065	1	5814	10205	6914
Series b No.1	1005	1297	7	3702	1	4812	9207	4342
Series c No.1	248	392	13	2734	2	3731	4305	3305
Series d No.1	189	290	4	1956	1	2866	5031	2615
Series e No.1	230	855	3	2936	1	4733	8307	8105
Two-sided welded element No.1	71	228	7	2250	2	3217	5647	5610
Weld of undetermined quality No.1	68	155	8	2600	2	3718	6526	4820

would allow obtaining more valid prediction results either by establishing special coefficients for such a kind of loading, or through adding new standards, on which identification of material state is based.

At the same time it should be noted that the detected prediction error is not critical, firstly, because the lower limit of predicted breaking load falls within the admissible error range, secondly because the hazard warning which is represented by the red colour of the indicator (see Figure 13), is generated by EMA-3.92 program in advance, before the material yield limit has been reached.

Thus, even without making corrections in prediction setting, EMA type systems can provide timely warning about the danger of welded joint breaking up.

Conclusions

1. In the presence of a welded joint in the sample, it is the main AE source. Number of AE events in the samples with welded joints, as a rule, is higher than that in monolithic samples.

2. The process of welded sample destruction is characterized by a more uniform in time AE activity in samples with largest volume of welded joint material and less uniform for samples with a smallest volume of welded joint material.

3. The maximum number and amplitude of AE events correspond to largest volumes of welded joint material, which one can see at comparison of the results of testing samples of *a*, *c* and *e* series with those of *b* and *d* series.

4. Samples with welded joints are characterized by greater diversity of the obtained pattern of AE event distribution in time, amplitude and other characteristics for unwelded samples that is indicative of the influence of welded joint quality on the amount of damage introduced by them into the material. AE activity depends on the level of material damage, caused by welding.

5. The breaking load prediction for the majority of the samples gives satisfactory values. For samples of *b*, *c* and *d* series subjected to off-center tension during testing, the destruction prediction yields somewhat higher breaking load values. This should be taken into account at testing structures, where such a kind of welded joint loading is in place.

6. The sum of AE events is the parameter which can serve the characteristic of damage of welded joint metal. The angle of inflexion of the curve of AE event sum allows distinguishing between testing monolithic metal and metal with welded joint. Ability to assess the volume of metal involved in welding can increase the validity of this characteristic application.

1. Nedoseka, A.Ya., Nedoseka, S.A. (2020) *Fundamentals of calculation and diagnostics of welded structures.* Ed. by B.E. Paton. 5th Ed. Kiev, Indprom [in Russian].
2. Nedoseka, A.Ya., Nedoseka, S.A., Markashova, L.I. et al. (2018) Investigation by acoustic emission method of the kinetics of damage accumulation at fracture of materials. *Tekh. Diagnost. i Nerazrush. Kontrol,* **3**, 3–13 [in Ukrainian].
3. Nedoseka, S.A. (2007) Forecasting the fracture by the data of acoustic emission. *Ibid*., **2**, 3–9 [in Russian].
4. Skalsky, V.R. (2003) Evaluation of accumulation of bulk damage in solids, based on acoustic emission signals. *Ibid*., **4**, 29–36 [in Russian].
5. Stone, D.E., Dingwall, P.F. (1977). Acoustic emission parameters and their interpretation. *NDT Int.*, **10**, 51–56.
6. Tetelman, A.S., Chow, R. (1971) Acoustic emission testing and micro cracking processes. In: *Proc. of Symposium presented at the December Committee Week American Society for Testing and Materials (Bal Harbour. 7–8 December, 1971)* 30–40.
7. Volkov, V.A. (1980) *Basic results of All-Union experiment on fracture mechanics of low-strength steel.* In: *Problems of metal fracture.* Moscow, MDNTN, 3–22 [in Russian].
8. Lebedev, A.A., Chausov, N.G. (1988) *Express-method of evaluation of crack resistance of plastic materials.* Kiev, AS of Ukr.SSR [in Russian].
9. Paton, B.E., Lobanov, L.M., Nedoseka, A.Ya. et al. (2012) *Acoustic emission and service life of structures: Theory, methods, technologies, facilities, application.* Kiev, Indprom [in Russian].

Received 22.12.2020